Electrical Characterisation of Unidirectional Thermoplastic Composite Tapes

Influence of Microstructure and Manufacturing Route

Dennis Colaianni

Delft University of Technology

TU Delft

Electrical Characterisation of Unidirectional Thermoplastic Composite Tapes

Influence of Microstructure and Manufacturing Route

Master Thesis Master of Science Thesis

by

Dennis Colaianni

to obtain the degree of Master of Science
at the Delft University of Technology,
to be defended publicly on Tuesday May 12th, 2026

Thesis committee:

Chair:	Dr. J. J. E. Teuwen
Supervisor:	Dr. B. Çağlar
External Examiner:	Dr. ir. O. K. Bergsma
Company Supervisor:	Dr. ir. A. J. de Wit
External Supervisors:	E. ul-Haq, Dr. O. Eryilmaz
Project Duration:	August, 2025 - May, 2026
Faculty:	Faculty of Aerospace Engineering, Delft

Style: TU Delft Report Style, with modifications by Daan Zwaneveld

TU Delft

Preface

This report presents the results of my graduation research, completing my MSc in Aerospace Engineering at TU Delft. The research was conducted at the Aerospace Structures and Materials (ASM) department in collaboration with the Royal Netherlands Aerospace Centre (NLR) in Amsterdam.

First and foremost, I would like to express my sincere gratitude to my main supervisor, Baris Caglar, for his trust in this project and for his continuous guidance. I am also very thankful to Ehshan ul-haq and Oguz Eryilmaz for their daily supervision, as well as for their friendship throughout this work.

I would like to extend my appreciation to my company supervisor, Albert Jan de Wit, for generously sharing his expertise and for always being available to provide valuable insights. Special thanks also go to Shailee, Burak, Maissaloun, Clement, and all the members of the ASM tape line group for their support and assistance whenever needed.

I am grateful to my classmates and friends for sharing both challenges and the enjoyable moments of this journey, making this master's experience not only valuable but also truly memorable.

Finally, I would like to thank my family and friends for their unwavering support, encouragement, and belief in me, which have motivated me to always go the extra mile.

Dennis Colaianni
Delft, April 2026

Abstract

The increasing use of thermoplastic composites (TPC) in aerospace structures calls for a better understanding of their functional properties, particularly for unidirectional (UD) tapes. These materials offer advantages in automated manufacturing and weldability, but their electrical behaviour is inherently complex due to strong anisotropy and microstructural variability. This study therefore investigates the relationship between manufacturing route, microstructure, and electrical conductivity of UD TPC tapes, with an outlook on their applicability in the induction welding process.

A multi-method experimental approach was adopted, combining six probe electrical measurements, infrared thermography, eddy current testing, and optical microscopy. Four different UD TPC tape systems, produced via distinct manufacturing routes, were characterised and compared. The results demonstrate that electrical conductivity is primarily governed by fibre volume fraction, but is significantly influenced by microstructural features such as fibre distribution, polymer rich regions, defects, and thickness variations. Deviations from idealised models, such as the Rule of Mixtures, highlight the importance of local fibre connectivity and interfacial effects in determining conductive behaviour.

Infrared thermography and eddy current testing revealed that electric current pathways are highly dependent on both internal architecture and surface condition, with polymer rich layers limiting current injection and promoting localised conduction. Microstructural analysis confirmed that manufacturing routes directly influence fibre arrangement and polymer distribution, resulting in distinct electrical responses across the investigated materials.

This study also identified limitations in conventional conductivity measurements, particularly related to geometric assumptions and thickness variability, and proposed a normalisation approach to reduce associated uncertainties. Furthermore, finite element modelling of inductive heating demonstrated that the strong anisotropy of UD TPC tapes limits the formation of effective eddy currents, leading to poor heat generation compared with more isotropic laminate configurations.

Overall, this work establishes a direct link between manufacturing, microstructure, and electrical behaviour in UD TPC tapes. The findings provide valuable insights for improving material characterisation, enhancing modelling accuracy, and enabling practical applications such as in-situ quality control during tape manufacturing and optimisation of induction-based processing techniques.

Contents

Preface i

Summary ii

Nomenclature ix

1 Introduction 1
- 1.1 Motivation . . . 1
- 1.2 Research Questions, Scope, and Objectives . . . 2
- 1.3 Outline and Approach . . . 3

2 Literature Review 5
- 2.1 Thermoplastic Composites . . . 5
  - 2.1.1 Temperature Phases . . . 5
  - 2.1.2 Material Manufacturing . . . 6
  - 2.1.3 Manufacturing Process . . . 7
- 2.2 Electrical Behaviour of Composites . . . 10
  - 2.2.1 Induction Welding . . . 10
  - 2.2.2 Anisotropic Electrical Properties of CFRP . . . 10
  - 2.2.3 Heating Mechanism During Induction Welding . . . 11
  - 2.2.4 Influence of Interface on Electrical Conductivity . . . 12
- 2.3 Electrical Conductivity Characterisation . . . 14
  - 2.3.1 Rule of Mixtures . . . 14
  - 2.3.2 Methods of Characterisation of Electrical Conductivity in CFRP Composites . . . 16
  - 2.3.3 The Six probe Voltage Measurement Method . . . 18
  - 2.3.4 Eddy Current Testing . . . 21

3 Methodology 23
- 3.1 Material Preparation . . . 23
  - 3.1.1 Tape Preparation and Specimen Geometry . . . 25
  - 3.1.2 8 Layer UD TPC Laminate Preparation . . . 25
- 3.2 Electrical Characterisation . . . 27
  - 3.2.1 Six-probes Electrical Conductivity Test . . . 27
  - 3.2.2 Infrared Thermography . . . 34
  - 3.2.3 Through-thickness Eddy Current Measurement Test . . . 35
- 3.3 Microscopy Characterisation . . . 38
  - 3.3.1 Sample Preparation . . . 38
  - 3.3.2 Micrograph Acquisition and Processing . . . 39
  - 3.3.3 Assumptions and Limitations . . . 41
- 3.4 Induction Welding Outlook . . . 42
  - 3.4.1 FEM Simulation . . . 42
  - 3.4.2 Static Induction Heating Experiment . . . 45

4 Results & Discussion 47
- 4.1 Electrical Characterisation of UD TPC Tapes . . . 47
  - 4.1.1 Electrical Conductivity . . . 47
  - 4.1.2 Fibre Volume Fraction Determination . . . 49
  - 4.1.3 Comparison with Rule of Mixtures (ROM) . . . 51
  - 4.1.4 Current Injection Behaviour . . . 52
  - 4.1.5 Eddy Current Sensor Results . . . 55
- 4.2 Microstructural Characterisation . . . 59

4.2.1 Microstructural Features of UD Tapes . . . 59
4.2.2 Thickness Variations of UD Tapes . . . 61
4.3 Influence of Manufacturing Route on Microstructure and Electrical Behaviour . . . 66
4.4 Induction Welding Outlook . . . 67
4.4.1 FEM Simulation of Static Induction Heating . . . 67
4.4.2 Experimental Induction Heating Validation . . . 69
4.4.3 FEM Modelling and Microstructural Features . . . 70
4.5 In-situ Quality Control for Tape Manufacturing . . . 72

5 Conclusion **74**

References **76**

A Material Preparation **82**
A.0.1 Tape preparation . . . 82
A.0.2 Laminate preparation . . . 83

B Six probes design and adjustments **86**
B.1 set-up design & adjustments . . . 86

C Six probe data acquisition code **90**

D Results **95**
D.1 Electrical Conductivity . . . 95
D.1.1 TC 1225 tape . . . 95
D.1.2 DPR tape . . . 96
D.1.3 TPR tape . . . 97
D.1.4 Hybrid tape . . . 98
D.2 Microscopy . . . 99
D.2.1 TC 1225 tape . . . 99
D.2.2 DPR tape . . . 100
D.2.3 TPR tape . . . 101
D.2.4 Hybrid tape . . . 102

List of Figures

1.1 Schematic structure of thesis approach . . . 3

2.1 Temperature profile of thermoplastics indicating glass transition, crystalline, and melting temperature phases . . . 6
2.2 Typical TPC processing cycle from raw material to structure . . . 7
2.3 TPR in-line production setup at TU Delft . . . 7
2.4 DPR in-line production setup at TU Delft . . . 8
2.5 Overview of induction welding process . . . 10
2.6 Eddy current formation in a (i) woven fabric unit cell and (ii) to a UD ply-based reinforcement 11
2.7 Energy dissipation mechanisms by eddy currents . . . 11
2.8 Percolation stages in conductive composite . . . 12
2.9 Corresponding fibre-fibre contact for percolation threshold . . . 13
2.10 Conductivity in three dimensions . . . 14
2.11 Measured data for longitudinal conductivity from literature . . . 15
2.12 Typical electrical conductivity measurement methods . . . 16
2.13 Cross section of the UD tape undergoing a six-probe measurement . . . 18
2.14 Real and approximated current density through anisotropic materials . . . 19
2.15 Effect of geometry on voltage drop in specimen during the six probe measurement . . . 20

3.1 UD TPC tape preparation . . . 25
3.2 Six probes setup schematic representation . . . 27
3.3 Six probes DC electrical circuit diagram . . . 28
3.4 Six probes schematic representation of measurement configuration . . . 28
3.5 Six probes cabling setup . . . 29
3.6 flowchart of the Python application to calculate anisotropic electrical conductivities from six probes measurements . . . 30
3.7 Sketch of cross sectional area for longitudinal resistivity calculations . . . 32
3.8 Infrared Thermography Diagram . . . 34
3.9 DC & AC electrical circuit diagram . . . 35
3.10 Schematic view of eddy current setup . . . 36
3.11 Eddy Current Sensor Gain and Phase Shift Diagrams of UD TPC Tape . . . 36
3.12 Polished microscopy samples . . . 39
3.13 Micrograph of a Toray TC1225 cross section . . . 39
3.14 Flowchart of python code to analyse micrograph . . . 40
3.15 Cross sectional micrograph with fibre detected by red circles . . . 40
3.16 Flowchart FEM Model . . . 42
3.17 Geometry of Induction Welding setup . . . 43
3.18 Induction welding experiment setup at SAM XL . . . 45

4.1 Longitudinal electrical conductivity of 4 UD tapes . . . 48
4.2 Through-thickness electrical conductivity of 4 UD tapes . . . 48
4.3 FVF python micrograph analysis . . . 49
4.4 Longitudinal conductivity of four tape systems compared to literature values and ROM . 50
4.5 Thermography of TC 1225 tapes: low vs full clamping pressure . . . 53
4.6 Thermography of DPR tapes: low vs full clamping pressure . . . 53
4.7 Thermography of TPR tapes: low vs full clamping pressure . . . 53
4.8 Thermography of Hybrid tapes: low vs full clamping pressure . . . 54
4.9 Thermography of 8 layer UD TC 1225 laminate . . . 55
4.10 Eddy Current Gain and Phase Shift Response of TC_4 and TC_5 tapes . . . 56

4.11 Eddy Current Gain and Phase Shift Response of DPR 1_3 and 1_7 tapes 56
4.12 Eddy Current Gain and Phase Shift Response of TPR 3_1 and 3_2 tapes 57
4.13 Eddy Current Gain and Phase Shift Response of Hybrid 2_1 and 2_3 tapes 58
4.14 Micrography of TC 1225 tape 59
4.15 Micrography of DPR tape 60
4.16 Micrography of TPR tape 60
4.17 Micrography of Hybrid tape 61
4.18 Micrograph of DPR tape used for thickness variation 61
4.19 Thickness variance mask of DPR tape 61
4.20 Thickness variance of TC 1225 tape 62
4.21 Thickness variance of DPR tape 62
4.22 Thickness variance of TPR tape 63
4.23 Thickness variance of Hybrid tape 63
4.24 Longitudinal electrical conductivity of 4 UD tapes 64
4.25 Longitudinal electrical conductivity of 4 UD tapes with normalised thickness 64
4.26 Longitudinal electrical conductivity of 4 UD tapes with normalised FVF 65
4.27 Top view heat map of simulated temperature distribution of TC 1225 tape after 1 second 68
4.28 Top view heat map of simulated temperature distribution of TC 1225 tape after 10 second 68
4.29 IR thermography results for woven laminate under $300\ A$ coil excitation 69
4.30 Top view heat map of simulated temperature distribution of woven laminate after 3 second 70
4.31 Cross section of TPR tape with polymer rich regions highlighted in red and bulk fibre concentration highlighted in blue 70
4.32 Top view heat map of simulated temperature distribution of woven laminate after 3 second 71
4.33 Schematic view of six probe and IR thermography for in-situ quality control for tape manufacturing 72
4.34 Schematic view of in-situ placement in TPR tape production line 73

A.1 Toray TC1225 tape 82
A.2 Preparation of sample geometry 82
A.3 2 layer UD laminate stack 83
A.4 Hot press 83
A.5 De-moulding of 2 layer laminates 84
A.6 Defects from hot press process 84
A.7 Trimming of flow-out material 85
A.8 30x30cm 8 layer laminate 85
A.9 Trimmed 8 layers laminate 85

B.1 Six-probe test of aluminium t-bone 86
B.2 Thickness effect on calculated resistivity of stainless steel strips 86
B.3 NI USB-6009 DAQ 87
B.4 Python live visualisation of top and bottom resistivity, and calculated through-thickness conductivity of the tape 87
B.5 Electrode geometry effect on acquired longitudinal conductivity 88
B.6 Clamping pressure effect on acquired longitudinal resistivity 88
B.7 Current effect on acquired longitudinal conductivity 89
B.8 Resistivity variance over a time frame of four minutes 89

D.1 Longitudinal conductivity of TC 1225 tape sections 95
D.2 Through thickness conductivity of TC 1225 tape sections 96
D.3 Longitudinal conductivity of DPR tape sections 96
D.4 Through thickness conductivity of DPR tape sections 96
D.5 Longitudinal conductivity of TPR tape sections 97
D.6 Through thickness conductivity of TPR tape sections 97
D.7 Longitudinal conductivity of Hybrid tape sections 98
D.8 Through thickness conductivity of Hybrid tape sections 98
D.9 Micrograph of TC1225 tape TC_4_1 99
D.10 Micrograph of TC1225 tape TC_4_2 99

D.11 Micrograph of TC1225 tape TC_5_1 99
D.12 Micrograph of TC1225 tape TC_5_2 100
D.13 Micrograph of DPR tape 1_3_1 100
D.14 Micrograph of DPR tape 1_3_2 100
D.15 Micrograph of DPR tape 1_7_1 101
D.16 Micrograph of DPR tape 1_7_2 101
D.17 Micrograph of TPR tape 3_1_1 101
D.18 Micrograph of TPR tape 3_1_2 102
D.19 Micrograph of TPR tape 3_2_1 102
D.20 Micrograph of TPR tape 3_2_2 102
D.21 Micrograph of Hybrid tape 2_1_1 103
D.22 Micrograph of Hybrid tape 2_1_2 103
D.23 Micrograph of Hybrid tape 2_3_1 103
D.24 Micrograph of Hybrid tape 2_3_2 103

List of Tables

2.1 Overview of literature data on longitudinal electrical conductivity of pan fibre-based cfrps with a ud lay-up. In this listing, studies were included solely if there was traceable information on the fibre type, fibre volume fraction, and measured longitudinal electrical conductivity σ_1. 15
2.2 Electrical conductivities characteristic for commercially available pan-based carbon fibres as reported by the manufacturers. 16

3.1 Torayca™-M40J fibre and functional properties 24
3.2 Torayca™-T800s fibre and functional properties 24
3.3 Grinding and polishing program used for sample preparation 38
3.4 Material properties Toray TC1225 43

4.1 FVF comparison to manufacturing route and respective conductivity 50
4.2 FVF determination per material system 51
4.3 ROM conductivity calculation for each tape system 52
4.4 Nominal tape thickness used for conductivity calculations 52
4.5 Thickness variance results from cross section analysis 63
4.6 Electrical conductivity properties of UD TC 1225 tape input for FEM model 67
4.7 Electrical conductivity properties of woven laminate input for FEM model 69

A.1 Hot Press Production Plan - Toray TC1225 laminate 83

Nomenclature

Abbreviations

Abbreviation	Definition
NLR	Netherlands Aerospace Centre
TPC	Thermoplastic composite
UD	Unidirectional
TPR	Thermoplastic extrusion impregnation
DPR	Water based dispersion impregnation
CFRP	Carbon fibre-reinforced polymer
FVF	Fibre volume fraction
CTO	Closed tolerance orifice
FEM	Finite element method
ROM	Rule of mixtures
PAN	Polyacrylonitrile
ECT	Eddy current testing
NDT	Non-destructive test
Rx	Receiver
Tx	Transmitter
KVL	Kirchoff's voltage law
LM-PAEK	Low-melting polyaryletherketone
PEEK	Polyetheretherketone
CTE	Coefficient of thermal expansion
DAQ	Data acquisition
NI	National Instruments
AI	Analog Input
AC	Alternating current
DC	Direct current
CLAHE	Contrast limited adaptive histogram equalization

Symbols

Symbol	Definition	Unit
T_m	Melting temperature	[°C]
T_g	Glass transition temperature	[°C]
T_c	Crystallization temperature	[°C]
q	Flow rate area	$[m^2]$
K	Permeability	$[m^2]$
$\frac{dp}{dz}$	Pressure gradient	$[Pa/m]$
Δt	Impregnation time	$[s]$
Δp	Pressure gradient	$[Pa]$
z	Impregnation path	$[m]$
k	Thermal conductivity	$[W/(m{\cdot}K)]$
k_m	Matrix thermal conductivity	$[W/(m{\cdot}K)]$
k_f	Fibre thermal conductivity	$[W/(m{\cdot}K)]$
v_f	Fibre volume fraction	[%]
v_m	Matrix volume fraction	[%]
I	Current	$[A]$
V	Voltage	$[v]$
V_t	Top surface voltage drop	$[v]$
V_b	Bottom surface voltage drop	$[v]$
w	Width	$[m]$
t	Thickness	$[m]$
l	Length inner probes	$[m]$
L	Length outer electrodes	$[m]$
R	Resistance	[Ω]
z_{eff}	Effective penetration depth of current	$[m]$
t_{eff}	Effective thickness	$[m]$
$J_x(z)$	Current density	$[A/m^2]$
L	Inductance	$[H]$
M	Mutual inductance between coils	$[H]$
Z	Impedance	[Ω]
S	Scattering transmission coefficient	[-]
f	Frequency	$[Hz]$
R_{top}	Top surface resistance	[Ω]
R_{bottom}	Bottom surface resistance	[Ω]
R_f	Bulk fibre resistance	[Ω]
FVF	Fibre volume fraction	[%]
H	Magnetic field strength	$[A/m]$
B	Magnetic flux density	$[T]$
D	Electric displacement field	$[C/m^2]$
η	Dynamic viscosity	$[Pa{\cdot}s]$
ρ	Resistivity	$[\Omega/m]$
σ	Conductivity	$[S/m]$
σ_f	Fibre conductivity	$[S/m]$
σ_m	Matrix conductivity	$[S/m]$
ω	Angular frequency	$[rad/s]$
δ	Penetration depth	$[m]$
μ	Magnetic permeability	$[H/m]$
ϵ	Permittivity	$[-]$
δ_{imp}	Impregnation efficiency coefficient	$[m]$

1

Introduction

The following research is carried out at TU Delft with the support from the Royal Netherlands Aerospace Centre (NLR) in Amsterdam, with the scope of investigating the qualitative and quantitative relationship between UD tapes microstructure and their electrical properties. This chapter introduces the motivation behind the study, presents the research questions, and provides an overview of the structure of the thesis.

1.1. Motivation

The increasing demand for cost efficient and high rate manufacturing of large composite structures in the aerospace industry has accelerated the transition from metallic materials to fibre-reinforced polymers [1]. These materials offer superior specific strength and stiffness, while enabling significant weight reduction and improved fuel efficiency in modern aircraft [2]. Among composite systems, thermoplastic composites (TPC) have gained growing attention due to their enhanced impact resistance, recyclability, and their ability to be welded, making them particularly attractive for automated manufacturing processes [3, 4].

Unidirectional (UD) thermoplastic composite tapes represent a key building block for advanced composite structures. However, their performance is not only governed by intrinsic material properties, but also by their microstructural architecture, which is strongly influenced by the manufacturing route [5]. Processes such as thermoplastic extrusion impregnation (TPR) [6] and water based dispersion impregnation (DPR) [7] can produce tapes with varying fibre volume fraction, fibre distribution, and resin rich regions. As a result, even identical tapes may exhibit significant local variability in their internal structure, leading to differences in functional properties.

One property of particular interest for the present study is the electrical conductivity of UD TPC tapes. Due to the presence of carbon fibres, these materials exhibit anisotropic electrical behaviour, where conductivity is significantly higher along the fibre direction than in transverse and through thickness directions [8]. Due to the material anisotropy, electrical performance can not be fully described by idealised models such as Rule of Mixtures [9]. It is strongly affected by microstructural features such as fibre distribution, heterogeneity, defects, and the presence of polymer rich layers [10, 11].

Understanding the relationship between microstructure and electrical behaviour is therefore essential. Electrical conductivity measurements, when combined with qualitative techniques, provide insight into current pathway formation within the material. These pathways reflect the effective connectivity of the fibre network and can serve as indirect indicator of microstructural quality [8].

This relationship is particularly relevant for manufacturing and processing applications. In induction based processes, such as induction welding, heat generation relies on the formation of eddy currents within the material. However, in UD TPC systems, strong electrical anisotropy and microstructural features, such as polymer rich regions, can limit current flow and reduce heating efficiency [12].

Although induction welding is applied to components manufactured from UD TPC tapes rather than

to individual tapes themselves, the electrical behaviour of single tapes remains fundamental. The arrangement and connectivity of tapes within a structure are directly governed by their intrinsic properties and microstructure. While induction welding has been successfully applied to woven composites, its application to UD tape based structures is more challenging due to the difficulty in achieving predictable and homogeneous current pathways.

Induction welding is a method that is already being used in the aerospace industry to assemble thermoplastic composite structures. For example, the empennage of the Gulfstream G650 [13], elevators of the Dassault F5X [14, 8], and the access doors to the fuel tank of the Airbus A220 [15, 8]. However, as mentioned, these successful technologies are based on woven fabric-reinforced thermoplastic composites, whereas unidirectional tape-based TPC have yet to take flight [8]. This is the consequence of a complex process not readily applicable to UD-ply based reinforcements, due to the difficulties in achieving consistent and predictable heat generation at the interface [8].

In this context, a detailed understanding of how manufacturing routes influence microstructure, and how microstructure in turn governs electrical behaviour, is essential. Such knowledge not only contributes to the fundamental understanding of composite materials but also enables practical applications. These include improving accuracy of finite element models for predicting induction welding processes and developing in-situ quality control strategies for tape manufacturing based on electrical measurements.

1.2. Research Questions, Scope, and Objectives

This research aims to investigate the qualitative and quantitative relationship between the electrical performance of unidirectional thermoplastic composite tapes and their microstructural features and respective manufacturing route.

Based on this scope, the study is guided by the following main research question:

How do microstructural features and manufacturing routes of unidirectional thermoplastic composite (UD TPC) tapes influence their electrical conductivity and current pathway formation, and how can these relationship be utilised for improved characterisation and process application?

The following sub-questions forms a backbone for the methodology:

- Which microstructural features govern electrical conductivity and current pathway distribution in UD TPC tapes?
- How do different tape manufacturing routes influence the microstructural architecture of UD TPC tapes, and how does this affect their electrical conductivity and current distribution behaviour?
- How can the electrical conductivity of UD TPC tapes be accurately quantified, considering anisotropy, microstructural variability, and geometric uncertainties?
- How can electrical measurements, infrared thermography, eddy current testing, and microstructural analysis be combined to provide a comprehensive understanding of current pathways in UD TPC tapes?
- How do anisotropic electrical properties and microstructural characteristics of UD TPC tapes influence their behaviour under inductive heating conditions?
- How can electrical characterisation methods be applied for in-situ quality control of UD TPC tape manufacturing processes?

To address the research questions outlined in this study, the following objectives are defined:

1. To characterise the anisotropic electrical conductivity of UD TPC tapes using the six probe method, and to evaluate the reliability and limitations of this approach in relation to geometrical and measurement uncertainties.

2. To investigate the relationship between microstructural features and electrical behaviour, with particular focus on fibre volume fraction, fibre distribution, resin rich regions, and thickness variations.

3. To investigate the influence of manufacturing routes such as TPR and DPR on microstructural architecture, and to assess how these differences affect electrical conductivity and current pathway formation.

4. To integrate multiple characterisation techniques, including infrared thermography, eddy current testing, and optical microscopy, in order to establish an analysis of current distribution within UD TPC tapes.

5. To evaluate the impact of anisotropic electrical properties on inductive heating behaviour, through the implementation and validation of a finite element model.

6. To explore the potential application of electrical characterisation methods for in-situ quality control, enabling real time assessment of tape manufacturing processes.

Therefore, this study focuses on the experimental characterisation of the electrical behaviour of UD TPC tapes, with particular emphasis on the influence of microstructural features and manufacturing routes. By combining conductivity measurements, current pathway visualisation, local electrical response, and detailed microstructural analysis, an understanding of the material behaviour is established.

The outcomes of this work provide new insights into the relation between microstructure and electrical performance of UD TPC tapes, while also demonstrating the potential of electrical characterisation as a tool for process optimisation, modelling, and quality control in composite manufacturing.

1.3. Outline and Approach

To achieve the project scope, a multi-scale approach is adopted, combining material preparation, electrical and microstructural characterisation, and both experimental and numerical methods. This integrated methodology enables a comprehensive understanding of how microstructural features and their representative manufacturing route influence the electrical behaviour, and how these properties may impact applications such as induction welding of UD TPC composite structures.

Based on this scope, the study is guided by the following structure:

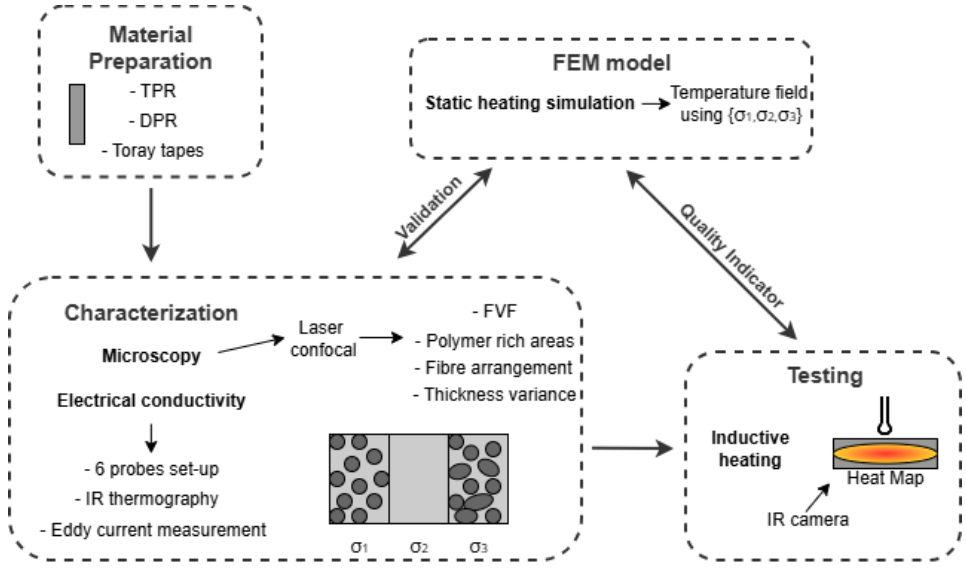

Figure 1.1: Schematic structure of thesis approach

As illustrated in Figure 1.1, the overall structure of this thesis follows a systematic approach to investigate the relationship between manufacturing route, microstructure, and electrical behaviour of UD TPC tapes. The study begins with the preparation and selection of materials produced via different manufacturing routes, namely TPR and DPR, which are compared against a reference Toray UD TPC tape.

The characterisation is divided into two complementary components: electrical and microstructural analysis. Electrical characterisation includes the use of six probe method for conductivity measurements, infrared thermography for visualising current pathway distribution, and eddy current testing for assessing local electrical response. Microstructural characterisation is performed using optical microscopy

combined with image analysis, enabling the evaluation of features such as fibre volume fraction, fibre distribution, polymer rich regions, and thickness variations.

In addition, the study extends to an application outlook by investigating the behaviour of UD TPC tapes under inductive heating conditions. A static induction experiment is conducted and analysed with infrared thermography to assess the thermal response of the material. This behaviour is further modelled using a finite element method simulation, in which the experimentally determined electrical properties are implemented.

The comparison between experimental and numerical results provide validation of the electrical characterisation and offers insight into the challenges associated with processing UD TPC materials in induction welding. Overall, this integrated approach enables understanding of how manufacturing, microstructure, and electrical behaviour are interconnected.

2

Literature Review

This chapter presents the literature review that forms the theoretical foundation for this study and supports the formulation of the research questions. It provides a comprehensive overview of unidirectional thermoplastic composite materials, with particular emphasis on their manufacturing, microstructural characteristics, and electrical behaviour.

The review begins with an introduction to thermoplastic composites and their intrinsic material properties, followed by an overview of manufacturing techniques used to produce TPC tapes, including the specific processes investigated in this work. Subsequently, the electrical behaviour of carbon fibre reinforced composites is discussed, with focus on anisotropic conductivity and the underlying conduction mechanisms.

In addition, the chapter examines induction welding processing, including the fundamental heating mechanisms involved and the challenges associated with UD composites. Particular attention is given to the influence of microstructure on electrical conductivity.

Finally, existing methods for electrical characterisation are reviewed, including the Rule of Mixtures (ROM), six probe measurements, and eddy current testing, as well as reported conductivity values in the literature. This review establishes the current state of art and identifies the gaps addressed in this study.

2.1. Thermoplastic Composites

Thermoplastic composites (TPC) exhibit enhanced performance compared to traditional thermoset composites, notably surpassing them in terms of fracture toughness and impact resistance. Moreover, the intrinsic characteristics of TPC enable them to be welded, potentially eliminating the requirement for mechanical fasteners and adhesive bonding in aircraft design [16]. TPC are materials that combine thermoplastic polymer matrix with reinforcing fibres, such as carbon fibres.

2.1.1. Temperature Phases

The thermoplastic matrix polymer material exhibit distinct temperature phases, as shown in Figure. 2.1, that affect their mechanical properties. As temperature rises, the polymer transition through different phases, including the glass transition temperature (Tg), at which the glassy state polymer changes to a rubbery state, characterised by reduced stiffness and increased ductility. Further heating leads to the melting temperature (Tm), where the polymer melts, becoming a viscous fluid with decreased stiffness and strength. Upon cooling, the polymer can crystallize below the crystallization temperature (Tc), forming a semi-ordered structure which improves mechanical properties and dimensional stability [17].

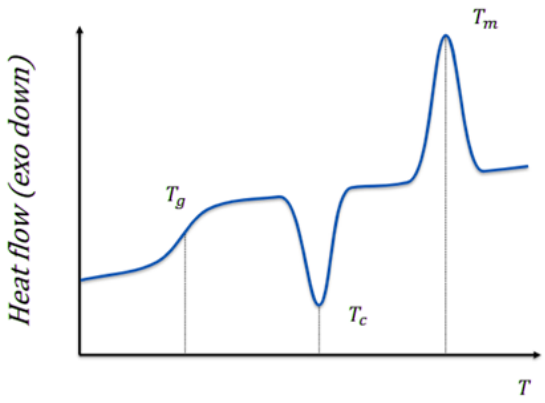

Figure 2.1: Temperature profile of thermoplastics indicating glass transition, crystalline, and melting temperature phases

A key aspect of TPC is their temperature dependent behaviour. Thermoplastic matrices can be repeatedly melted and solidified, meaning their processing is governed by temperature phases such as melting, consolidation, and cooling. These stages control fibre impregnation and polymer distribution, ultimately defining the material's microstructure [18, 17, 19, 20].

During cooling, the matrix solidifies and develops a semi-crystalline structure, influenced by factors such as temperature history and cooling rate. As a result, different manufacturing routes produce distinct microstructures [8, 17], including variations in fibre distribution and the formation of features such as polymer rich regions and heterogeneous interfaces [12, 16].

These microstructural characteristics directly influence electrical behaviour. In particular, polymer rich regions and interfacial zones can disrupt fibre connectivity, limiting current transfer and promoting non uniform current pathways. This is especially relevant for processes such as induction welding, where heat generation through Joule heating depends on continuous conductive networks. Understanding these temperature driven effects is therefore essential to link manufacturing processing, microstructure, and electrical performance.

2.1.2. Material Manufacturing

Unidirectional tape-based thermoplastic composites have been gaining increased attention in recent times. The UD tapes are characterised by their non-woven structure, with continuous fibres oriented in a single direction. These tapes are notably suitable for automated manufacturing of composite components, regardless of their size, due to their slender shape and ability to be easily handled and processed by machines. Moreover, UD reinforcements provide high stiffness and strength in the fibre direction due to their aligned fibre architecture. Consequently, the aerospace industry is extensively exploring the use of UD tapes for rapid manufacturing of larger load-bearing structures in future aircraft, such as wing boxes [21] and fuselage sections [22]. The key to higher production rates of TPC, compared to thermoset composites, lies in the ability of thermoplastic polymer to undergo rapid processing across multiple stages [23]. The manufacturing route for TPC aircraft structures involves several steps as shown in Figure 2.2, starting with impregnation, where material manufacturers impregnate carbon fibres with thermoplastic polymer to create UD tapes. These tapes are then cut to size, stacked, and consolidated into laminates using a hot press, a process referred to as laminate creation. The consolidated laminates are subsequently reshaped using processes like press forming or overmoulding to create three-dimensional features, in a step known as reshaping. This sequence allows for high automation, with each step applying heat and pressure to soften the thermoplastic polymer, transforming the composite into the next intermediate product.

The final stage of assembling TPC parts currently relies on traditional methods, such as fasteners or adhesive bonding, which are labour intensive. With the increasing use of TPC joints in airframes, there is a growing need for a processing technology that can offer advantages in terms of time, cost, structural integrity, and weight savings, which can be achieved by welding.

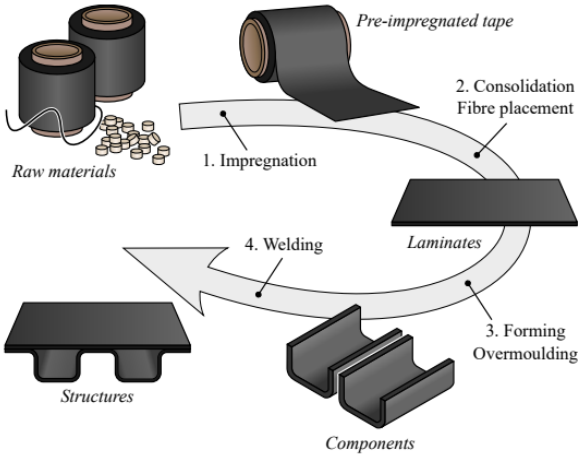

Figure 2.2: Typical TPC processing cycle from raw material to structure [8]

2.1.3. Manufacturing Process

Compared to thermoset composites, UD tapes offer both economical and environmental advantages. Their use results in reduced material waste and enables automated processing methods, such as automated tape laying, due to their ability to be reheated and reshaped.

Uniform impregnation of reinforcing fibres is essential to ensure a homogeneous distribution of the matrix, minimising defects such as fibre misalignment, waviness, fibre-fibre contact, and voids [7]. TPC have been manufactured since the 1970s using various techniques, including film stacking, melt pultrusion, and powder impregnation [7]. In this work, only thermoplastic extrusion impregnation (TPR) and water based slurry dispersion impregnation (DPR) are considered, as these are the processes used at the TU Delft tape line facility.

In the TPR process, the matrix is introduced as commercially available polymer granules [24]. The quality of the resulting UD tapes depends on both material properties, such as matrix viscosity and fibre characteristics, and process parameters, including production speed and die temperature. Among all stages, the impregnation unit is the most critical, as fibres are drawn through a die and impregnated with polymer melt from an extruder, governing fibre wet-out and matrix distribution. The TPR set-up used in this study is shown in Figure 2.3.

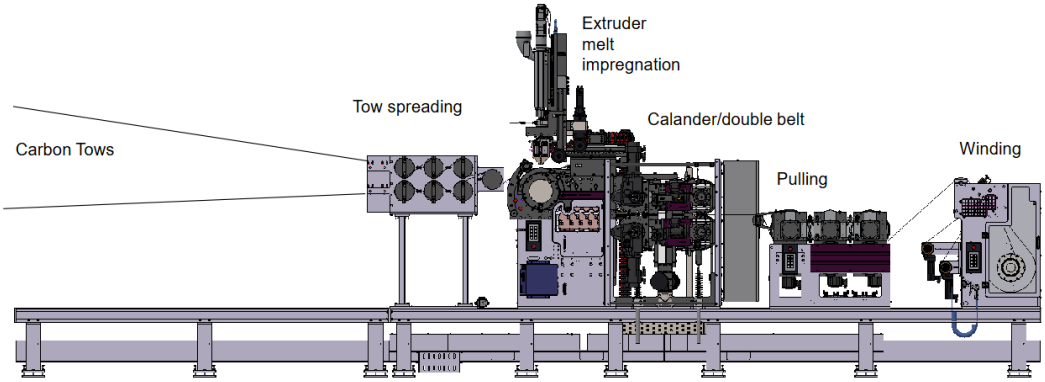

Figure 2.3: TPR in-line production setup at TU Delft

The fibres are impregnated by means of parallel and perpendicular flow to the fibre orientation, with the main perpendicular flow dominating. As a result, the impregnation process can be approximated by the Darcy law in Equation 2.1, which describes the flow of a fluid through a porous medium [6, 25].

$$q = \frac{K}{\eta} = \frac{dp}{dz} \tag{2.1}$$

where q is the flow rate area, K is the permeability of the fibre bundle, η is the dynamic viscosity of the polymer, and dp/dz is the pressure gradient perpendicular to the fibre direction [6]. By integration, the impregnation time Δt can be approximated as in Equation 2.2 (assuming permeability is not dependent of pressure):

$$\Delta t = \frac{\eta * z^2}{2 * K * \Delta p} \tag{2.2}$$

where Δp represents the pressure difference between the start and end of the impregnation path z (perpendicular to the fibre direction).

According to Darcy's law, efficient impregnation requires low matrix viscosity and short flow paths, as well as high pressure gradients and fibre permeability. These factors influence the degree of impregnation and, consequently, the porosity and void content of the resulting UD tape [26].

In addition to porosity, tape quality is characterised by morphological parameters such as fibre volume fraction (FVF), fibre orientation, matrix distribution, fibre tortuosity, crystallinity, and the homogeneity of fibre distribution [27]. Among these, fibre distribution is particularly important, as inhomogeneities can not be corrected in downstream processing and can reduce transverse mechanical properties. Moreover, non-uniform fibre distribution leads to local variations in permeability, directly affecting impregnation quality. Therefore, achieving a homogeneous fibre spread prior to impregnation, typically through upstream spreading using redirection rolls, is essential [28].

Experimental work by *Hopmann et al.* [6] showed that increasing production speed leads to higher porosity due to reduced impregnation time, while increasing die temperature reduces porosity by lowering matrix viscosity. Additionally, fewer redirection rolls result in increased porosity, highlighting the importance of fibre spreading. These findings are consistent with the trends predicted by Darcy's law for melt impregnation processes.

In contrast, water-based dispersion impregnation (DPR) is a continuous fibre process in which dry fibre bundles are passed through a slurry containing thermoplastic powder [**Ramani1995** , 30]. The fibres are coated with the polymer and subsequently heated to consolidate the material. The DPR setup typically includes a creel, slurry bath, drying bridge, and winding system, as shown in Figure 2.4.

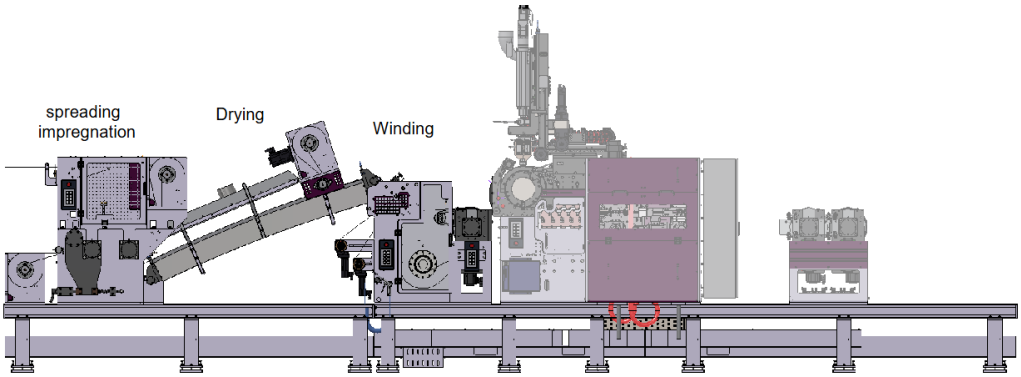

Figure 2.4: DPR in-line production setup at TU Delft

The fibre tows are initially fed from a creel, where each bobbin is equipped with a mechanical braking system. The applied braking force enables precise control of the initial tow tension, defining the mechanical state of the fibres prior to processing. A controlled and constant tension is then maintained during processing to ensure stable tow transport and consistent spreading, which are essential for achieving uniform impregnation.

The fibres are subsequently spread through a set of rollers within the slurry bath to promote uniform distribution of the thermoplastic powder. A closed tolerance orifice (CTO), or alternatively a set of rollers, is then employed to apply pressure to the tow, controlling the amount of resin adhering to the fibres. The impregnated tape is passed over a drying bridge to remove water from the slurry mixture, allowing the powder to coalesce and from a coating around the fibres.

Finally, the tape passes through a dynamic ceramic eye, which regulates the width of the towpreg, before being consolidated and wound onto a bobbin [29].

During the DPR process there are several fundamental variables that control the resin pickup. A higher fibre yield improves resin pickup as smaller fibre tows can be better spread within the slurry bath. The process velocity determines the amount of time that the fibre tow passes through the slurry bath, a longer time spent in the slurry bath improves resin pickup. The size of the CTO is also important, as less resin can pass through a smaller diameter, and therefore wet less the fibres. This effect is also directly proportional to process velocity. Fibre tension is a process parameter that mainly affects fibre distribution and spreading, whereas it has a negligible effect on resin pickup, as the fibre sizing already prevents fibre tows from spreading on the rollers in the bath [29]. Finally, the slurry composition is a clear process parameter that affects resin pickup, as different powder polymers have different material properties. Following the work of *Ramani et al.* [29], an interesting empirical equation that describes the drying step for through-thickness thermal conductivity k of the unidirectional composite can be found in Equation 2.3.

$$k = k_m + \frac{v_f}{\frac{1}{k_f - k_m} + \frac{v_m}{2k_m}} \tag{2.3}$$

where the thermal conductivity of the matrix k_m is a combination of the polymer, water, air, and vapour conductivities and k_m decreases as water evaporates. This approximation of the equivalent matrix thermal conductivity is based on the Maxwell model for conductivity of spherical particles [31].

2.2. Electrical Behaviour of Composites

In this section, a practical outlook on the process of induction welding of TPC components is given in order to better understand the electrical properties of composites.

2.2.1. Induction Welding

Figure 2.5 gives an overview of the induction welding process. The fundamental principle of the induction welding technology is initially discovered by Michael Faraday and later mathematically described by James Clerk Maxwell [8]. During the process, a coil circuit is excited by an alternating voltage, which generates an alternating electric field and electric current in the coil windings. In consequence, an alternating magnetic field is generated around the coil.

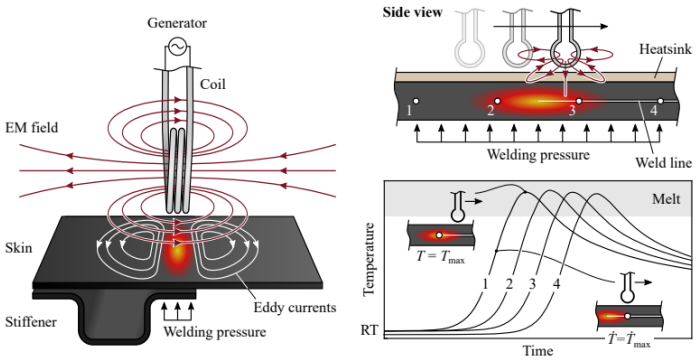

Figure 2.5: Overview of induction welding process [8]

The intensity of the magnetic field weakens with distance from the source. However, it can induce substantial current density in the form of eddy currents when the coil is placed close enough to the TPC assembly, assuming adequate electrical conductivity of the material. The electrical conductivity of TPC highly depends on the presence of carbon fibres, which will be explained in more detail later.

To realize an operational joint at the weld interface that can handle mechanical loading, enough heat must be generated to properly soften the thermoplastic polymer on both faces of the interface. Heating occurs as a result of electrical resistance of the conductive material, leading to a loss of energy by the eddy currents. Moreover, considering the shielding effect and the proximity of the coil, the magnetic field is strongest at the top surface of the assembly. As a consequence, the maximum density of eddy currents, and thus the highest heat generation, is found at the top surface rather than at the interface [8]. To mitigate this effect, during induction welding, the top surface is actively cooled by a heat sink, ensuring enough heat concentration at the weld line instead. A proper consolidation pressure should follow heating, with adequate dwell time and cooling, maintaining adequate intimate contact between the parts [32].

2.2.2. Anisotropic Electrical Properties of CFRP

As mentioned in Section 2.2.1, an important factor of induction heating in carbon fibre-reinforced TPC is the electrical conductivity of the fibres, which allows the material to efficiently induce current from the generated electromagnetic field. Whereas, the matrix polymer is an electrical insulator, hence closed-loop eddy currents can only generate through a network of carbon fibres in contact [8, 33]. Therefore, the eddy current generation is significantly impacted by the specific arrangement of the carbon fibres within a TPC. Hence the two main types of continuous reinforcements, woven fabric-based and UD ply-based, react differently to an applied electromagnetic field. Figure 2.6 depicts a unit cell for both reinforcement type, to show this contrast.

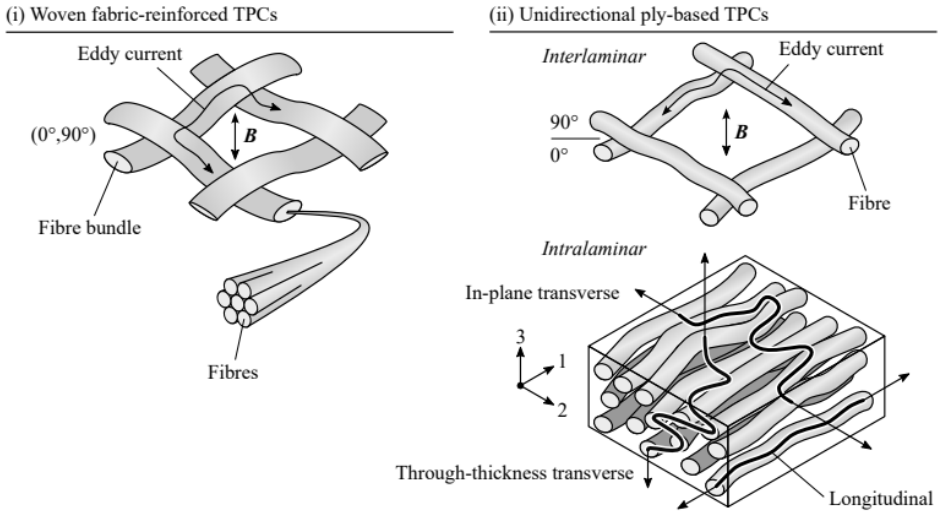

Figure 2.6: Eddy current formation in a (i) woven fabric unit cell and (ii) to a UD ply-based reinforcement [8]

A woven fabric reinforcement, as illustrated in Figure 2.6 (i), is composed of bundles of carbon fibres tightly interconnected, allowing for a high fibre-fibre contact ratio between warp and weft directions of the fabric. This high contact ratio allows for easy flow of current in both in-plane and out-of-plane directions within a single fabric ply, allowing for interlaminar eddy currents to generate with ease, even without the need of multiple stacked layers. For the UD ply, as illustrated in Figure 2.6 (ii), this is not the case, as eddy currents are not well defined. The amount of contacts between fibres is less common, as all the fibres are purposefully oriented in one direction. However, in reality, carbon fibres are not perfectly straight, allowing formation of a network of fibre segments in contact [8]. These contacts are the result of phenomena such as waviness, uneven distribution of components, and fibre tow twisting intrinsic in prepreg manufacturing processes [8]. As a consequence, current paths are not only possible along the longitudinal fibre direction, but also transversely in-plane and through the thickness of the composite.

Nonetheless, to enable transverse current flow, eddy current has to zigzag through the fibres, searching a network of contacts to cover substantial distance. As a consequence of the higher distance and amount of fibre-fibre contacts, eddy currents face notable electrical resistance in both transverse directions, restricting their advancement in these orientations. This behaviour is clearly observed with multiple orders of magnitude difference between the longitudinal electrical conductivity and both transverse orientations [10]. Hence, the electrical conductivity of UD tapes displays a high degree of anisotropy.

2.2.3. Heating Mechanism During Induction Welding

Energy dissipation by eddy currents is described in literature with three well-defined mechanisms: fibre heating, contact heating and dielectric hysteresis [8]. these mechanisms are illustrated in Figure 2.7.

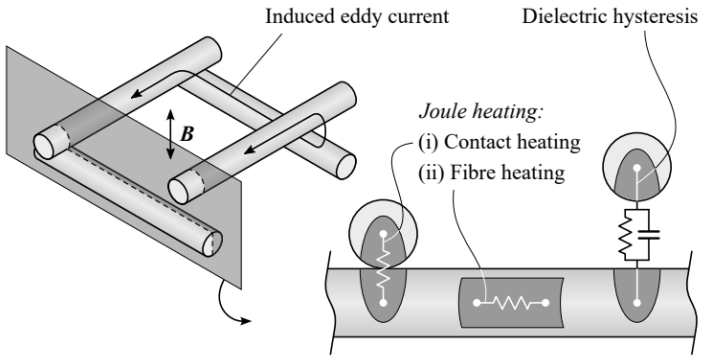

Figure 2.7: Energy dissipation mechanisms by eddy currents [8]

The first mechanism, fibre heating, is a result of longitudinal resistance of carbon fibres, it causes voltage losses that dissipate energy based on Joule's law. *Yarlagadda et al.* [34] considers this mechanism the most dominant when the fibre volume fraction is high and the contact between the fibres is intimate. This observation seems to follow recent numerical investigation of heating mechanisms in [35].

Both intralaminar and interlaminar fibre contacts present a second type of Joule heating. Restriction of electrical current in the thin contact point between fibres, and the resistance of the dividing polymer layer, slim enough to allow for electrons to pass through, delivering the required electrical resistance for substantial heating at the interfaces between plies [36]. Differentiating and identifying these types of Joule heating can potentially be essential for micro-modelling, or characterising interlaminar contact resistance [37]. However, when analysing interlaminar transverse current flow, the eddy currents meet alternately with fibre and contact constriction resistance [8]. Therefore, relative to the point of view, it could be more suitable and relevant to consider both type of Joule heating through a combined description.

The presence of the matrix polymer connects the fibres capacitively and acts as a separating layer which can introduce a third heating mechanism known as dielectric hysteresis [33]. As the electric field alternates, small displacements can occur in chain segments of the polymer molecules, given that the polymer is adequately enough polarisable. The vibrations caused by the changing polarisation can induce dielectric losses directly within the polymer. The magnitude of this mechanism is dependent greatly of factors such as the distance between fibres, the material properties of the polymer and field frequency [33]. Recent work of [10, 38] into modelling of induction heating behaviour of UD ply-based TPC have ignored the importance of dielectric heating while still finding good agreement with their experimental data. As stated by *De Wit et al.* [38], dielectric heating is relevant only at operating frequency higher than the ones associated to induction heating of TPC. Nonetheless, it is important to consider all three mechanisms when characterising electrical conductivity of UD TPC.

The work of *Gouin et al.* [13], while focusing on modelling the induction welding process, measures a range of electrical conductivities of composite adherends via a four wires Ohms measurement. Electrical conductivity is implemented in the FEM model as a temperature-dependent parameter. This is because, as the heating rate increases after an amount of time, it results in a loss of polymer viscosity. As the resin flows, the fibres within the adherends move around and by getting closer, creating more contacts, and therefore increasing the electrical conductivity of the composite. Thus, this higher electrical conductivity increases the heating rate.

2.2.4. Influence of Interface on Electrical Conductivity

Thermal properties of composites require homogeneous and robust adhesion between carbon fibre reinforcements and the polymer matrix, differently, electrical conductivity requires formation of continuous electrical conductive network between the fibres [39, 40, 41, 42, 43]. The mechanism of electrical conductivity can be divided in three main stages, (i) before, (ii) during, and (iii) after the percolation threshold [44, 45]. The three main stages of carbon fibres in a polymer host are illustrated in Figure 2.8 and Figure 2.9.

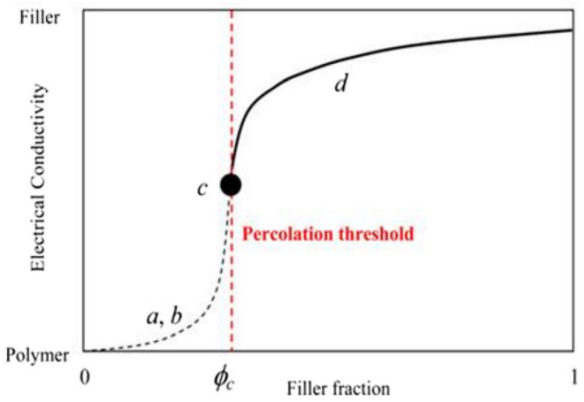

Figure 2.8: Percolation stages in conductive composite [46]

In the first stage, due to the low fibre volume fraction, the electrical conductivity is closest to the conductivity of the polymer. After which, by linearly increasing the amount of fillers in the host and their connections, the electrical conductivity moderately increases by the tunnelling effect, a similar mechanism to dielectric hysteresis discussed in Section 2.2.3, as shown in Figure 2.9b. Nonetheless, at this stage a complete pathway for conduction is not completed yet. By continuously increasing the amount of fibres present in the host, the first conductive pathway is achieved as shown by the red lines in Figure 2.9c. The volume fraction of the fibres at this stage is called percolation threshold [46]. Finally, increasing the fibre volume fraction generates more conductive pathways, which creates a higher conductive network as shown in Figure 2.9d. The percolation threshold is characterised by an acute drop of electrical resistance and it's dependent of size and aspect ratio of the fibres [40, 47], their distribution [48], interfacial interaction, and tortuosity [49].

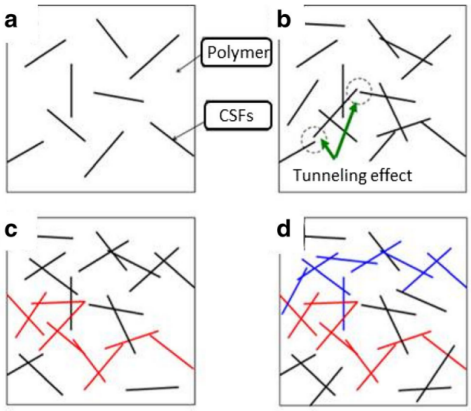

Figure 2.9: Corresponding fibre-fibre contact for percolation threshold [46]

The presence of the thin layer of polymer around the carbon fibres, as discussed in Section 2.1.1, hinders the perfect formation of a continuous network and creates a tunnelling barrier between them [46, 50]. Therefore, the polymer filler has two different features. As mentioned above, it enhances the distribution of the fibres into the host [51]. Continuous conductive network, which improves electrical conductivity, is the result of well-dispersed fibres into the polymer matrix [52]. In contrast, The matrix polymer that interacts with the fibre on its surface also acts as an electrical insulator, which has a negative effect for the electrical conductivity improvement [53]. This is also important when considering induction welding of composites, as between each consolidated ply there is a resin film (thickness 7-10 μm [12]) which acts as an insulator for the generated eddy currents throughout the conductor network.

Overall, the negative effect of electrical insulation of the polymer is outweighed by its positive influence on dispersion of fibres [50]. As shown above, plentiful of studies on composites and their electrical properties prove the importance of the interaction at the polymer-filler interfaces. It is proven that the electrical performance highly depends on the quality of the interfacial interactions [46].

2.3. Electrical Conductivity Characterisation

This section reviews the most commonly used electrical characterisation techniques reported in the literature. It introduces the idealised Rule of Mixtures approach and provides a detailed description of the analytical framework of the six probe method, which is adopted in the methodology of this study. In addition, an overview of eddy current testing is presented as a complementary technique for assessing electrical behaviour.

2.3.1. Rule of Mixtures

The electrical properties of UD TPC are defined by assigning the electrical conductivity along the three principal axes. The average conductivity tensor of an UD tape can be expressed as in [8]

$$\boldsymbol{\sigma} = \begin{bmatrix} \sigma_1 & 0 & 0 \\ 0 & \sigma_2 & 0 \\ 0 & 0 & \sigma_3 \end{bmatrix} \tag{2.4}$$

σ_1 expressed in $[S/m]$ represents the longitudinal electrical conductivity, that follows the unidirectionality of the fibres. σ_2 represents the transverse conductivity, and σ_3 the through-thickness conductivity. In theory, the polymer surrounding the fibres acts as an insulator (hence $\sigma_m \approx 0$), therefore σ_1 is primarily dependent on the fibre conductivity σ_f and the volume fraction v_f, which follow the rule of mixtures (ROM):

$$\sigma_1 = \sigma_f v_f + \sigma_m v_m \approx \sigma_f v_f, \quad (\sigma_m \approx 0) \tag{2.5}$$

This handy relation can not be easily applied to the remaining conductivities, as the fibre distribution in these two remaining principal axes is not as straightforward. Fibre waviness and clustering generate more unpredictable fibre-fibre contacts in the microstructure of the composite. These unorthodox contacts introduce stochastic tortuous paths, which become available for some transverse electrical currents to pass through, as shown in Figure 2.10. As a consequence, σ_2 and σ_3 can not be determined from the intrinsic electrical properties of the constituents, like for σ_1. Rather, they are the outcome of the microstructural topology.

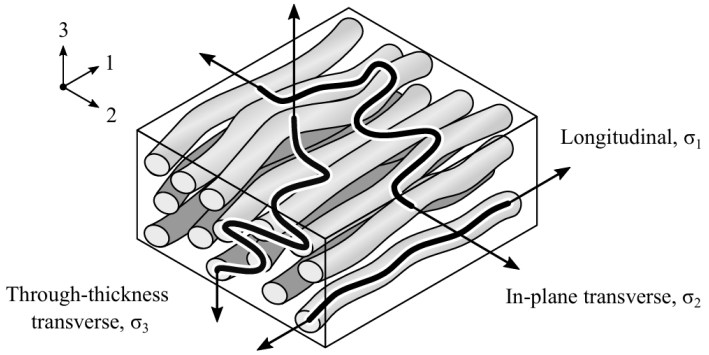

Figure 2.10: Conductivity in three dimensions [8]

The rule of mixtures has been introduced long ago in literature to calculate electrical conductivity of carbon fibre reinforced polymers (CFRP). Its early application can be found in studies that date back as 1981 [9], in which Equation 2.5 was used to determine the longitudinal conductivity σ_1. However, current literature on electrical conductivity of CFRP lacks a general agreement on how to apply the rule of mixtures for longitudinal conductivity. *Buser et al.* [8] included a dataset based on existing literature, as shown in Figure 2.11 and Table 2.1

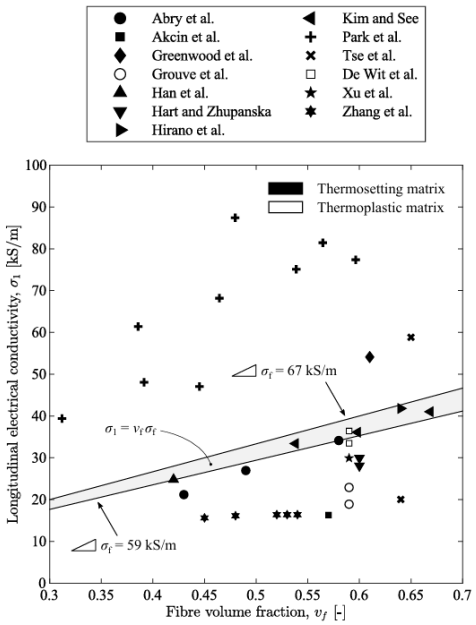

Figure 2.11: Measured data for longitudinal conductivity from literature [8]

As *Buser et al.* [8] correctly mentions, the inconsistency of data found from the literature and depicted in Figure 2.11, proves that measuring σ_1 is a complex task, and requires further investigation on different approaches. It is also important to pay attention when comparing data from different studies. As the material properties of carbon fibres highly depend on their manufacturing process and objective application. For example, the study of *Šafářová and Grégr* [54] found considerable difference in σ_f between carbon fibres manufactured with PAN or pitch. Based on literature, pitch-based carbon fibres exhibit electrical conductivities up to 900 kS/m [55], which is an order of magnitude higher than PAN-based carbon fibres (Table 2.1). Hence, Figure 2.11 and Table 2.1 only include data from papers which explicitly communicate that the carbon fibres are PAN-based and what their v_f is. This is done to minimize possible differences in sample preparation between found literature results.

Table 2.1: Overview of literature data on longitudinal electrical conductivity of pan fibre-based cfrps with a ud lay-up. In this listing, studies were included solely if there was traceable information on the fibre type, fibre volume fraction, and measured longitudinal electrical conductivity σ_1.

Author	Year	Method	v_f [-]	σ_1 [kS/m]	σ_3 [S/m]
Abry et al. [56]	1999	Two-probe	0.43–0.58	21.2–34.1	–
Akcin et al. [57]	2016	Two-probe	0.57[a]	24.8	–
Greenwood et al. [58]	1975	Two-probe	0.61	54.1	–
Grouve et al. [10]	2021	Four-probe	0.59	18.9–22.9	0.103
Han et al. [59]	2022	Two-probe	0.42	24.8	0.86
Hart and Zhupanska [60]	2020	Six-probe	0.60	28.1–29.9	0.287
Hirano et al. [61]	2016	Four-probe	0.64	41.8	0.021
Kim and See [62]	1990	Unspecified	0.54–0.71	33.4–44.3	–
Park et al. [63]	2006	Six-probe	0.31–0.60	39.4–87.4	–
Tse et al. [9]	1981	Four-probe	0.64–0.65	20.0–58.8	0.5
De Wit et al. [38]	2023	Two-probe	0.59	33.5–36.4	0.055
Xu et al. [37]	2018	Two-probe	0.59[b]	29.9	1.1
Zhang et al. [64]	2020	Two-probe[d]	0.45–0.54	15.6–16.4[c]	–

[a] Fibre volume fraction retrieved from another study [24].
[b] An educated guess by the authors based on a reported resin content of 33%.
[c] Conflicting orders of magnitude are reported throughout this study. The authors have adopted the higher electrical conductivity values in the literature survey.

Table 2.2: Electrical conductivities characteristic for commercially available pan-based carbon fibres as reported by the manufacturers.

Fibre	σ_f [kS/m]	Ref.
Hexcel AS4	59	[65]
Hexcel IM7	67	[66]
Toray T700S	63	[67]
Toray T700G	67	[68]

Figure 2.11 shows a grey area, which illustrates the expected electrical conductivity range of PAN-based CFRP following the rule of mixtures. Table 2.2 gives the conductivity values typically used by manufacturers of PAN-based fibres, which are directly used to determine the upper and lower limit of the grey area in Figure 2.11. It is important to mention, that in [8] the data of Hexcel is verified, and appears to be a result of testing fibres in tow form with a four-probe measurement with direct current (DC).

Whilst values found by *Han et al.* [59], *Hirano et al.* [61], and *Kim and See* [62] closely match the visualised ROM, other observed values from the remaining studies clearly disagree with it. In fact, this disagreement shows the difficulty in correctly assessing longitudinal electrical conductivity. This lack of consistency between papers underlies the uncertain state of ROM validation. Moreover, most of the studies shown in Figure 2.11 analysed an epoxy-based resin CFRP, and only two studies focused on thermoplastic polymer as matrix. This leaves even more gaps in knowledge on characterising electrical conductivity in thermoplastic-based UD tapes.

2.3.2. Methods of Characterisation of Electrical Conductivity in CFRP Composites

Various methods exist to determine the electrical conductivity of anisotropic composites. These methods can be grouped in uniform and non-uniform current density methods. Figure 2.12 gives an illustrative overview, which shows the basic principles of these measurement methods.

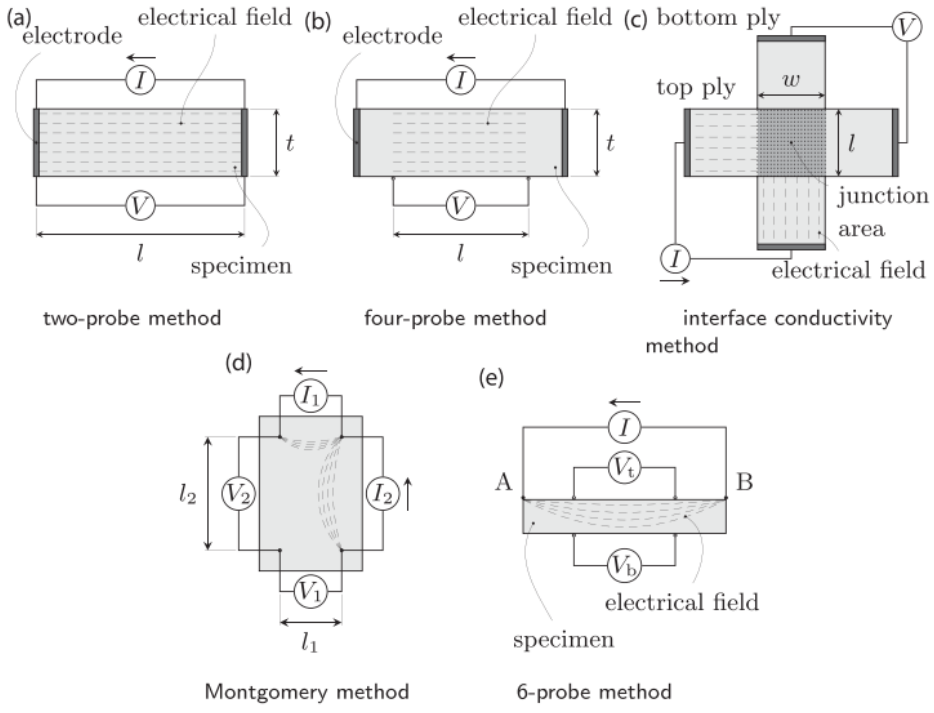

Figure 2.12: Typical electrical conductivity measurement methods [69]

In the majority of studies for characterisation of electrical conductivity of TPC, a uniform current density method is used. The most known uniform current density method is the two probe method as shown in Figure 2.12.a. *Schulte et al., Kim et al, and Todoroki et al.* [70, 36, 71] applied a two-probe measurement in their study. With this approach, a direct current I is applied by electrodes installed at two opposing parallel edges of the specimen. The objective is to achieve a uniform distribution of the current density across the specimen's cross-section, as described with dashed lines in Figure 2.12.a. The voltage drop V that is measured between the electrodes, along the length l, is required to calculate the conductivity by using Ohm's law,

$$\sigma = \frac{I}{V}\frac{wt}{l} \tag{2.6}$$

where w is the width of the specimen and t its thickness. Consequently, a resistance $(R = V/I)$ can be measured, which is a combination of resistance in the electrode, the contact resistance between specimen and electrode, and the resistance of the specimen. Typically, the resistance of the electrode is neglected, as its resistance is of higher magnitude than the specimen's resistance. Moreover, the resistance between the sample and the electrode must be minimized to ensure a proper current introduction within the specimen's conductor. A uniform current density into the conductor is also dependent on the quality of intimate contact between electrode and specimen. This can be achieved with laborious contact surface pretreatment and ensuring enough clamping force between electrode and specimen.

The four probe method, shown in Figure 2.12.b., is used in [72, 73, 74, 11] to characterise longitudinal electrical conductivity. Comparable to the two-probe approach, a direct current I is applied by electrodes placed in two opposite faces of the specimen. Two extra probes placed in between the two electrodes are used to measure the voltage drop. Both a point contact [11] and a line contact [72] can be used as measurement approach of resistivity. The additional probes eliminate the electrode resistance. The current distribution is expected to be distributed uniformly between the voltage measurement probes, resulting in a method less affected by the contact quality between the electrodes and the specimen, therefore also less laborious compared to the surface preparations required for the two probe method. The voltage drop V that is measured over the distance l, is required to calculate the conductivity by using Ohm's law, as in Equation 2.6. *Wang et al.* [75] and *Guerrero et al.* [76] analysed the electrical conductivity of the interface within each ply of a composite laminate. Their method, shown in Figure 2.12.c, assumes a uniform distribution of current along the junction area. The conductivity of the interface's contact, σ_c, is found by,

$$\sigma_c = \frac{I}{V}\frac{1}{wl} \tag{2.7}$$

For non-uniform current density methods a specific distribution of the current within the specimen must be designed. A recognised non-uniform current approach to calculate conductivity in anisotropic materials is the Montgomery method [77], and is shown in Figure 2.12.d. Specific voltage measurements between the probes are needed to obtain the anisotropic electrical conductivities. This approach, is only fitting for characterising the in-plane anisotropic conductivities of composites.

In more recent studies, the six probe measurement method is analysed by *Hart and Zhupanska* [60], as shown in Figure 2.12.e. This method is specifically applied to characterise electrical conductivity in uni-directional composites. This method therefore is specifically applied to characterise the electrical behaviour of UD TPC tapes in this research.

2.3.3. The Six probe Voltage Measurement Method

In this section, the six probe measurement method is described and analytically defined to derive the anisotropic electrical conductivities in UD TPC tapes.

Relevance of Electrical Characterisation

The six probe method involves applying a direct electrical current to the top surface of the UD tape between points A and B, along the distance L, as illustrated in Figure 2.13.

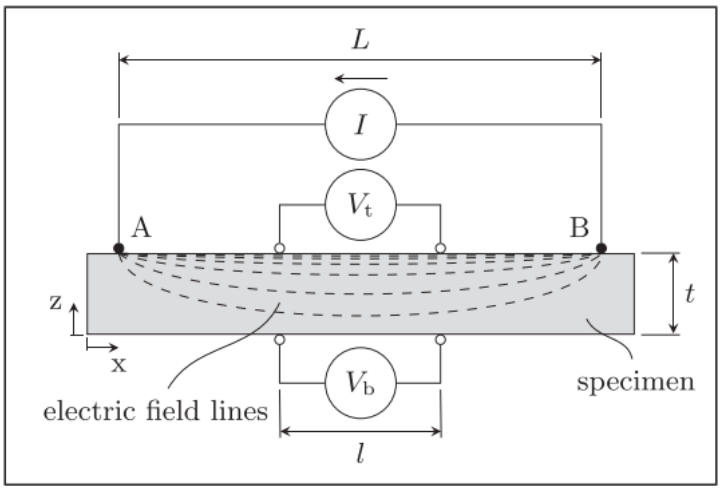

Figure 2.13: Cross section of the UD tape undergoing a six-probe measurement [69]

The application of current I generates a non-uniform electrical field density within the tape, as indicated by the dashed lines in Figure 2.13. The voltage drops measured over the distance l at the top surface (V_t) and the bottom surface (V_b) are not equal [69]. The distribution of the electrical field depends on distance L, tape thickness, in-plane specific electrical conductivity, and out-of-plane electrical specific conductivity. For the method described and the UD material in question, it is assumed that the electrical current distributes evenly across the tape's width due to the fibre bundles' orientation [69]. The six probe method is considered the most practical approach for achieving reliable contact between the sample and the probe. It does not require surface pretreatment of the tapes, as the line contact spans the entire sample, ensuring transverse homogeneity of the current across the tape's width. More importantly, a single experiment can simultaneously determine both the in-plane and out-of-plane electrical conductivity of composites.

Analytical Model Description

As discussed in Section 2.3.3, the six probe measurement method has several advantages. However, determining anisotropic electrical conductivity is more complex compared to methods using a uniform current, such as the two probe method. Previous studies by *Busch et al. and Hart and Zhupanska [78, 60]* have developed an analytical approximation and a numerical method, which are illustrated in this section. The analytical approximation, originally developed by *Busch et al.* for measuring electrical conductivity in highly anisotropic single crystals, can also be applied to UD tapes on a macroscopic scale. The analytical approximation is derived by solving the differential equation that describes the two-dimensional potential distribution $V(x, z)$ in the tape sample during the experiment, as shown in Equation 2.8.

$$\frac{1}{\rho_x}\frac{\partial^2 V}{\partial x^2} + \frac{1}{\rho_z}\frac{\partial^2 V}{\partial z^2} = 0 \tag{2.8}$$

A proper solution is given by the expansion in Equation 2.9:

$$V(x,z) = \sum_{n=1,3,5,\ldots} V_n \sin\left(\frac{n\pi x}{L}\right) \cosh\left(\sqrt{\frac{\rho z}{\rho x}}\frac{n\pi z}{L}\right) \tag{2.9}$$

where ρ represents the electrical resistivity, the reciprocal of electrical conductivity σ. The x and z indicate the direction of the resistivity, as shown in Figure.2.13. *Busch et al.* derived an approximation of $V(x,z)$ by considering the lowest $n=1$ term, giving:

$$V(x,z) \approx -\frac{I}{w}\sqrt{\rho_z \rho_x}\frac{\sin\left(\frac{\pi x}{L}\right)}{\sinh\left(\frac{\pi t}{L}\sqrt{\rho_z \rho_x}\right)}\cosh\left(\frac{\pi z}{L}\sqrt{\frac{\rho_z}{\rho_x}}\right) \tag{2.10}$$

By using the measured voltage V_t and V_b in the known locations, the ratio $\frac{V_t}{V_b}$ can be obtained,

$$\sqrt{\frac{\rho_z}{\rho_x}} \approx \frac{L}{\pi t}\cosh^{-1}\left(\frac{V_t}{V_b}\right) \tag{2.11}$$

and from V_t,

$$\sqrt{\rho_z \rho_x} \approx \frac{V_t w}{2I\sin\left(\frac{\pi l}{2L}\right)}\tanh\left(\frac{\pi t}{L}\sqrt{\frac{\rho_z}{\rho_x}}\right) \tag{2.12}$$

Multiplying the result of Equation 2.12 by the result of Equation 2.11 gives ρ_z; dividing Equation 2.12 by the result of Equation 2.11 gives ρ_x. If the ratio of ρ_z to ρ_x is significantly large, as typically for TPC composites, then by applying Taylor series expansions in Equation 2.12, a further approximation can be derived, giving:

$$\sqrt{\rho_z \rho_x} \approx \frac{V_t w L}{I \pi L} \tag{2.13}$$

A particularity of Equation 2.13 is that the expression of thickness has been eliminated with Equation 2.13, suggesting that the electric current is confined to a portion of the tape's cross-sectional area, rather that uniformly occupying the entire area. *Busch et al.* [78] found that in electrically anisotropic materials, such as UD TPC, the penetration of current density j_x is exponentially damped and limited to a thin surface layer. The current density distribution through the thickness can be expressed as [60]:

$$j_x(z) \approx j_x^0 e^{-\frac{|z|}{z_{\text{eff}}}} \tag{2.14}$$

Here z_{eff} represents the effective penetration depth of current.

$$z_{\text{eff}} = \frac{L}{\pi}\sqrt{\frac{\rho_z}{\rho_x}} \tag{2.15}$$

The penetration depth of the current is influenced by the degree of electrical anisotropy of the material. As illustrated in Figure 2.14 , the distribution of current across the thickness of an electrically anisotropic material can be described as follows: Figure 2.14a shows the actual distribution, where electric current density is exponentially damped and mainly confined within the region defined by the effective thickness z_{eff}. Figure 2.14b provides an approximate representation of this distribution.

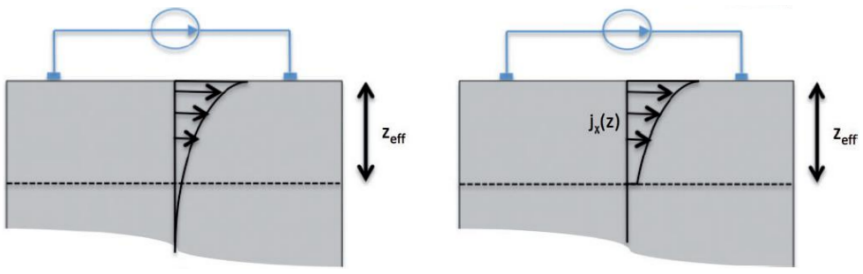

(a) Current density distribution through thickness **(b)** Approximation of current density

Figure 2.14: Real and approximated current density through anisotropic materials [60, 79]

Multiplying Equation 2.15 and Equation 2.13 give an approximate value for the in-plane electrical resistivity ρ_x, which can be calculated as follows:

$$\rho_x \approx \frac{V_t w z_{\text{eff}}}{Il} \approx \frac{R_t w z_{\text{eff}}}{l} \tag{2.16}$$

It should be noted that for composites with a high resistivity ratio $(\frac{\rho_z}{\rho_x})$, the effective penetration depth of the current z_{eff} may exceed the physical thickness of the sample. To address this, *Hart and Zhupanska* [60] suggest that the current penetration depth should be expressed as the minimum value between the sample thickness t and z_{eff}.

$$t_{\text{eff}} = min(t, z_{\text{eff}}) \tag{2.17}$$

The effective thickness through which the current can penetrate the composite material is indicated by t_{eff}. The approximate expression for the in-plane electrical resistivity ρ_x is:

$$\rho_x \approx \frac{R_t w t_{\text{eff}}}{l} \tag{2.18}$$

By substituting the calculated in-plane resistivity ρ_x into Equation 2.13, the out-of-plane electrical resistivity ρ_z can be determined as follows:

$$\rho_z \approx (\frac{V_t w L}{I \pi l})^2 \frac{1}{\rho_x} \tag{2.19}$$

Given the dimensions of the UD tape, the applied current, and the measured voltage drops at the top (V_t) and bottom (V_b) of the tape, Equation 2.18 and Equation 2.19 yield approximate values for in-plane (ρ_x) and out-of-plane (ρ_z) resistivities of the UD TPC. The electrical conductivity can consequently be calculated using the following relationship:

$$\sigma = \frac{1}{\rho} \tag{2.20}$$

Effect of the Geometry of the Specimen on the Electrical Conductivity

In the previous work of [69], *Van der Berg et al.* discussed the influence of specimen parameters such as width, and thickness of a composite on their voltage drop differential based on the a six probe experiment. Figure 2.15 shows this effect.

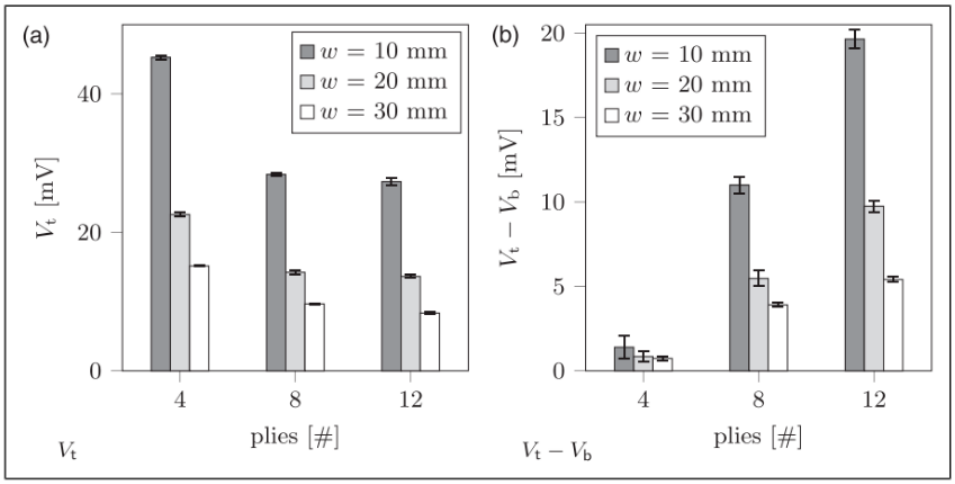

Figure 2.15: Effect of geometry on voltage drop in specimen during the six probe measurement [69]

Van der Berg et al. [69] showed that the longitudinal conductivity σ_x is independent of both the number of plies consolidated in the laminate. In contrast, the through thickness conductivity σ_z is affected by the laminate thickness. This behaviour is illustrated in Figure 2.15, where an increase in the number of plies, and thus specimen thickness, leads to a larger voltage drop differential between the top and bottom surfaces. This indicates a decrease of through thickness conductivity with increasing thickness, consistent with the higher proportion of insulating matrix material in thicker laminates.

This also suggests that, for thin materials such as unidirectional thermoplastic composite tapes, the voltage drop measured during six probe experiments may be very small. As a result, the extraction of reliable through thickness conductivity values can be challenging due to limited measurable potential differences.

Furthermore, it can be observed that for this materials, variations in specimen width have negligible effect on the measured voltage drop differential.

Reliability of Characterisation

Van der Berg et al. [69] compared the numerically calculated σ_x with the values obtained using the approach by *Busch et al.* [78] and the σ_x with the values obtained from the two probe measurement. The overview showed high consistency with the σ_x between each method. Differently, the overview of σ_z resulted in a discrepancy between the two probe measurement method and the one of *Busch et al.* It is observed that the σ_z values found with the *Busch et al.* method converge fairly quickly compared to other methods, especially for the thinner 4-ply specimens. It is believed that the constrained number of terms $(n = 1)$ assumed in Equation 2.9 is inadequate to accurately describe the potential distribution $V(x, z)$ when the ratio $\frac{V_t}{V_b}$ is small, which is the case for low ply numbers or single UD tapes.

Nonetheless, compared to the two probe method, the six probe measurement does not require tests on specimens with different thicknesses to characterise the anisotropic electrical behaviour, hence it is a faster approach to analytically approximate the though-thickness conductivity [69]. Moreover, compared to other methods such as two probe, surface treatment of the specimen is not required while still ensuring proper electrical current introduction, resulting in a less laborious setup.

2.3.4. Eddy Current Testing

Another technique used to characterise electrical behaviour of conductive carbon fibres is the eddy current testing (ECT) method, in which via an applied drive current an alternating magnetic field is generated to induce eddy currents within the conductor. This technique is utilized as a non-destructive test (NDT) such as defect detection, conductivity characterisation, thickness measurements, and in induction welding as explained in section 2.2.1. For NDT approaches the eddy currents are induced by a driver coil, whereas a pick-up coil at a different location can act as a magnetic field sensor and detect a change in local electrical conductivity [80] and give information about the conductor properties. This technique evolved from the use of single-frequency excitation ECT [81], to multiple-frequency ECT [82], and swept-frequency ECT [83, 84], to the most updated pulsed/transient ECT [85]. This is important, as using a single frequency hinders the results, the sensitivity is dependent on the skin depth effect for surface or subsurface characterisation. A swept-frequency excitation is needed to obtain information and conductivity parameters at different depth of the sample [86]. A Tx-Rx ECT system is composed of an excitation circuit, a coil as receiver (Rx) and a transmitter (Tx). Parallel or series connection of elements like inductors and capacitors ensure the resonance property is achieved. Current flows through each element of the circuit and voltage drop can be found via Kirchoff's laws. Kirchoff's voltage law (KVL) states that the total voltage sum within a closed loop in a circuit is zero. For a circuit with a three-loops coil the KVL is described in Equation 2.21.

$$\begin{pmatrix} V \\ 0 \\ 0 \end{pmatrix} = \begin{pmatrix} Z_1 & -j\omega M_{12} & -j\omega M_{1s} \\ -j\omega M_{12} & Z_2 & j\omega M_{2s} \\ -j\omega M_{1s} & j\omega M_{2s} & Z_s \end{pmatrix} \begin{pmatrix} I_1 \\ I_2 \\ I_s \end{pmatrix} \tag{2.21}$$

where M_{12}, M_{1s}, M_{2s} are inductances for the transmitter and receiver samples, and their equivalent impedances Z_1, Z_2, Z_s are described as:

$$Z_1 = r_s + (\frac{1}{j\omega C_1})//R_1 + j\omega L_1 \tag{2.22}$$

$$Z_2 = (R_2 + j\omega L_2) + (\frac{1}{j\omega C_2})//R_L \tag{2.23}$$

$$Z_s = R_s + j\omega L_s \tag{2.24}$$

Equation 2.21 is used to determine the resistance and inductance in every resonant circuit as a function of the sample and coil parameters. Self-inductance and self-resistance are the most predominant coil parameters, which are highly dependant on the sample conductivity, permeability and geometry due to eddy current interference. This is the main approach to sense defects or anisotropic features in a sample, as such different sample's feature affect the voltage and current responses. The difference between the input and output voltages at the resonance point can provide valuable information about the electrical conductivity and magnetic permeability of the sample, which can be used to characterise the anisotropic electrical behaviour of UD TPC. The performance of such setup is measured by the forward voltage gain, which can be explained using a parameter's scattering transmission coefficient, S_{21}, as shown in Equation 2.25 [87, 88, 89].

$$S_{21} = 2\frac{V_L(\omega)}{V(\omega)}\sqrt{\frac{r_s}{R_L}} \tag{2.25}$$

$$\vec{J}_d = \vec{J}_0 e^{-\frac{d}{\delta}} \tag{2.26}$$

Where:
$\vec{J}_d =$ Current density at a distance d from the surface of the HE (A/m^2)
$\vec{J}_0 =$ Current density at the surface of the HE (A/m^2)

The penetration depth can be calculated from:

$$\delta = \sqrt{\frac{\rho_e}{\pi f \mu}} \tag{2.27}$$

The reviewed electrical characterisation techniques provide a comprehensive framework for analysing the electrical behaviour of UD TPC tapes. While the six probe method enables quantitative evaluation of electrical conductivity, it relies on idealised assumptions that may not fully capture the inherent microstructural variability of composite materials.

In this context, eddy current testing offers a valuable complementary approach, providing spatially resolved insight into local variations in electrical response and current pathway distribution. When combined with techniques such as infrared thermography, it enables a more complete interpretation of how microstructural features affect electrical behaviour.

Based on this literature review, the methodology of this study integrates these techniques, using six probe method for quantitative conductivity evaluation, while eddy current testing and infrared thermography are employed to support the interpretation of results relation to microstructure and manufacturing route.

3

Methodology

This chapter discusses the experimental and analytical methodology implemented to characterise the electrical conductivity behaviour of UD TPC tapes. First, the materials used in this research and the sample preparation are described. Subsequently, the electrical investigation techniques employed in this study are introduced, including the six probes method for in-plane and out-of-plane conductivity measurements an infrared thermography technique and an eddy current sensing approach to assess visual variations in electrical behaviour. In order to compare the measured electrical properties to the material architecture, microstructural characterisation using laser optical microscopy is also presented, alongside with the image analysis procedures used to quantify relevant features. Finally, an outlook on the applications of the measured electrical behaviour for induction welding is provided via a combination of finite element modelling and validating experimental trials.

3.1. Material Preparation

UD TPC are used in this study to investigate the electrical conductivity behaviour of tapes. The materials analysed consist of low melting polyaryletherketone (LM-PAEK) and polyetheretherketone (PEEK) matrices reinforced with carbon fibres. These material are selected due to their increasing use in high performance structural applications and their relevance of automated composite manufacturing processes as described in Section 2.1.3.

For this research, UD tapes are obtained from two different sources. A commercially available prepreg tape supplied by Toray (Cetex® TC1225) is used as a reference material. In addition, several tapes are manufactured in-house using the tapeline facility at TU Delft, allowing different reinforcement configurations and processing routes to be investigated. The in-house manufactured tapes are produced using VICTREX™700 series PEEK powered-based slurry and carbon fibre rovings.

To investigate the influence of manufacturing processes and fibre architecture on electrical behaviour, four different UD tape materials were selected. These materials represent different processing routes and reinforcement configurations:

- a commercial Toray Cetex® TC1225 T700 LM-PAEK prepreg tape,
- a DPR-based PEEK tape reinforced with Torayca™T800SC-24K-10E fibres,
- a TPR-based PEEK tape reinforced with Torayca™T800SC-24K-10E fibres,
- a DPR-based Hybrid tape combining Torayca™T800 and M40J carbon fibres.

The fibre and material properties of the investigated reinforcements are summarised in Tables 3.1, and 3.2. By analysing materials produced using different processing routes and fibre types, it becomes possible to evaluate how microstructural features and manufacturing variability influence the electrical conductivity behaviour of UD TPC tapes.

Table 3.1: Torayca™-M40J fibre and functional properties [90]

PROPERTY	UNIT	FILAMENT COUNT	NOMINAL VALUE	METHOD
Tensile Strength	MPa (kgf/mm²)	-	4400 (450)	TY-QA-002
Tensile Modulus	GPa (10³kgf/mm²)	-	377 (38.5)	TY-QA-002
Elongation	%	-	1.2	TY-QA-002
Density	g/cm³	-	1.75	TY-QA-003
Yield	g/1000m	6 000 12 000	225 450	TY-QA-004
Specific Heat	Cal/g.°C	-	0.17	-
Electric Resistivity	x 10^{-3} Ω.cm	-	1.0	-
CTE	$\alpha 10^{-6}/°$C	-	-0.83	-
Thermal Conductivity	Cal/cm.S.°C	-	0.164	-
Filament Diameter	μm	-	5	-
Cross Sectional Area	mm²	6 000 12 000	0.13 0.25	-

Table 3.2: Torayca™-T800s fibre and functional properties [91]

PROPERTY	ENGLISH	METRIC	METHOD
Tensile Strength	853 ksi	5,880 MPa	TY-030B-01
Tensile Modulus	42.7 Msi	294 GPa	TY-030B-01
Strain at Failure	-	2.0%	TY-030B-01
Density	-	1.80 g/cm³	TY-030B-02
Filament Diameter	-	5 μm	-
Yield	12K	515 g/1000m	TY-030B-03
	24K	1,030 g/1000m	TY-030B-03
CTE	-	-0.4 $\alpha \cdot 10^{-6}/°$C	-
Specific Heat	-	0.740 J/g $\cdot$ °C	-
Thermal Conductivity	-	0.113 J/cm $\cdot$ s $\cdot$ °C	-
Electric Resistivity	-	1.3×10^{-3} $\Omega\cdot$ cm	-
Chemical Composition: Carbon	-	$>$96%	-
Na + K	-	$<$50 ppm	-

3.1.1. Tape Preparation and Specimen Geometry

Prior to electrical characterisation, the UD tapes are cut and prepared to obtain specimens with geometries compatible with the experimental setups described in Section 3.2. Ensuring consistent specimen dimensions is important in order to minimise experimental variability and maintain repeatable electrical measurements.

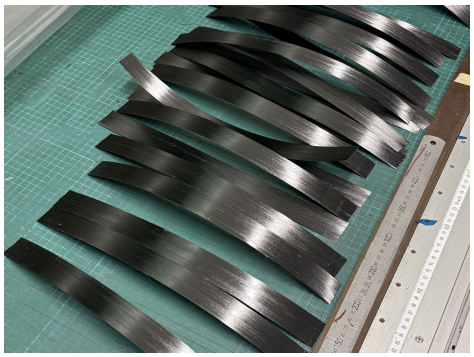

Figure 3.1: UD TPC tape preparation

For the six probe electrical conductivity measurements, as shown in Figure 3.1, the tapes are prepared with a length of $200\ mm$, ensuring that the specimen could be fully positioned between the outer current electrodes of the setup. A minimum contact length of $150\ mm$ is required for proper electrical injection, as that is the distance between the outer electrodes. Therefore, the additional length ensures that the specimen edges remain sufficiently far from the electrodes, reducing potential edge effects during the measurements.

The tape width is selected based on the objectives of the electrical characterisation. Since the primary focus of this work is the longitudinal and through thickness electrical behaviour of UD TPC tapes, rather than transverse conductivity, relatively narrow specimens are preferred. This approach helps minimise the contribution of transverse current pathways and reduces potential noise associated with lateral current distribution within the tape.

The selection of a $30\ mm$ width is further supported by the findings of *Van der Berg et al.* of Section 2.3.3, who investigated specimens with width of 10, 20, and $30\ mm$ and demonstrated that the longitudinal conductivity σ_x is independent of specimen width. In contrast, their results showed that the voltage drop associated with through thickness measurements increases only marginally with width for thin UD laminates, indicating that width has a limited influence on the measured electrical response in this configuration.

Within this context, a width of $30\ mm$ is chosen as a compromise between maintaining a narrow geometry and ensuring sufficient measurable voltage drop for reliable through thickness conductivity estimation. Finally, the selected width remains well within the operational limits of the six probe fixture ($100\ mm$), ensuring proper electrode contact and measurement reliability.

Once the specimens are prepared and their geometrical characteristics defined, they are ready for electrical characterisation. The prepared UD tapes are subsequently analysed using the experimental techniques described in the following section, which aim to quantify their electrical behaviour. Additional illustrations of the tape preparation procedure are provided in Appendix A.

3.1.2. 8 Layer UD TPC Laminate Preparation

This study primarily focuses on the electrical characterisation of UD TPC tapes, with particular emphasis on their microstructural features and associated manufacturing routes. Processes such as TPR and DPR are directly investigated to understand how in-line tape manufacturing influences fibre architecture, electrical conductivity, and current pathway formation.

To extend this analysis beyond individual tapes, an 8 layer UD laminate is manufactured from Toray TC 1225 UD TPC tape. This approach enables the evaluation of how subsequent processing steps, such as stacking and consolidation, influence the resulting microstructure and electrical performance.

The laminate is produced by stacking eight UD tapes in a unidirectional configuration, followed by consolidation in a hot press under controlled temperature and pressure conditions. The objective of this process is to replicate a simplified composite manufacturing step and assess its impact on fibre distribution, interfacial characteristics, and overall electrical behaviour.

The manufactured laminate is subsequently characterised using the six probe method to evaluate its electrical conductivity, and infrared thermography is employed to analyse current pathway formation and distribution. The detailed manufacturing procedure for the laminate is provided in Appendix A.

3.2. Electrical Characterisation

Electrical characterisation is performed using three complementary techniques. A six probe method is introduced to measure the in and out of plane electrical conductivity of UD tapes, while an eddy current sensing approach is implemented to investigate local variations in electrical behaviour, and an infrared thermography technique to visualise current injection. The methodology for each technique is described in the following sections.

3.2.1. Six-probes Electrical Conductivity Test

Measurement Principle

The six probe electrical conductivity measurement implemented in this work is based on the method proposed by *Busch et al.* [78], described in Section 2.3.3. In this method, a direct electrical current is injected into a UD tape using a set of six probes arranged along the specimen surface. The resulting voltage drops are measured at different probe locations on the upper and lower surfaces of the sample. By comparing these voltage measurements, a voltage differential ratio can be determined, which provides information on the anisotropic electrical behaviour of the material, including both the longitudinal conductivity along the fibre direction and the through thickness conductivity of the tape. A schematic representation of the six probe configuration used in this study is shown in Figure 3.2.

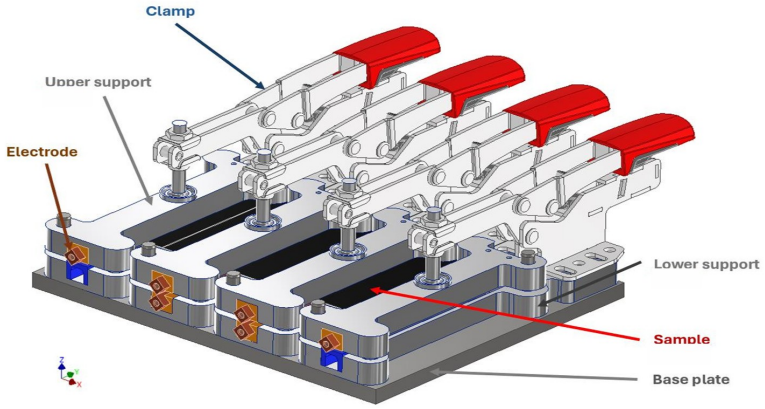

Figure 3.2: Six probes setup schematic representation [79]

UD TPC exhibit strong anisotropic electrical behaviour due to the orientation and distribution of the conductive fibres within the insulating polymer matrix. As described in Section 2.2.2, electrical conduction occurs predominantly along the fibre direction, where continuous fibres provide highly conductive pathways. In contrast, electrical transport in the transverse and through thickness directions is significantly lower, as current must pass through fibre-fibre contact points or jumping across the polymer matrix separating adjacent fibres.

As a result of this anisotropic nature, the electrical response measured across the UD tape depends on the direction of current flow and the available conductive pathways within the material. When an electrical current is injected through the six probe setup, the current preferentially passes via the fibre direction while only limited current flows through the thickness of the tape. The voltage differential measured at the probe locations therefore reflect the combined effect of longitudinal fibre conduction and transverse resistive pathways within the composite.

The electrical behaviour of the UD tape can be represented using a respective resistive network, as illustrated in Figure 3.3.

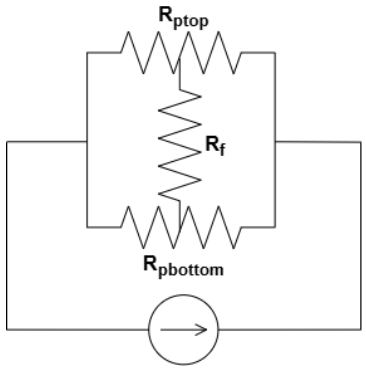

Figure 3.3: Six probes DC electrical circuit diagram

In this representation, the conductive carbon fibres embedded within the polymer matrix form the primary conductive pathway inside the material, represented by R_f. In contrast, the outer surfaces of the UD tape are dominated by polymer matrix, which exhibits significantly higher electrical resistance. These surfaces are therefore represented by the resistances $R_{p,top}$ and $R_{p,bottom}$, corresponding to the top and bottom surfaces of the tape respectively.

The equivalent circuit illustrates the principle behind the voltage measurements performed in the six probe setup. As shown in Figure 3.3, the polymer-dominated regions at the top and bottom surfaces of the tape introduce resistive pathways, while the internal fibre network forms the primary conductive path. During the measurement, the voltage probes placed on the top and bottom surface of the tape capture voltage drops associated to these regions. The simultaneous acquisition of top and bottom voltage signals reflects how the injected current distributes between the thickness of the material. By evaluating the ratio between measured voltage drops, an approximation of the relative contribution of through-thickness conductivity can be calculated, providing an indirect estimate of the effective through thickness conductivity of the UD tape.

Experimental Setup

The six probe electrical conductivity measurements are performed using a custom-built setup based on the work of *Y. Buser et al.* [8], designed to allow controlled current injection and voltage measurements along the surface of UD TPC tapes. A schematic representation of the measurement configuration is shown in Figure 3.4.

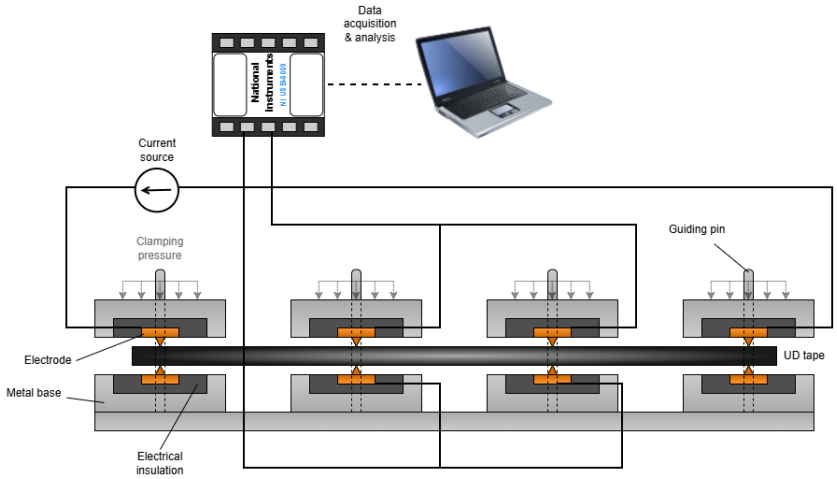

Figure 3.4: Six probes schematic representation of measurement configuration

The setup consists of six cylindrical probes placed linearly along the surface of the specimen. The outer probes are used to inject a direct electrical current through the tape, while the intermediate probes mea-

sure the resulting voltage drops across the material. The probes are positioned on a non-conductive support structure to ensure electrical isolation and stable tape contact during measurements. The probe spacing is chosen to ensure a sufficient distance between current injection points and voltage acquiring locations, thereby reducing the influence of contact resistance on the measured signal.

Electrical current is supplied using a controlled current source, while the voltage signals are acquired using a data acquisition (DAQ) system connected to the intermediate sensing probes. The wiring configurations follows the equivalent approach described in Section 3.2.1, allowing the voltage differential between top and bottom intermediate probes to be recorded simultaneously. The acquired signals are transmitted to a computer where they are processed using a custom Python-based data acquisition and analysis application.

To ensure consistent electrical contact, the probes are clamped onto the tape with constant pressure that maintains constant probe spacing and contact during testing. The entire setup is designed to allow rapid positioning of specimens while maintaining repeatable measurement conditions.

Electrical Instrumentation and Data Acquisition

To improve the stability and reproducibility of the measurements, an automated data acquisition system is implemented. A National Instruments USB-6009 DAQ device is used to interface the six probe setup with a computer via USB connection. The DAQ device enables the acquisition of analogue voltage signals from the probes and allows direct communication with a custom Python measurement application. Through this interface, voltage signals from the probes can be recorded continuously and processed in real time during th experiment.

In order to capture the voltage drop at the intermediate probes, four cables form the DAQ input ports are connected to the corresponding voltage probes of the setup. The wiring configuration is designed to allow simultaneous measurement of voltage drops at both the top and bottom surfaces of the UD tape. A schematic representation of the cabling arrangement is shown in Figure 3.5.

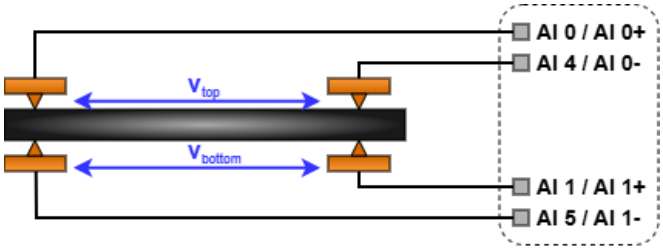

Figure 3.5: Six probes cabling setup

The two probes located on the top surfaces of the tape are connected to analogue input channel AI0 of the DAQ device in differential mode (AI0+ and AI0-), allowing the voltage drop between the two probes to be measured as

$$V_{top} = V_{top_{left}} - V_{top_{right}} \tag{3.1}$$

Similarly, the two probes located on the bottom surface are connected to the channel AI1, also in differential mode, giving the bottom voltage drop

$$V_{bottom} = V_{bottom_{left}} - V_{bottom_{right}} \tag{3.2}$$

No probe is connected to the DAQ ground, ensuring true differential measurements and avoiding ground loop effects. This configuration allows the top and bottom surface voltages to be acquired simultaneously while the electrical current is injected through the separate outer electrodes of the six probe setup.

Data processing and Analysis

Data acquisition and processing are implemented using a custom Python application developed for the six probe measurement setup. The initial implementation of the program is based on the work of *E. ul-Haq* [92], who used the same DAQ system to acquire electrical and mechanical data during the impregnation of TPC tapes. The code is adapted to the present six probe configuration in order to process the differential voltage signals obtained from the probe arrangement. The Python application performs three main tasks: acquisition of voltage signals from the DAQ system, real time calculation of electrical parameters, and automated storage of the measured data for further analysis. A flowchart of the data acquisition and processing routine is shown in Figure 3.6.

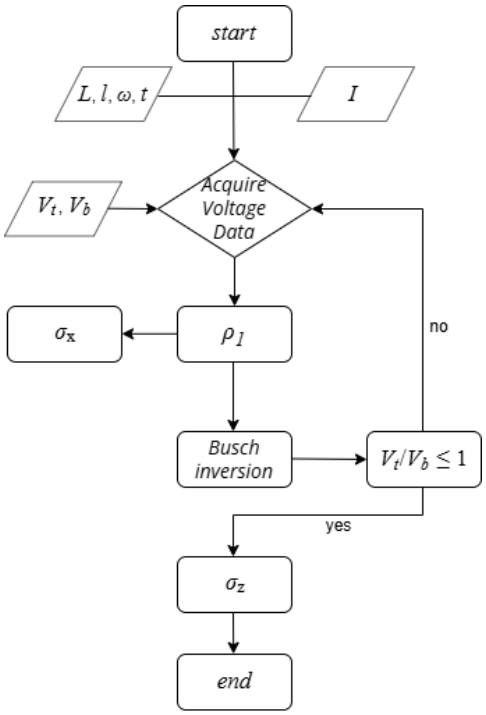

Figure 3.6: flowchart of the Python application to calculate anisotropic electrical conductivities from six probes measurements

The electrical conductivity of the UD tapes is calculated following the analytical model proposed by *Busch et al.*, described in Section 2.3.3. In this approach, the geometry of the specimen is defined by the outer electrode spacing L, the inner voltage probe spacing l, the tape width w, and the specimen thickness t. During the measurement, a constant current I is injected through the outer electrodes, generating a predominantly longitudinal current field within the anisotropic material.

The voltage drops measured at the top and bottom probes are continuously recorded and averaged in order to reduce noise and offset errors. From the measured voltage values, the apparent longitudinal resistance is first determined using Ohm's law

$$R = \frac{V}{I} \tag{3.3}$$

The corresponding apparent longitudinal resistivity of the tape can then be estimated as

$$\rho_x = \frac{Rwt}{l} \tag{3.4}$$

This expression provides an initial estimate of the longitudinal resistivity independent of the inversion procedure used by *Busch et al*.

The electrical anisotropy of the composite is exploited by comparing the voltage drops measured at the top and bottom surfaces of the specimen. In particular, the ratio V_t/V_b provides information about the distribution of the current field within the material. When this voltage ratio satisfies the conditions defined by ***Busch et al.*** model ($V_t/V_b \leq 1$), an effective penetration depth can be calculated from the analytical solution of the anisotropic Laplace equation. This leads to the definition of an effective thickness t_{eff}, which may differ from the physical thickness of the specimen for thin anisotropic materials.

Using the calculated effective thickness, the longitudinal resistivity ρ_x and the through thickness resistivity ρ_z can be determined. The corresponding electrical conductivities are obtained as

$$\sigma_x = \frac{1}{\rho_x}, \sigma_z = \frac{1}{\rho_z} \tag{3.5}$$

If the voltage asymmetry between the top and bottom probes is insufficient, the *Busch* inversion can not be applied and only the longitudinal conductivity can be determined.

During the measurement, the Python application displays real-time plots of the calculated electrical parameters, including the top and bottom resistivity values and the estimated through thickness conductivity. This real-time monitoring allows potential anomalies or measurement errors to be identified during the experiment, reducing the need for repeated testing. Once the measurement sequence is completed, the program automatically stores the recorded data in text files containing the voltage signals and calculated conductivity values. These files can subsequently be analysed using Python or external software such as Microsoft Excel for further quantitative and qualitative evaluation.

In addition to the conductivity values obtained from the six probe measurements, the calculated longitudinal electrical conductivity of the UD tapes is compared with theoretical predictions based on the Rule of Mixtures (ROM) described in Section 2.3.1. According to this approach, the longitudinal conductivity of a composite can be approximated by

$$\sigma_1 = \sigma_f v_f + \sigma_m v_m \approx \sigma_f v_f, \sigma_m \approx 0 \tag{3.6}$$

where σ_f and σ_m represent the electrical conductivities of the fibre and matrix, respectively, and v_f and v_m correspond to their respective volume fractions. For CFRP composites, the electrical conductivity of the polymer matrix is several orders of magnitude lower than that of the carbon fibres and can therefore be neglected in the approximation. The dry fibre conductivity values used in this work are obtained from the literature and summarised in Tables 3.1, 3.2.

The Rule of Mixtures provides an idealised estimate of the electrical conductivity of a composite based solely on its fibre volume fraction. However, this simplified approach does not account for manufacturing related effects such as fibre misalignment, non-uniform fibre distribution, resin-rich regions, voids, or defects within the material. As a result, the ROM prediction represents an optimistic theoretical approximation of longitudinal conductivity.

Comparing the experimentally measured conductivity obtained from the six probe method with the ROM prediction therefore provides useful insight into how processing conditions and microstructural features influence the electrical behaviour of UD tapes. These deviations from the ROM model can be further investigated through the microstructural methodology presented in Section 3.3, where the internal architecture of the material is examined using microscopy.

Measurement Procedure

Once the six probe setup and instrumentation is configured, electrical characterisation of the UD tape can be performed. The measurement procedure consists of specimen preparation, installation in the six probe fixture, and automated voltage acquisition using the data acquisition system.

Before testing, the geometric dimensions of each specimen are measured and defined as input parameters for the Python data processing script. The tape width w is measured using a caliper, while the specimen thickness t is measured using a micrometer. Due to local thickness variations observed in UD tapes, five measurements are recorded at different locations along the specimen. The average

value of these measurements is then used to define the effective cross-sectional dimension used in the conductivity calculations.

After dimensional measurements, the specimen is positioned within the six probe fixture. The tape is first aligned between the bottom probes, ensuring that the specimen is centred and perpendicular to the probe alignment. The top electrodes and probes are then lowered onto the specimen using the guiding pins of the fixture to ensure consistent probe positioning.

To maintain uniform contact pressure between the probes and the specimen surface, a metal bar with rubber insulation is placed above the probes. The clamping mechanism of the fixture is then tightened to secure the assembly and ensure stable electrical contact during the measurement.

The outer electrodes of the six probe setup are connected to a DC power supply using crocodile clamps in order to inject a constant current through the specimen. The four intermediate probes are connected to the NI DAQ device according to the wiring configuration described in Figure 3.5.

Once all electrical connections are verified, a constant current of $0.5\ A$ is supplied to the outer electrodes. The Python data acquisition program is then initiated to continuously record the voltage drops measured at the top and bottom probes.

During measurement ($10 - 20\ s$), the Python application acquires voltage signals from the DAQ device and processes them in real time according to the methodology described in the Figure 3.6 flow chart. When the measurement is completed, the acquisition is terminated using the program command, after which the processed data is automatically saved to a text file in a predefined directory.

The generated data files contain the recorded voltage signals as well as the calculated electrical parameters, including longitudinal conductivity and through thickness conductivity of the specimen. These files are subsequently used to further analysis of the electrical behaviour of the investigated materials.

The complete measurement procedure, including specimen installation, voltage acquisition, and data storage, required approximately five minutes per specimen, allowing efficient electrical characterisation of multiple UD tapes.

Measurement Assumptions and Limitations

The six probe methodology used in this work relies on several geometric assumptions and experimental parameters that influence the accuracy and repeatability of the conductivity measurements. These assumptions mainly relate to specimen geometry, probe contact conditions, applied current, and measurement duration. The following section describes the main limitations associated with the measurement approach.

The Python data processing routine requires the geometric parameters of the specimen to calculate the electrical resistivity. In particular, the tape width w and thickness t are required in order to estimate the cross sectional area used in the longitudinal resistivity calculation. These parameters are therefore measured prior to each test using a caliper and micrometer. A schematic representation of the assumed cross sectional area used in the resistivity calculations is shown in Figure 3.7.

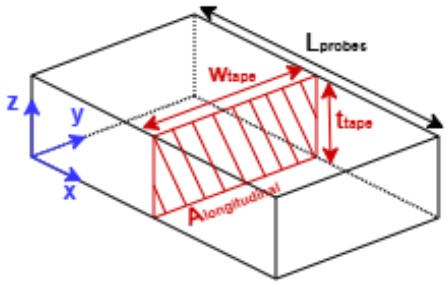

Figure 3.7: Sketch of cross sectional area for longitudinal resistivity calculations

UD TPC tapes are typically very thin, with thicknesses ranging between $0.1\ mm$ and $0.2\ mm$, and often exhibit local thickness variations along their length due to manufacturing processes. As a result, the

thickness value used in the calculations can not represent the exact geometry of the entire specimen. To reduce this uncertainty, the thickness of each tape is measured at five different locations, and the average value is used as an input parameter for the data processing program.

In addition, the cross sectional area of the tape is assumed to be rectangular when calculating resistivity. In practice, microstructural observations from 3.3 show that the surfaces of UD tapes are not perfectly flat and often exhibit local waviness due to fibre packing and uneven polymer distribution. Consequently, the rectangular cross section assumption introduces a simplification in the resistivity calculation.

Another important factor affecting the measurement is the geometry of the probes. In the initial setup, triangular electrodes were used. When clamped onto the specimen, these electrodes generated high local contact pressure, leading to visible surface indentations on the composite tapes. Such damage is undesirable because the six probe technique aims to provide a non-destructive characterisation (NDT) method.

Furthermore, for very thin tapes (particularly DPR tapes below $0.1mm$ thickness), the high contact pressure introduced by triangular electrodes reduced the voltage differential between top and bottom surfaces. This effect is likely due to a reduction in effective through thickness contact resistance under excessive pressure, which alters the measured voltage distribution.

In this context, the concept of effective conducting thickness is less critical for the present UD TPC tapes. The formulation by *Busch et al.* is mainly relevant for thicker composite laminates, where strong anisotropy leads to a reduced electrically active thickness. For the thin tapes investigated here, the specimen thickness is sufficiently small that current is expected to traverse the full thickness, making the geometric thickness a reasonable approximation for through thickness conductivity evaluation.

To mitigate this issue, round copper probes are implemented. The circular geometry distributes the contact pressure more uniformly and reduces the risk of damaging the tape surface while preventing measurable voltage differential between the two surfaces. However, this modification introduces a trade-off, by reducing the contact pressure, a higher electrode-material contact resistance increases, resulting in higher apparent resistivity values. The influence of probe geometry on the measured conductivity is illustrated in Figure B.5.

The electrical contact between the probes and the specimen is also affected by the applied clamping pressure. Variations in contact pressure modify the effective contact resistance between the electrodes and the tape surface, which directly influences the measured voltage drop.

Experimental observations show that higher clamping pressures generally result in lower measured resistivity values, as improved electrical contact reduces the overall contact resistance. However, defining a precise and reproducible clamping force remains challenging due to the mechanical characteristics of the setup. In order to maintain consistency across all measurements in this work, each test is performed under full clamp conditions, ensuring similar probe contact conditions for all specimens. The influence of clamping pressure on the measured conductivity is shown in Figure B.6.

Another parameter influencing the measurement is the magnitude of the electrical current injected into the specimen. UD TPC exhibit high electrical resistance, meaning that high current levels induce Joule heating within the fibres as explained in Section 2.2.3. This heating effect is undesirable because the measurements should be conducted under isothermal conditions to avoid altering the intrinsic electrical properties of the material or affecting the microstructure.

To determine a suitable current level, preliminary tests are conducted using currents ranging from $1\ A$ to $0.009\ A$. The results indicate that below $0.5\ A$ the measured conductivity decreases due to insufficient signal levels, while above this value the measured conductivity stabilises. Based on these observations, a constant current of $0.5\ A$ is selected for all measurements, providing a compromise between signal stability and minimal thermal effects. The preliminary test results on the injected current intensity effect on the measured conductivity are illustrated in Figure B.7.

The duration of the measurements also influences the stability of the acquired data. Continuous current injection may cause gradual temperature changes within the specimen due to Joule heating, which could affect the measured resistivity over time.

Tests performed with a constant current of $0.5\ A$ over a four minute period show that the measured resistivity initially decreases slightly during the first minute and then stabilises. The small variations observed may also be partially attributed to measurement noise within the DAQ system. Since the resistivity values measured within the first 20 seconds are consistent with those obtained over longer durations, extended acquisition times are not required.

For this reason, the duration of most conductivity measurements in this work is limited to approximately 20 seconds, allowing efficient characterisation of a large number of specimens while maintaining reliable conditions. The influence of test duration of acquired resistivity is illustrated in Figure B.8.

The six probe methodology used in this work provides a practical approach to characterise the electrical behaviour of UD TPC tapes by measuring the voltage drop across the specimen and analysing it through an anisotropic conductivity model. Despite the geometric simplifications and experimental limitations discussed above, the method allows reliable estimation of the longitudinal conductivity, and under suitable conditions, an approximation of the through thickness conductivity of the material. The automated data acquisition and processing system improves the efficiency and repeatability of the measurements, enabling the characterisation of a large number of specimens within minimal manual intervention.

However, the six probe technique provides information on the observed conductivity in the full material without directly capturing spatial variations in electrical behaviour across the surface of the material. To complement these measurements and obtain a more qualitative visualisation of conductivity variations, infrared thermography and eddy current sensing are also employed. The methodology used for the infrared thermography characterisation is described in the following section.

3.2.2. Infrared Thermography

As generation of current pathways in anisotropic UD TPC tapes is not yet fully understood, an infrared (IR) thermography technique is introduced in this study as a qualitative visualisation method. Infrared thermography employs an IR camera to capture the thermal response of a material, enabling the observation of temperature distributions as the specimen heats up under electrical loading.

This approach is applied to visualise the injected current paths in UD tapes during the six probe measurements. Carbon fibres exhibit relatively high electrical resistance. Therefore, when a DC current is applied, Joule heating occurs along the conductive pathways. In the six probe configuration, the outer electrodes introduce the DC current, while the IR camera records the resulting temperature distribution across the tape. The setup diagram is illustrated in Figure 3.8.

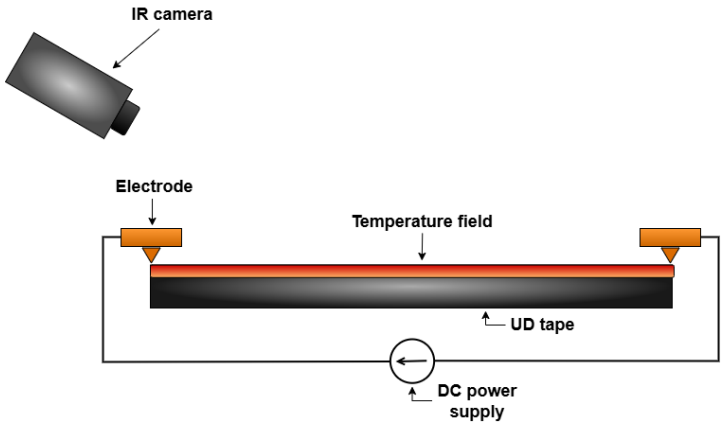

Figure 3.8: Infrared Thermography Diagram

Given that the surrounding polymer matrix has an electrical conductivity several orders of magnitude lower than that of the carbon fibres, short duration DC current injection is expected to highlight the most conductive fibre networks, which represent the preferential current pathways. For longer current

application times, heat diffusion leads to a more uniform temperature distribution across the tape width, including regions dominated by the polymer matrix. This technique not only reveals the preferential current paths but also provides insight into contact resistance at the electrode-tape interface. In particular, it enables evaluation of how applied pressure influences voltage drop measurements in the six probe setup. Furthermore, it offers indirect information on surface quality, which can be linked to the manufacturing route of UD tapes. For instance, the presence of polymer rich surface films may hinder efficient current injection, thereby affecting the observed thermal and electrical response. Finally, an additional visualisation technique, eddy current testing, is introduced in the following section to further investigate the electrical behaviour of UD TPC tapes.

3.2.3. Through-thickness Eddy Current Measurement Test

In addition to the six probe methodology described in Section 3.2.1, an eddy current sensing technique is used to further investigate the electrical behaviour of UD TPC tapes. This approach, developed and optimised by *E. ul-Haq*, provides a complementary method for analysing the electrical response of conductive composites by using alternating current (AC) electromagnetic excitation rather than the direct current (DC) injection employed in the six probe method.

Nevertheless, the fundamental operating principle and its application within this work can be described.

Unlike the six probe method, which characterises electrical conductivity through direct voltage measurement, the eddy current technique relies on electromagnetic induction. When an alternating current flows through an excitation coil, a time-varying magnetic field is generated. When a conductive material such as carbon fibre reinforced composite is placed within the magnetic field, circulating electrical currents, known as eddy currents, are induced within the material. These currents cause energy losses within the conductor and influence the intensity of the magnetic field once it is picked up.

The electrical response of the material under AC excitation is therefore governed by its impedance, which includes contributions from resistance R, inductance L, and capacitance C. A schematic comparison between DC conduction mechanism used in the six probe method and the AC electromagnetic response involved in eddy current sensing is illustrated in Figure 3.9.

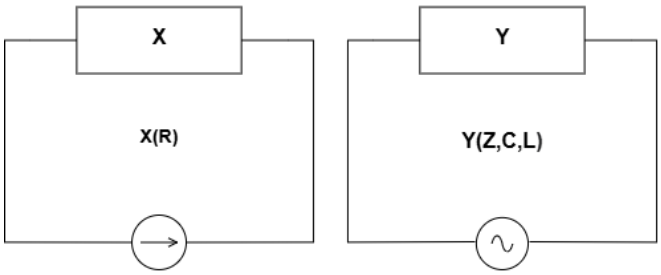

Figure 3.9: DC & AC electrical circuit diagram

The measurement setup consists of an excitation coil positioned above the specimen and a receiving coil which can be located where most desired. The excitation coil generates a controlled alternating magnetic field, which penetrates the UD tape and induces eddy currents within the conductive carbon fibres. The receiving coil then detects the modified magnetic field after interaction with the material. Part of the electromagnetic energy is dissipated within the specimen due to the induced eddy currents, resulting in measurable changes in the detected signal. A schematic representation of the eddy current sensor configuration used in this study is shown in Figure 3.10.

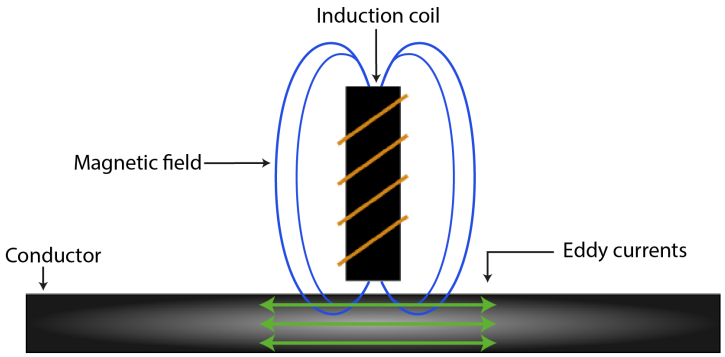

Figure 3.10: Schematic view of eddy current setup

These changes can be quantified in terms of signal gain and phase shift between excitation and received signals. Variations in these parameters are directly related to the electromagnetic properties of the specimen and therefore provide information about the local behaviour of the material. Regions with higher electrical conductivity or possible higher fibre concentration typically induce stronger eddy currents, leading to greater attenuation of the magnetic field and measurable changes in the detected signal.

The measurement system is coupled to a custom Python application that processes the acquired signals and analyses the response of the material under different excitation frequencies. The resulting data are used to generate two dimensional field maps of the specimen surface, representing the spatial distribution of phase and gain variations across the UD tape.

An example of such measurements is shown in Figure 3.11, where two UD tapes placed side by side are analysed using the eddy current sensor system. The resulting phase and gain maps provide qualitative visualisation of the local electromagnetic response of the materials.

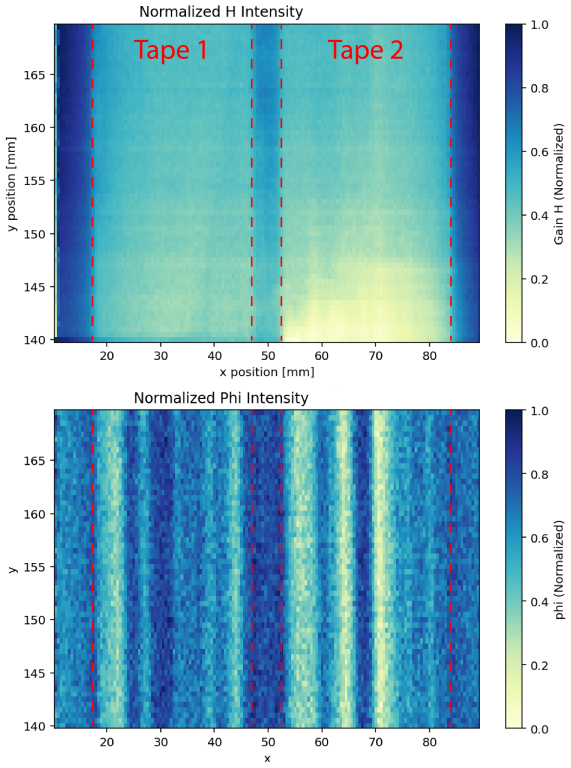

Figure 3.11: Eddy Current Sensor Gain and Phase Shift Diagrams of UD TPC Tape

These spatial representations allow regions with different electrical behaviour to be identified across the tape surface. Areas showing higher signal attenuation may indicate regions with increased fibre concentration or more efficient conductive pathways, whereas lower attenuation may correspond to regions with lower fibre volume fraction or polymer rich regions.

The eddy current sensor technique therefore complements the six probe conductivity measurements by providing spatially resolved qualitative information about the electrical behaviour of the composite material. While the six probe method provides quantitative estimates of longitudinal and through thickness conductivity at discrete locations, the eddy current approach enables the visualisation of local variations across the specimen surface. In combination with the microstructural analysis presented in Section 3.3, these measurements allow correlations to be established between electrical response and the underlying microstructure of the UD thermoplastic composite tapes.

Together, these techniques form the experimental methodology used in this work to investigate the electrical behaviour of anisotropic UD thermoplastic composite tapes.

3.3. Microscopy Characterisation

To better interpret the electrical behaviour observed during conductivity measurements, microstructural analysis of the UD TPC tapes is performed. The electrical conductivity of CFRP is strongly influenced by microstructural characteristics such as fibre distribution, fibre volume fraction, resin rich regions, voids, and the connectivity of conductive fibre networks. These features can significantly affect the formation of electrical pathways within the material and therefore influence the measured conductivity as described in Section 2.3.

Microscopy provides direct insight into the internal architecture of the composite tapes and enables the identification of local structural features that may influence the electrical response of the material. By analysing cross sectional micrographs of the specimens, it becomes possible to correlate the electrical behaviour with the underlying microstructure of the tapes.

For this purpose, selected specimens are prepared for optical microscopy following the electrical characterisation described in Section 3.2.

3.3.1. Sample Preparation

After completing the electrical characterisation tests, selected tape specimens are sectioned for microstructural analysis. Small cross sectional samples are trimmed from the tapes described in Section 3.1. Since microscopy preparation and analysis are relatively labour-intensive processes, only a limited number of samples are selected for detailed investigation.

For each material, two representative specimens are chosen based on their electrical performance: one corresponding to the upper-bound of the measured conductivity and one corresponding to the lower-bound of the measured conductivity.This selection strategy allows the microstructural features associated with the best and worst electrical performance to be investigated while keeping the number of analysed samples manageable.

The trimmed samples are carefully labelled to ensure proper identification throughout the preparation and analysis process. Because the objective of the microscopy analysis is to examine the cross sectional microstructure, the samples are cut such that the entire tape width (approximately $30\ mm$) is included in the analysed cross section. The specimen length is kept relatively short, as it does not influence the cross sectional micrograph analysis and allows the samples to fit within the embedding moulds used during preparation.

The specimens are embedded using the EpoFix epoxy mounting system. The epoxy resin and hardener are mixed according to the manufacturer's recommended weight ratio $25:3$ and poured into the moulds containing the samples. To minimise the presence of entrapped air bubbles, the moulds are placed under vacuum to allow trapped air to escape before curing. The mounted samples are then cured at room temperature for 24 hours.

After curing and demoulding, the embedded samples are polished using a Struers Tegramin-20 preparation machine in order to obtain a smooth cross sectional surface suitable for microscopy. The grinding and polishing procedure used for sample preparation is summarised in Table 3.3.

Table 3.3: Grinding and polishing program used for sample preparation

Grit / Polishing Foil	Time
500 (SiC paper)	30 s
1000 (SiC paper)	1 min
2000 (SiC paper)	1 min 20 s
4000 (SiC paper)	2 min
DUR 3 μm	4 min
DUR 1 μm	5 min

Once the polishing procedure is completed, the prepared samples obtained a smooth cross sectional surface exposing the internal fibre architecture of the UD tapes.

Figure 3.12: Polished microscopy samples

Figure 3.12 shows four embedded samples representing the material systems from different manufacturing routes (TC 1225, DPR, TPR, and Hybrid). Each sample contains two cross sections from different tapes, selected based on six probe conductivity measurements, with one exhibiting higher and the other lower conductivity to capture the range within each system.

The polished samples are then handled and stored carefully after preparation, as surface scratches or contamination could degrade the quality of the acquired micrographs.

3.3.2. Micrograph Acquisition and Processing

Cross sectional micrographs of the prepared specimens are acquired using a Keyence VK-X1000 laser confocal microscope. The microscope is operated with a lens providing a working distance of $3.1\ mm$ and a magnification of 20x, allowing detailed observation of microstructural features such as fibre distribution, resin rich regions, and potential voids within the material.

To capture larger regions of the tape cross section, multiple micrographs are acquired and combined using an image stitching technique. This approach enables the reconstruction of a larger field of view while maintaining the high spatial resolution required to analyse the fibre architecture. An example of an acquired cross sectional micrograph is shown in Figure 3.13.

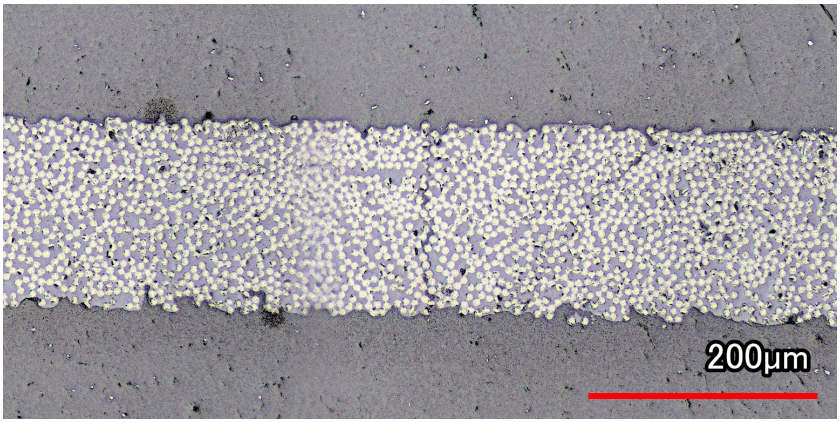

Figure 3.13: Micrograph of a Toray TC1225 cross section

The acquired micrographs are first used for qualitative visual assessment of the microstructure and are compared with the electrical conductivity results obtained in Section 3.2. In addition, the micrographs are analysed quantitively to estimate the fibre volume fraction of the tapes.

For this purpose, a Python-based image processing application, developed in collaboration with *O. Eryilmaz*, is used to analyse the micrographs. The algorithm processes the images through several steps in order to identify the circular cross sections of the carbon fibres and calculates their relative area within the composite. The workflow of the analysis algorithm is illustrated in Figure 3.14.

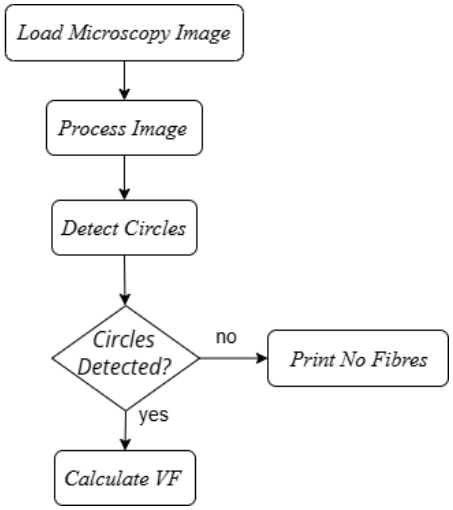

Figure 3.14: Flowchart of python code to analyse micrograph

The image processing procedure begins by loading the microscopy image and converting it to greyscale, as the fibre volume fraction calculation only requires pixel intensity information. The greyscale image is then inverted so that the carbon fibres appear bright while the polymer matrix appears darker, which improves contrast between the two phases.

To further enhance local contrast and improve the visibility of fibre boundaries, contrast limited adaptive histogram equalization (CLAHE) is applied. This is followed by a Gaussian blur operation to reduce image noise and smooth the data before fibre detection.

The processed image is then analysed using the Hough circle transform, which identifies circular geometries corresponding to the fibre cross sections. When fibres are successfully detected, circles are drawn around the identified fibre regions. The area of each detected fibre is calculated using $A = \pi r^2$, and the total fibre area is divided by the total image area to estimate the fibre volume fraction of the composite.

The program finally outputs the processed image together with the calculated fibre volume fraction, as illustrated in Figure 3.15.

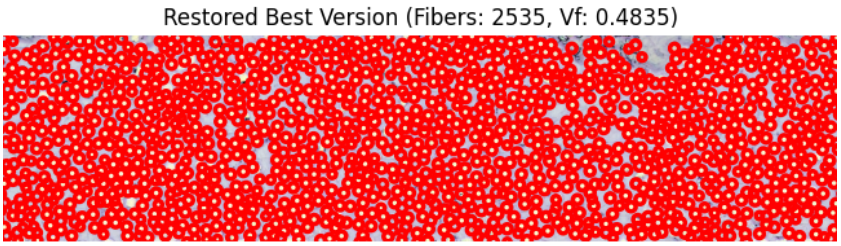

Figure 3.15: Cross sectional micrograph with fibre detected by red circles

This analysis provides quantitative information about the fibre volume fraction and the quality of fibre impregnation within the UD tapes. The obtained fibre volume fraction values can be directly compared with the electrical conductivity measurements and eddy current analysis presented in Section 3.2. Furthermore, the micrographs enable the identification of local microstructural features and defects associated with the different manufacturing processes, allowing qualitative comparison between the investigated materials.

3.3.3. Assumptions and Limitations

Several assumptions and limitations are associated with the microstructural characterisation methodology used in this work. These mainly relate to the spatial sampling of the micrographs, the estimation of fibre volume fraction, and the automated image analysis procedure.

A first limitation concerns the spatial representativeness of the acquired micrographs. Due to the relatively high magnification used during imaging (20x), it is not practical to capture the entire tape cross section within a single micrograph. Acquiring images covering the full width of the tape would require a very large number of stitched images, resulting in extremely large datasets that would be difficult to process efficiently using the image analysis workflow in Figure 3.14. For this reason, only selected regions of interest along the cross section are analysed. These regions typically correspond to image sections of approximately $500 - 1000\ \mu m$ in length, within which local features are examined at smaller scales of approximately $100 - 200\ \mu m$. Consequently, the analysed micrographs represent only local sections of the tape rather than the full cross sectional width.

As a result, the calculated fibre volume fraction (FVF) values are also derived from these local image regions. It is therefore assumed that the analysed sections are representative of the overall tape microstructure. In practice, however, the microstructure of UD composite tapes can vary along the width due to local variations. The reported fibre volume fraction values should therefore be interpreted as local approximations rather than exact values representative of the entire tape.

Additional uncertainties arise from the image processing procedure for fibre detection. The Python based analysis algorithm identifies fibre cross section using contrast enhancement and circle detection methods. However, the detection accuracy can be affected by image noise, variations in contrast, shadows, or scratches introduced during the polishing process. In some cases, the algorithm may therefore slightly under or over detect fibre cross sections. Furthermore, certain algorithm parameters require manual adjustment depending on the specific micrograph being analysed, meaning that a single fully automated parameter set can not always be applied to all images. Although more advanced automated optimisation methods could be implemented to improve detection robustness, this is beyond the scope of the present work.

Finally, another limitation concerns the number of analysed samples. Due to the time intensive nature of microscopy preparation and analysis, only two representative specimens per material are selected for detailed microstructural investigation. These correspond to the tapes with higher and lower bounds in measured electrical conductivity within each material group analysed in Section 3.2. While this approach enables a qualitative comparison between microstructure and electrical performance, it does not capture the full variability of all specimens tested during the electrical characterisation.

Despite these limitations, the microscopy analysis provides qualitative and semi quantitative information on the fibre architecture and impregnation quality of the investigated tapes. The obtained observations are used to support the interpretation of the electrical characterisation results presented in Section 4.1. The analysis focuses on features such as fibre distribution and microstructural variations within the tapes.

3.4. Induction Welding Outlook

Understanding the anisotropic electrical behaviour of UD TPC tapes not only contributes to the scientific understanding of these materiels, but also supports their implementation in industrial manufacturing processes. In particular, this section explores the implications of the measured electrical properties for the induction welding of TPC structures. To investigate this, a finite element method model (FEM) is developed to simulate the electromagnetic heating behaviour of the UD tapes manufactured in Section 3.1 when subjected to a static induction welding setup. The electrical conductivity values obtained from the six probe measurements in Section 3.2 are used as input parameters for the simulations. Finally, a static inductive heating experiment is conducted at SAM XL to validate the FEM model and to observe thermographic heating behaviour of the UD tapes.

3.4.1. FEM Simulation

Induction welding is a promising technique for joining TPC that offers potential improvement in the aerospace sector. To optimize this process, numerical simulations using Finite Element Method software COMSOL are employed to predict the thermal response of the component during induction welding.

This exercise helps to understand the highly anisotropic nature of UD TPC tapes and the difficulty in being welded with induction welding. As mentioned in Section 2.2.1, Induction welding is possible by introducing a magnetic field that induces eddy currents in the composite, and via Joule effect, heat up the material and melt it. As magnetic fields, induced currents, and heat transfer all occur at once, a multi-physics simulation is required. This is the reason why the FEM model is modelled with the software COMSOL Multiphysics. Shown below is a flowchart of the FEM model with each step required to simulate this manufacturing process.

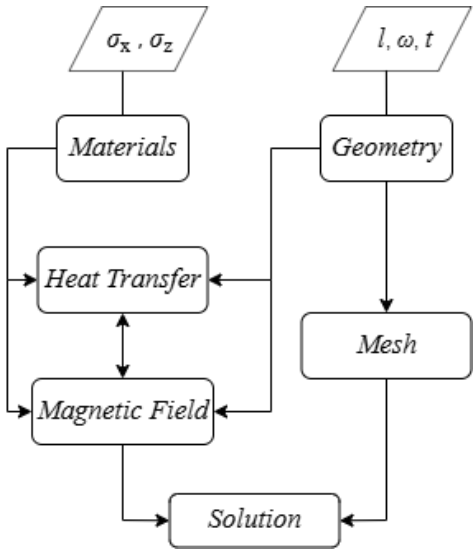

Figure 3.16: Flowchart FEM Model

The methodology employed in this FEM model involves capturing the coupled electromagnetic-thermal phenomena involved in induction welding of UD TPC tapes. The COMSOL model involves defining the geometry of the system, assigning material properties, simulating the electromagnetic field, and predicting the thermal behaviour of the UD tape.

Geometry

As a first step the geometry of the system is defined, which represents the components involved in the static inductive heating of a UD tape. The system consists of three main components: the inductive coil, the UD TPC tape, and an air domain surrounding these components. Each component is separately defined and modelled, to ensure different material properties and physics are defined. Shown below is the geometry of the full system.

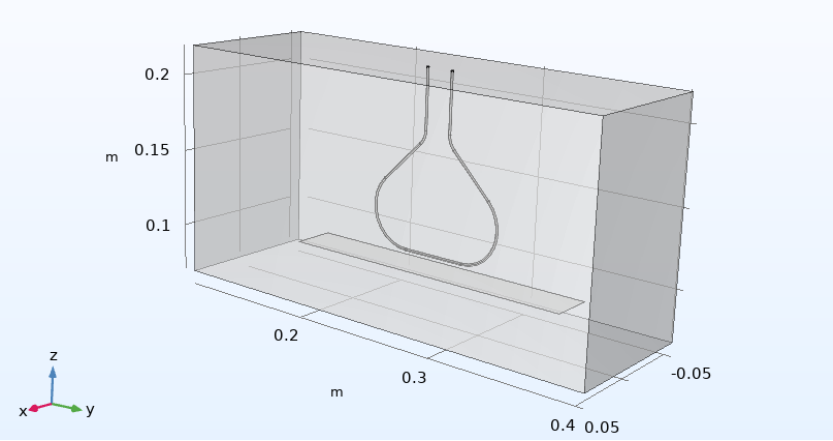

Figure 3.17: Geometry of Induction Welding setup

As can be seen in Figure 3.17, the UD tape is placed perpendicularly under the coil as during the experiment, moreover the air domain is simplified by a box around the system.

Materials

Following the geometry, the materials properties of each component are assigned. Without material properties a FEM simulation is not able to calculate and predict any physics. Hence it is fundamental to correctly define proper material input. To do this, the electrical properties of the Toray TC1225 UD tape are taken from the conductivity study made in Section 3.2.1. Other electro-magnetic properties such as relative permeability and permittivity are found from [12]. The coil used at SAM XL is the one from KVE, which is a bell-shaped copper coil. Shown below in Table 3.4 are the material properties used as input for the TC 1225 UD TPC tape modelled on COMSOL.

Table 3.4: Material properties Toray TC1225

Property	Variable	Value	Unit
Relative Permeability	μ	1	$-$
Relative Permittivity	ε	3.7	$-$
Electrical Conductivity	σ	$(35,000;\ 0.1;\ 0.1)$	S/m
CTE	α	$(-0.2e-6;\ 24e-6;\ 24e-6)$	$1/K$
Heat Capacity	C_p	$C_p(T)$	$J/Kg*K$
Density	ρ	$Rho(T)$	kg/m^3
Thermal Conductivity	k	$(K_{11}(T);\ K_{22}(T);\ K_{22}(T))$	$W/(m*K)$

Parameters such as heat capacity, density, and thermal conductivity are expressed as a function of temperature based on the work of *van Hoorn et al.* [12].

Magnetic Field

Once the geometry and the material parameters of the system are defined, the electro-magnetic physics of the model can then be defined.

The air domain is necessary as it determines the medium in which the magnetic field passes through. It is described with Maxwell equation, which represents a form of Faraday's law of induction.

$$E = -j\omega A \tag{3.7}$$

The electric field E is related to the magnetic vector potential A, where j is the imaginary unit, and ω represents the angular frequency.

$$\nabla X H = j \tag{3.8}$$

Equation 3.4.1 represents Ampere's law with the Maxwell's correction, in which H is the magnetic field strength, j the current density and ∇ the curl operator.

$$B = \nabla X A \tag{3.9}$$

Equation 3.9 defines the magnetic flux density B in terms of magnetic vector potential A.

$$J = \sigma E + j\omega D \tag{3.10}$$

Equation 3.10 represents the current density J as a function of the electric field E, electrical conductivity σ, and the displacement field D.

$$B = \mu_0 H \tag{3.11}$$

$$D = \varepsilon_0 E \tag{3.12}$$

Equation 3.11 and Equation 3.12 relate the magnetic flux density B to the magnetic field strength H through the permeability μ_0, and the electric displacement field D to the electric field E through the permittivity ε_0

Heat Transfer

The heat transfer physics for the system is divided in three mechanisms: conduction, convection, and radiation in solids.

$$\rho C_p u * \nabla T + \nabla * q = Q + Q_{ted} \tag{3.13}$$

Equation 3.13 is used to model transient heat transfer in the UD tape with convection and conduction. ρ is the density, C_p is the heat capacity, u is the velocity vector, T is the temperature, q is the heat flux, Q is the heat source, and Q_{ted} is the thermal energy dissipation.

$$q = -k\nabla T \tag{3.14}$$

Equation 3.14 represents Fourier's law of heat conduction, which introduces the relationship between the heat flux q and the temperature gradient and thermal conductivity $\nabla T * k$ within the UD tape.

$$q_0 = h(T_{ext} - T) \tag{3.15}$$

Equation 3.15 describes the convective boundary condition, where h is the convective heat transfer coefficient, T_{ext} is the external temperature, and T is the surface temperature of the UD tape. This equation represents the heat transfer exchanged between the tape's surfaces and the surrounding air.

$$-n * q = \varepsilon\sigma(T_{amb}^4 - T^4) \tag{3.16}$$

Equation 3.16 is the radiative boundary condition, where $n * q$ is the surface heat flux, ε is the surface emissivity, σ is the Stefan-Boltzmann constant, T_{amb} is the ambient temperature, and T is the surface temperature. This equation governs the radiative heat transfer present between the UD tape and the surrounding medium.

Mesh and Solver

The model requires a mesh to divide the complex geometries into smaller elements in order to assess the boundary conditions described above. For this model the default mesh type in COMSOL, tetrahedral elements, is applied. As it can be used to mesh complex 3D geometries, while requiring minimal input, and offering computational robustness. It is less accurate than hexahedral mesh sizes, but faster and easier to compute. Therefore for this study it is an acceptable mesh type.

Once the model mesh is fully built, it is required to select the necessary study steps to compute the system. To simulate the induction welding process three couples steps are required to combine all the multiphysics. The first step is the Coil Geometry Analysis, which computes the current flow in the complex 3D coil model. This study step solves the total alternating current vectors of the coil geometry. This step is based upon the coil excitation of $300\ A$ used during the experiment at SAM XL. Consequently, the magnetic field is compute via a Frequency Domain study step. This step computes the response of a linear model subjected to an harmonic excitation with a frequency of $300\ kHz$, the frequency used at SAM XL during the experiment. Finally, a Time-Dependent Solver is used to compute the heat transfer in the UD tape and to couple it to the electromagnetic heating. This step shows how the UD tape heats up in a time frame of $10\ s$.

Once all the study steps have been computed, the model realistically simulates the experiment of statically heating a UD tape with magnetic field excitation. This can be seen by plots of the temperature field, which can later be compared to an infra-red camera during the static heating experiment.

3.4.2. Static Induction Heating Experiment

In order to validate the FEM model and confirm its results, the same static inductive heating test is done at SAM XL. For this experiment the fanuc robot cell is used to control and move the KVE coil on top of the UD tape. The tape is placed on an insulated plastic bar to simulate the tape floating in the FEM model. This plastic bar should not have impact on how the eddy currents are generated within the tape, and should have negligible conduction heat sink properties that effect heat transfer. Shown below is the induction welding experiment setup.

Figure 3.18: Induction welding experiment setup at SAM XL

In Figure 3.18 the coil is being stationed perpendicularly on top of the UD tape, with a height difference of

$2\ mm$ as in the FEM model. This is possible by manually controlling the robotic arm via a controller. The coil is directly connected to an AC power supply which can deliver up to $500\ A$ with the corresponding frequency required. The temperature of the coil surface is acquired via internal thermocouples within the coil's case. In order to keep its temperature under control, the coil has a hollow shape in which cooling water can pass within. Moreover, the AC power supply and the full system is connected to an external computer which via a software can be used to set required process parameters such as time, current intensity, and temperature. In the software, the parameters used in the FEM model are implemented. Finally, an infrared camera is used to capture the heat map of the tape surface, in order to compare it to the FEM results.

Overall, the applied methodology combines electrical characterisation, microstructural analysis, and an induction related assessment to investigate the behaviour of UD TPC tapes. These approaches provide the basis for analysing the materials from both an electrical and structural perspective. The results obtained using this methodology are presented in the following chapter.

4

Results & Discussion

This chapter presents and discusses the quantitative and qualitative results obtained in this study, focusing on the anisotropic electrical behaviour of unidirectional thermoplastic composites tapes. Particular attention is given to the influence of manufacturing route, material system, fibre type, and microstructural characteristics on the electrical conductivity of the tapes.

Based on the methodology described in Section 3, this section presents the experimental results of this study, structured around electrical characterisation, microstructural analysis, and the influence of manufacturing route. An outlook on induction welding is then provided, followed by a brief discussion on potential practical applications.

4.1. Electrical Characterisation of UD TPC Tapes

This section presents the electrical behaviour of the investigated UD TPC tapes. The analysis focuses on the anisotropic properties of the materials and their variation across the different tape systems.

The results include conductivity measurements and observations of current distribution within the tapes, providing a basis for comparison with theoretical models and for correlation with microstructural features.

4.1.1. Electrical Conductivity

This subsection presents the electrical conductivity of the UD TPC tapes obtained from the six probe measurements. Both longitudinal and through thickness conductivities are evaluated in order to characterise the electrical behaviour of the materials and to enable comparison across the investigated tape systems.

The measured values are consequently compared with theoretical predictions based on the Rule of Mixtures (ROM). For this purpose, fibre volume fraction (FVF) values derived from the microstructural analysis are included, as they are required for the ROM based estimations of longitudinal conductivity.

Longitudinal Electrical Conductivity

Figure 4.1 presents the average longitudinal electrical conductivity of the four investigated UD TPC tape systems obtained form the six probe measurements. The values shown correspond to the mean conductivity of eight individual tape specimens per material system, while the error bars represent the standard deviation. The conductivity of each individual tape are provided in Appendix D.

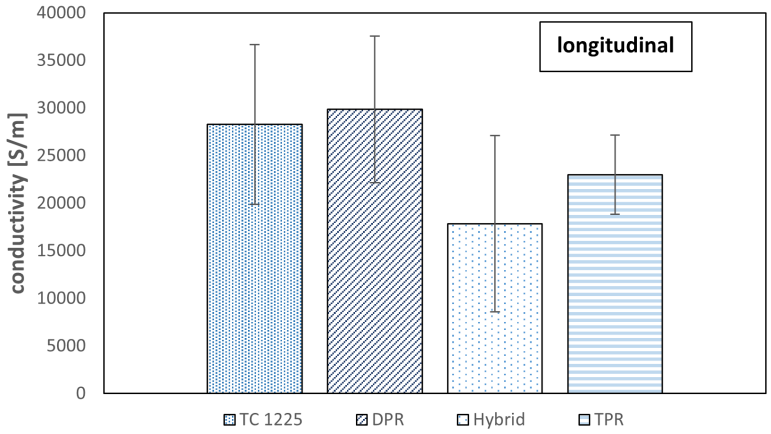

Figure 4.1: Longitudinal electrical conductivity of 4 UD tapes

Among the investigated materials, the DPR-based tapes exhibit the highest average longitudinal conductivity with a value of $29,843\ S/m$ with upper bounds up to $38,000\ S/m$. The TC 1225 tapes show a slightly lower average conductivity of $28,270\ S/m$, followed by the TPR tapes with an average of $22,990\ S/m$. The hybrid tape system presents the lowest longitudinal conductivity, with an average of $17,838\ S/m$.

These results suggest that the DPR route may promote slightly higher conductivity along the fibre direction, with TC 1225 tape showing nearly equivalent performance. In contrast, the low conductivity of the Hybrid tapes is unexpected, as they contain both T800 and highly conductive M40J fibres, which would suggest a higher overall conductivity. This discrepancy points to limitations in effective fibre connectivity or microstructural heterogeneity that restrict current transport. Further insight into these differences is provided by the microstructural analysis in Section 4.2.

Through-Thickness Electrical Conductivity

Figure 4.2 presents the measured through-thickness electrical conductivity of the four UD TPC tape systems. Similar to the longitudinal measurements, the plotted values represent the average conductivity obtained from eight individual tape specimens per material, with error bars indicating the standard deviation.

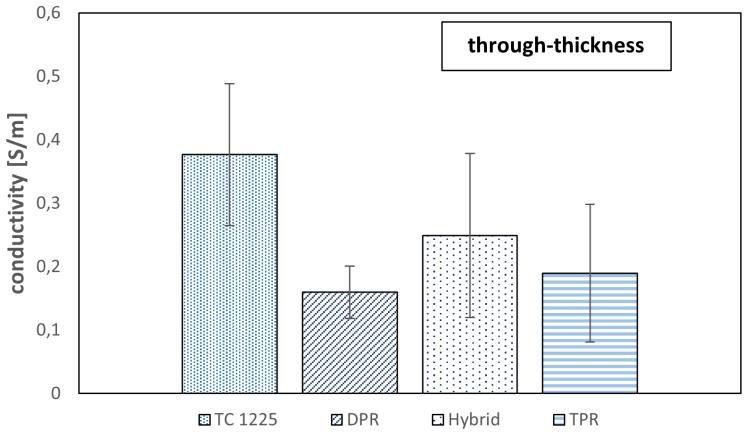

Figure 4.2: Through-thickness electrical conductivity of 4 UD tapes

The TC 1225 tapes exhibit the highest through-thickness conductivity with an average value of $0.38\ S/m$. This is followed by the hybrid material with an average conductivity of $0.28 S/m$, while the TPR and DPR

tapes present lower average values of $0.20\ S/m$ and $0.18\ S/m$ respectively.

One possible explanation for these differences is related to variations in tape thickness between the materials. For example, the TC 1225 tapes are relatively thicker compared to the DPR tapes, which can have a thickness below $100\ \mu m$. As reported in the literature of Figure 2.15, the thickness of the sample can influence the voltage drop measured during the six probe experiment, which in turns affects the calculated through-thickness conductivity. The six probe method implemented in this work, originally developed by *Busch et al.* for thicker composite laminates, may therefore introduce larger uncertainty when applied to very thin UD tapes.

The large difference between longitudinal and through-thickness conductivity confirms the strongly anisotropic electrical behaviour of UD TPC tapes, consistent with trends reported in the literature [60, 12]. However, uncertainty remains regarding the applied methodology, based on *Busch et al.*, particularly in estimating the effective thickness over which current density attenuates. As this approach was originally developed for thicker laminates rather than thin single ply UD tapes, it may introduce inaccuracies in the through thickness conductivity calculations.

4.1.2. Fibre Volume Fraction Determination

As the Rule of Mixtures (ROM) requires the fibre volume fraction (FVF) as an input parameter, this quantity must first be determined for the four investigated tape material systems. Since the FVF is not directly known for the manufactured tapes, it is estimated through the microstructural analysis described in Section 3.3. Optical micrographs of the cross sections are analysed using a Python based image processing application that detects the fibre cross sections and calculates the corresponding fibre area fraction, which is used as an approximation of the fibre volume fraction.

Figure 4.3 illustrates an example of this analysis procedure, where the Python algorithm identifies individual fibre circles within the micrograph and computes the corresponding FVF.

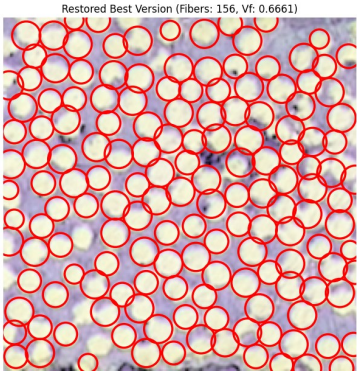

Figure 4.3: FVF python micrograph analysis

This analysis is repeated for multiple micrographs and locations across each tape material in order to obtain an approximate range of fibre volume fraction values. It should be noted that this approach assumes that the analysed micrograph regions are representative of the entire tape microstructure. While local variations in fibre distribution may exist along the tape width, the obtained values provide a reasonable approximation of the average FVF within the cross sectional area. Moreover, not every fibre cross section is consistently detected, as illustrated in Figure 4.3, where 6 out of 156 fibres are not included, resulting in an error of 3.8%. As each micrograph varies and requires individual adjustment for fibre detection, the error is not consistently this high across all images. Nevertheless, this variability should be considered when estimating fibre volume fraction ranges.

Table 4.1 summarises the investigated tape systems, including their manufacturing route (TC 1225, DPR, TPR, and Hybrid), the corresponding longitudinal conductivity values obtained from the six probe method, and the estimated fibre volume fraction derived from the micrograph analysis.

From this analysis, the TC 1225 tapes exhibit an estimated FVF between $46 - 48\%$, while the DPR tapes show the highest fibre volume fraction with values between $61 - 63\%$. The TPR tapes present

Table 4.1: FVF comparison to manufacturing route and respective conductivity

Manufacturing Route	Acquired conductivity $[S/m]$	FVF
Toray TC 1225	$28,270$	$46-48\%$
DPR	$29,843$	$61-63\%$
TPR	$22,990$	$38-44\%$
Hybrid	$17,838$	$28-29\%$

intermediate values ranging from $38-44\%$, whereas the hybrid tapes exhibit the lowest FVF, between $28-29\%$.

These observations are consistent with the experimentally measured longitudinal conductivity results obtained from the six probe measurements. In particular, the DPR tapes, which showed the highest fibre volume fraction, also exhibit the highest longitudinal conductivity, while the hybrid tapes present both the lowest FVF and the lowest measured conductivity.

The obtained fibre volume fraction values are subsequently used as input parameters for the ROM calculations to estimate the ideal longitudinal electrical conductivity of the investigated UD TPC tapes.

Comparison to Literature

It is important to compare the conductivity results obtained in this study with values reported in the literature in order to assess their validity. The measured longitudinal conductivities of the four investigated material systems are therefore benchmarked against literature data, as illustrated in Figure 2.11 in Section 2.3.1. Figure 4.4 instead presents the average longitudinal conductivity of each tape system, including their respective variability, in comparison with reported values of Section 2.3.1.

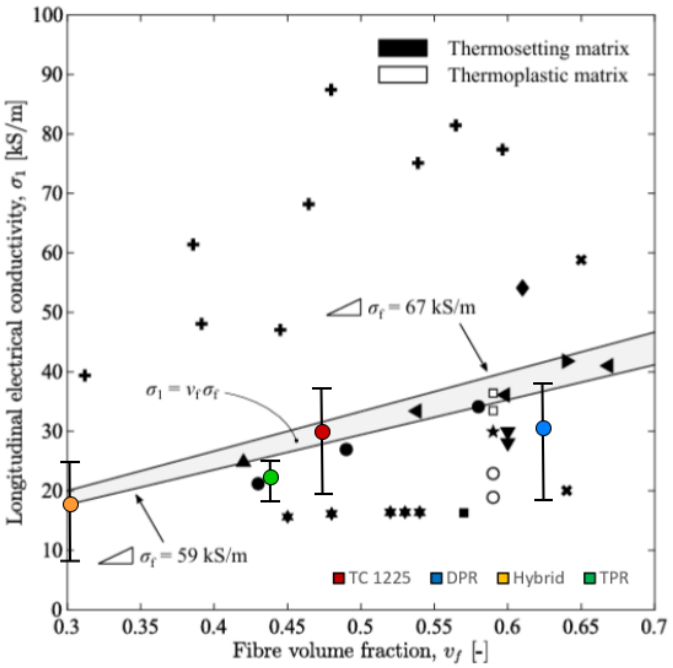

Figure 4.4: Longitudinal conductivity of four tape systems compared to literature values and ROM

As described in Section 2.3.1, the literature dataset includes both thermoplastic and thermoset based composites, with a grey region representing the expected conductivity range based on the Rule of Mixtures (ROM), assuming a fibre conductivity of $67\ kS/m$ and a fibre volume fraction between 30% and 70%.

From this comparison, it can be observed that the DPR tapes, despite exhibiting the highest FVF,

predominantly fall below the ROM prediction, with only their upper bound approaching the expected range. In contrast, the TC 1225 tape aligns closely with the ROM region for its corresponding FVF, indicating a stable and efficient microstructural architecture despite its lower fibre content. The TPR tapes also show slightly reduced conductivity compared to the ROM expectation, while the Hybrid tapes, characterised by the lowest FVF, fall within the lower bound of the grey region, although their conductivity remains lower than expected considering the presence of highly conductive M40J fibres.

Overall, the conductivity values obtained in this study show good agreement with literature data, particularly when compared to thermoplastic composite systems. This suggests that the applied methodology provides a reliable estimation of electrical performance. However, the in-house manufactured tapes (DPR and TPR) consistently exhibit conductivities below the idealised ROM prediction, reflecting the influence of microstructural imperfections and process related variability.

Furthermore, the upper bounds of the measured conductivity for all tape systems tend to approach the ROM region, indicating that the intrinsic material potential is partially achieved under favourable conditions. This observation suggests that deviations from ideal behaviour are primarily associated with microstructural features that hinder efficient current transport, such as limited fibre connectivity, heterogeneous distribution, and the presence of polymer rich regions.

4.1.3. Comparison with Rule of Mixtures (ROM)

The ROM provides an idealised estimate of the longitudinal electrical conductivity of fibre-reinforced composites. In this model, the conductivity is primarily governed by the conductivity of the reinforcing fibres and the fibre volume fraction, and can be approximated as

$$\sigma_1 \approx v_f \sigma_f \tag{4.1}$$

where v_f is the fibre volume fraction and σ_f is the electrical conductivity of the dry fibres. Because this analytical model assumes perfectly aligned fibres, homogeneous fibre distribution, and neglects potential manufacturing effects or microstructural irregularities, it represents an upper-bound approximation of the expected longitudinal conductivity.

Table 4.2 summarises the investigated tape systems, including their manufacturing route (TC 1225, DPR, TPR, and Hybrid), the reinforcement type (T700SC, T800SC, and M40J), the corresponding dry fibre conductivity values obtained from literature, and the estimated fibre volume fractions derived from the microstructural analysis.

Table 4.2: FVF determination per material system

Manufacturing Route	**Reinforcement**	**Dry fibre conductivity** $[S/m]$	**FVF**
Toray TC 1225	T700SC	$67,000$	$46-48\%$
DPR	T800SC	$77,000$	$61-63\%$
TPR	T800SC	$77,000$	$38-44\%$
Hybrid	T800SC + M40J	$77,000+100,000$	$28-29\%$

Using the ROM expression and the corresponding fibre properties and FVF values, the theoretical longitudinal conductivities of the tapes are calculated. Table 4.3 presents the resulting ROM-based conductivity values and compares them with the experimentally measured average conductivity obtained from the six probe measurements. The difference between the theoretical and experimental values is indicated by the corresponding conductivity deviation.

The results show that the ROM predictions are consistently higher than the experimentally measured conductivities.

In general, these results confirm that the ROM approach represents an idealised case in which manufacturing effects and microstructural features are not considered. In practice, factors such as fibre misalignment, imperfect packing, resin rich regions, and other irregularities can reduce the effective electrical conductivity of the composite. Nevertheless, the measured values remain within the typical range reported in the literature of TPC, indicating consistency with previously observed behaviour.

Table 4.3: ROM conductivity calculation for each tape system

Manufacturing Route	**ROM conductivity** $[S/m]$	**Acquired conductivity** $[S/m]$	**Delta** $[S/m]$
Toray TC 1225	$30,820 - 32,160$	$28,270$	$3,890$
DPR	$46,970 - 48,510$	$29,843$	$18,667$
TPR	$29,260 - 33,880$	$22,990$	$10,890$
Hybrid	$25,222$	$17,838$	$7,384$

A notable observation is that the DPR tapes exhibit the largest deviation from the ROM prediction. Based on the calculated FVF, the ROM model predicts a significantly higher conductivity that the value obtained experimentally. One possible explanation for this discrepancy may be related to uncertainties in the assumed cross sectional area used for the six probe calculations. Microstructural observations indicate that the actual tape thickness may be smaller than the nominal values used in the conductivity calculations, which could lead to an underestimation of the measured conductivity. The nominal thicknesses used for the six probe measurements are listed in Table 4.4, while the measured thickness variations for each material system are represented in Table 4.5.

Table 4.4: Nominal tape thickness used for conductivity calculations

Manufacturing Route	**Nominal Thickness** $[\mu m]$
Toray TC 1225	164
DPR	104
TPR	138
Hybrid	168

In contrast, the TC 1225 tapes show the smallest deviation from the ROM prediction. This may be related to the relatively uniform tape thickness observed in the microstructural analysis, which allows for a more accurate estimation of the cross sectional area used in the conductivity calculations.

Finally, the hybrid tape system presents an interesting case. This material contains M40J carbon fibres, which exhibit the highest electrical conductivity among the investigated fibre types as shown in Table 4.2. As a result, the ROM model predicts a relatively high longitudinal conductivity for this tape and its FVF. However, the experimentally measured conductivity is significantly lower than this theoretical value. Combined with the relatively low FVF observed in the micrographs, this result may indicate that the internal architecture of the hybrid tape limits the formation of efficient conductive pathways as will be discussed in Section 4.2.1, potentially due to the mixed fibre configuration or manufacturing related microstructural features.

4.1.4. Current Injection Behaviour

The electrical conductivity results presented in the previous sections highlight the strongly anisotropic nature of UD TPC tapes, as well as the influence of manufacturing route on their electrical performance. In addition, it was observed during the six probe measurements that certain material systems exhibit more unstable or noisy voltage signals, indicating that the current injection process may not be uniform or fully controlled.

This behaviour suggests that the manner in which current is injected into the material, particularly at the interface between the electrodes and the tape surface, may significantly influence the measured electrical response. In particular, contact resistance effects and potential variations in surface composition, such as polymer rich layers, may affect how the electrical current enters and distributes within the composite.

Infrared Thermography

Infrared thermography is used to qualitatively assess current pathways in UD TPC tapes. When direct current is applied, conductive carbon fibres generate heat via Joule heating, with heat initially concentrated in the fibre network due to their higher conductivity than the polymer matrix.

IR images reveal preferred current paths through localized temperature rises, before heat diffuses into the polymer. This enables a qualitative evaluation of current distribution and highlights the influence of surface conditions and contact resistance. Findings are further discussed alongside the microstructural features in Section 4.2.

Infrared Thermography Observations

Infrared thermography measurements are performed for all four investigated tape systems (TC 1225, DPR, TPR, and Hybrid) in order to visualise the current pathway during DC current injection. For each material system two different clamping conditions are investigated: a low clamping pressure and a full clamping pressure corresponding to the conditions used during the electrical conductivity measurements. The UD TPC tape is outlined by white dashed lines, while the electrode clamps are marked by red lines.

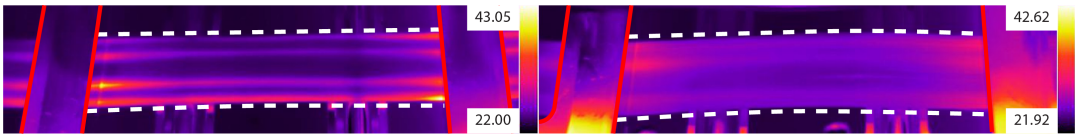

Figure 4.5: Thermography of TC 1225 tapes: low vs full clamping pressure

The thermographic response of the TC 1225 tapes is shown in Figure 4.5. Under low clamping pressure, several distinct fibre bundles can be observed to heat up rapidly after current injection. This indicates that the current is injected at multiple locations across the tape width, suggesting a non uniform electrical contact between the electrodes and the tape surface.

Under full clamping pressure, the thermal response becomes significantly more homogeneous. The temperature increase is distributed across the full width of the tape, indicating improved contact conditions and a more uniform current injection. This behaviour suggests that the TC 1225 tapes present a relatively uniform surface condition, allowing for a more stable electrical contact when sufficient pressure is applied.

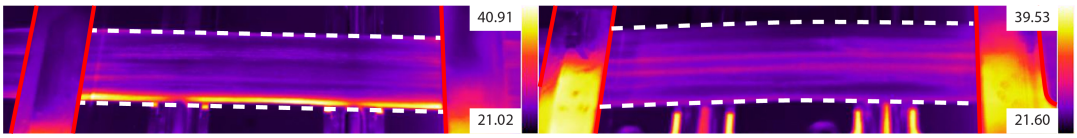

Figure 4.6: Thermography of DPR tapes: low vs full clamping pressure

Figure 4.6 illustrates the thermographic behaviour of the DPR tapes. Similarly to the TC 1225 material, multiple fibre bundles are observed to heat up under low clamping pressure, indicating localised current injection points.

When fully clamped, the heat distribution becomes more uniform, although some localised regions still exhibit higher temperature intensity. This may indicate local variations in tape thickness or fibre packing, leading to preferential current pathways even under improved contact conditions. This observation is consistent with the variability observed in the electrical conductivity measurements.

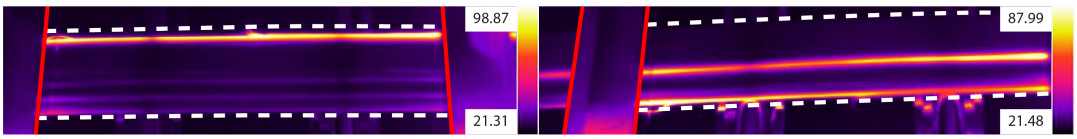

Figure 4.7: Thermography of TPR tapes: low vs full clamping pressure

The thermographic results for the TPR tapes are presented in Figure 4.7. Under low clamping pressure, the current injection appears highly localised, with one dominant fibre bundle exhibiting higher

temperature increase compared to the surrounding regions. This indicates that the electrical contact is concentrated at a limited number of locations, resulting in a non uniform distribution.

When fully clamped, the thermal response becomes more distributed, however, the current pathways remain partially localised. In some cases, the initially dominant heating region splits into two or more regions of lower intensity. This suggests that, even under improved contact conditions, the current injection is not fully homogeneous across the tape width. This behaviour may be attributed to surface or microstructural features that limit the effective conduction pathways.

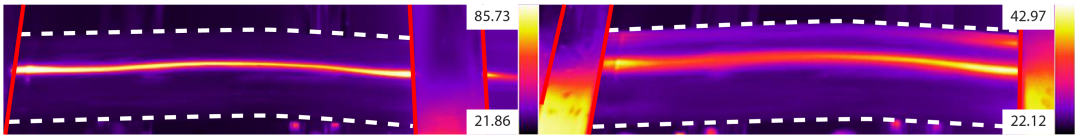

Figure 4.8: Thermography of Hybrid tapes: low vs full clamping pressure

Figure 4.8 shows the thermographic response of the Hybrid tapes. Similar to the TPR material, a highly localised heating pattern is observed under low clamping pressure, with a single dominant fibre bundle carrying most of the current.

Under full clamping pressure, the thermal distribution becomes slightly more uniform. However, distinct local regions of higher temperature remain visible. Compared to the other materials, the Hybrid tape shows a stronger tendency towards localised current pathways, even under improved contact conditions. As observed in the corresponding micrograph in Figure 4.17, the fibre bundles are not in direct contact, which limits the formation of continuous conductive networks. This behaviour is therefore expected and is likely further influenced by the lower fibre volume fraction and mixed fibre architecture.

Overall, these observations indicate that the current pathways during DC electrical measurements are strongly influenced by the contact resistance between the electrodes and the tape surface. Increasing the clamping pressure improves the electrical contact and promotes a more homogeneous current distribution; however, material dependent differences remain significant.

In particular, the TC 1225 and DPR tapes exhibit a more uniform current distribution under full clamping conditions, which also corresponds to their higher measured conductivities. This is especially notable for TC 1225, which achieves a highly uniform fibre distribution at 48% FVF, more challenging to realise than at higher FVF levels, such as the 63% in DPR. Additionally, as TC 1225 is a commercial tape, its superior homogeneity compared to the other materials, which originate from research trials, is not unexpected.

In contrast, the TPR and Hybrid tapes retain more localised current pathways. This behaviour suggests that surface quality, including resin rich layers, as well as local variations in thickness and fibre distribution, influence current injection. Overall, this highlights that electrical measurements in UD TPC tapes are governed not only by bulk properties but also by surface and interfacial effects.

Infrared Thermography of 8 Layer UD Laminate

As described in Section 3, this study primarily focuses on UD TPC tapes in order to establish a direct relationship between electrical performance, microstructure, and manufacturing route. To extend this analysis, an 8 layer UD laminate was manufactured from TC 1225 UD TPC tape to evaluate how electrical behaviour evolves when individual tapes are consolidated into a multi ply structure. The manufacturing procedure for this laminate is detailed in Appendix A.

During consolidation in the hot press, the laminate exhibited polymer flow-out, resulting in surfaces that are visibly resin rich and smooth. When tested using the six probe method, the laminate showed a significantly reduced conductivity of less than $5000\ S/m$, which is substantially lower than the average value of $28,000\ S/m$ measured for the individual tapes. This discrepancy indicates that the measured conductivity is not representative of the intrinsic material behaviour, but rather influenced by surface related effects introduced during manufacturing.

To investigate this further, the outer surfaces of the laminate were treated using a gas torch to remove the polymer rich layer and expose the underlaying carbon fibres. The objective of this approach was to

improve electrical contact between the electrodes and the fibre network during six probe measurements. Following this treatment, the measured conductivity increased to approximately $30,000\ S/m$. This finding is contradicting what *Van der Bert et al.* sates in Section 2.3.3, in which he states that surface treatment of the specimen is not required to ensure proper electrical current introduction. With an estimated FVF of $46-48\%$, this value aligns with the ROM prediction for TC 1225 and is consistent with the conductivity measured for the original tapes. This result confirms that the initially low conductivity was primarily due to high contact resistance at the surface, caused by the insulating polymer layer.

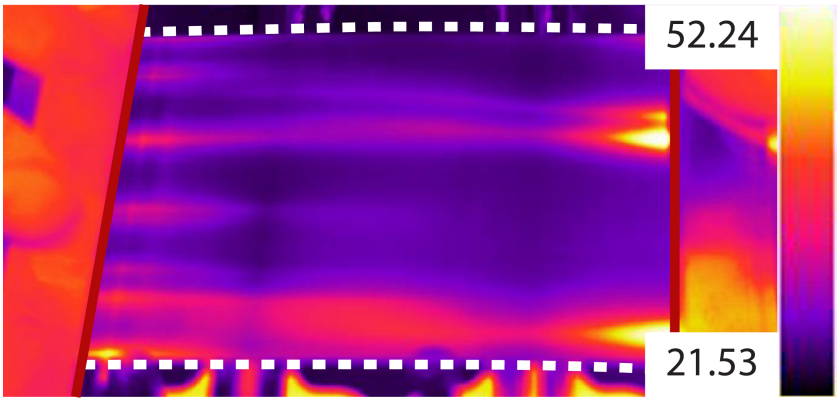

Figure 4.9: Thermography of 8 layer UD TC 1225 laminate

Based on this observation, the treated laminate was further analysed using infrared thermography. Figure 4.9 shows the thermal response of the 8 layer laminate with exposed fibre edges under electrical loading. In contrast to the untreated condition, multiple locations along the width of the laminate exhibit rapid heating upon current injection. This indicates the activation of multiple conductive pathways, facilitated by improved fibre-electrode contact.

These results demonstrate that surface condition plays a critical role in current injection and distribution in UD TPC materials. The removal of the polymer rich surface layer significantly enhances the ability of current to enter the fibre network, resulting in more distributed and efficient conduction. This finding provides further evidence that electrical performance is not solely governed by bulk material properties, but is strongly influenced by surface and interfacial characteristics introduced during manufacturing.

Overall, the behaviour of the 8 layer laminate reinforces the link between electrical measurements and underlying material structure. In particular, it helps explain the variability and instability observed in six probe measurements for materials such as TPR and Hybrid tapes, where polymer rich surfaces are more pronounced. A detailed analysis of the microstructural features is presented in Section 4.2.

4.1.5. Eddy Current Sensor Results

In addition to infrared thermography, eddy current testing is performed to further investigate the electrical behaviour of the UD TPC tapes. For each material system, two samples representing a lower and upper bounds of measured conductivity are analysed. This approach enables a direct comparison of electrical performance within the same manufacturing route and provides a means to validate the trends observed in the six probe measurements.

The eddy current sensor generates an alternating magnetic field, which induces circulating currents within the tape. The resulting energy dissipation is detected by a pickup coil and expressed through gain and phase shift signals. The gain response reflects the level of signal attenuation within the material, whereas the phase shift represents the temporal delay between the transmitted and received signals. This phase behaviour is influenced by the presence and distribution of conductive pathways and is often broadly correlated with gain, although the two signals capture distinct aspects of the material response.

In simple terms, gain indicates how much signal energy is lost, while phase shift describes how the signal is delayed during propagation through the material.

For each material system, two samples are placed side by side and analysed simultaneously. This configuration enables a direct visual comparison of their response under identical measurement conditions.

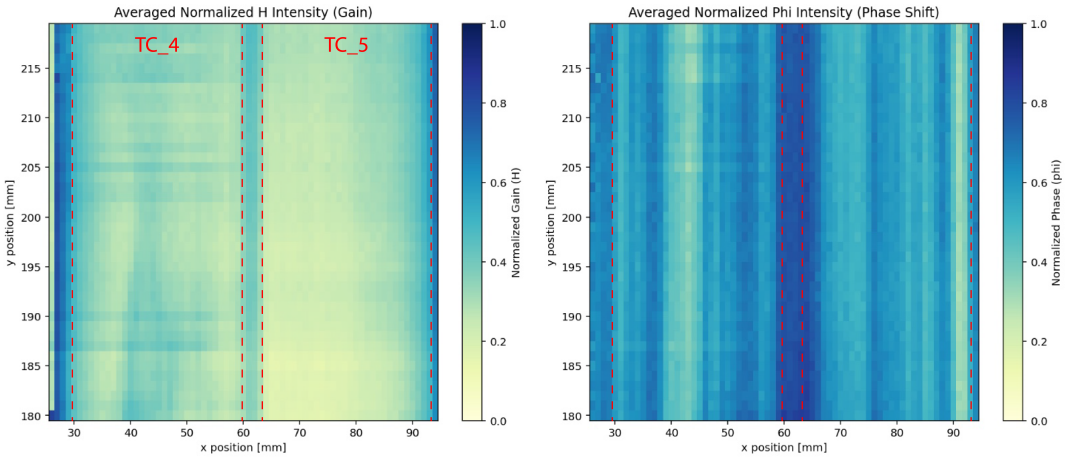

Figure 4.10: Eddy Current Gain and Phase Shift Response of TC_4 and TC_5 tapes

Figure 4.10 presents the gain and phase shift responses for two TC 1225 tapes with different conductivity levels. In the gain plot, brighter regions correspond to higher attenuation of the induced magnetic field, indicating stronger eddy current generation and, therefore, higher tape conductivity.

The more conductive tape (TC_5) exhibits a more uniform and intense attenuation across its width, while the least conductive sample (TC_4) shows a higher prevalence of lower intensity regions. This indicates a less efficient conductive network with reduced energy dissipation.

The phase shift plot provides additional insight into the current distribution, although it is less conclusive than the gain data. Both tapes exhibit predominantly longitudinal conductive pathways, consistent with their unidirectional fibre architecture. However, the less conductive tape shows more localised high intensity regions, indicating that current flow is concentrated within specific fibre bundles rather than being more uniformly distributed, as observed in the more conductive tape. This observation appears to be qualitatively similar to trends seen in infrared thermography, where more localised heating regions can be observed under non uniform current injection, although a direct comparison remains tentative.

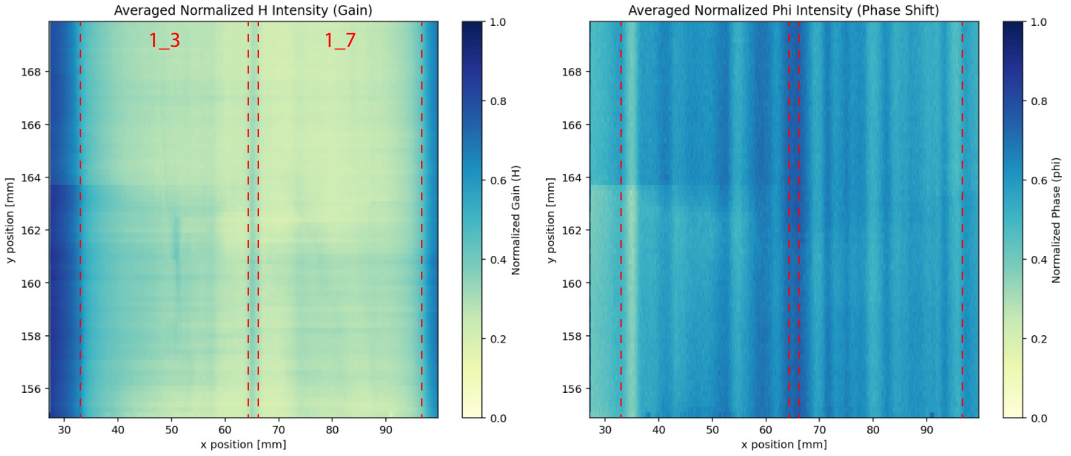

Figure 4.11: Eddy Current Gain and Phase Shift Response of DPR 1_3 and 1_7 tapes

The DPR tapes shown in Figure 4.11 exhibit trends similar to TC 1225, although the differences between the two samples are less pronounced. Overall, both tapes display comparable non uniform responses

in the gain and phase shift data. The higher conductivity tape (1_7) shows a slightly more homogeneous attenuation in the gain response, whereas the lower conductivity tape (1_3) appears marginally more variable, with some regions of reduced intensity.

A similar tendency can be observed in the phase shift response, however, the differences between the two samples remain subtle, and neither tape exhibits a fully uniform distribution. As such, while minor variations are present, the results suggest that both DPR tapes behave in a broadly similar manner.

These observations are consistent with the six probe measurements, indicating that even for DPR tapes with high fibre volume fraction, some variability in electrical response may arise, although the overall behaviour remains comparable between samples.

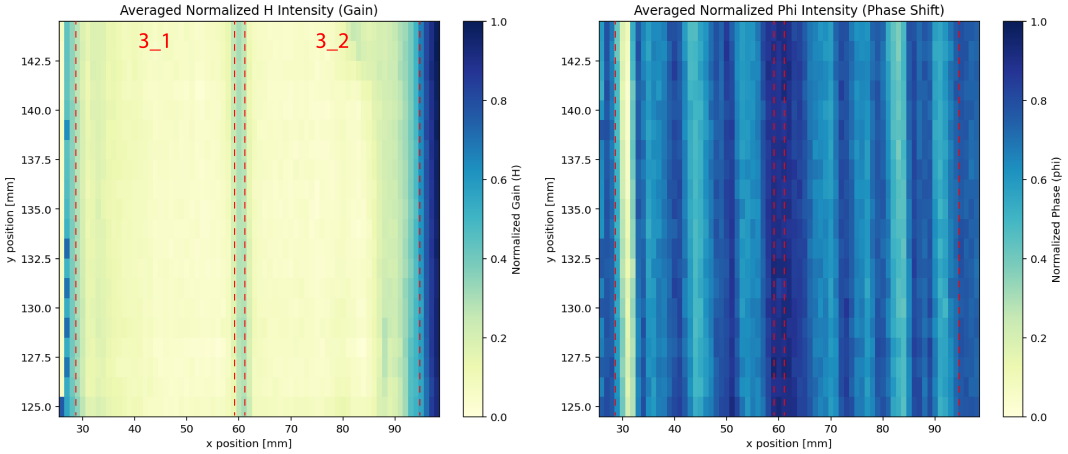

Figure 4.12: Eddy Current Gain and Phase Shift Response of TPR 3_1 and 3_2 tapes

The eddy current response of the TPR tapes differs from that of TC 1225 and DPR. As shown in Figure 4.12, both samples exhibit very similar attenuation levels in the gain plots, consistent with their comparable conductivity values. Consequently, the gain response provides limited contrast between the two tapes.

In contrast to TC1225 and DPR, both TPR tapes display a relatively uniform intensity distribution across their width, with only slight reductions in attenuation near the edges. This suggests that differences in the conductive network between the two tapes are limited, which is also consistent with the small variation in conductivity obtained from the six probe TPR measurements.

The phase shift plots, however, reveal some localised variations, with discontinuous regions of lower signal delay that may indicate the presence of resin rich areas between fibre bundles. In the lower conductivity tape (3_1), a notably bright region with higher signal delay is observed near the left edge. This region suggests that in that region of the tape there is a more conductive pathway that delays the signal. This feature appears qualitatively similar to the behaviour observed in the infrared thermography results, where a localised fibre bundle at the tape edge exhibits increased heating, although this comparison remains tentative.

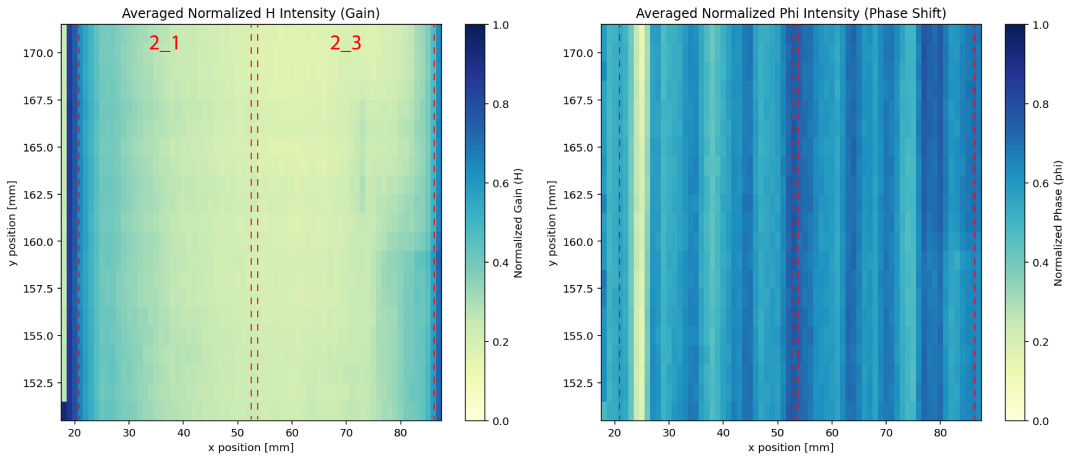

Figure 4.13: Eddy Current Gain and Phase Shift Response of Hybrid 2_1 and 2_3 tapes

Figure 4.13 illustrates the eddy current response of the Hybrid tapes. In the gain plot, both samples exhibit similar levels of attenuation, with darker regions observed near the outer edges. Overall, there is limited contrast between the two tapes, making it difficult to distinguish significant differences in their global electrical response using this metric alone. From the six probe measurements tape 2_1 conducts much less than tape 2_3, this suggests that the actual measured conductivity of 2_1 could be limited by signal attenuation from polymer rich areas at the surface or within the material. In reality, both tapes could have similar level of conductivity, hence the small variance in attenuation.

In contrast, the phase shift plots reveal a more distinct local features. In particular, the lest conductive tape (2_1) exhibits a region of higher intensity, indicating that eddy current generation is concentrated within that specific region. This suggests a highly localised conductive behaviour rather than a uniformly distributed current network. This could also be the reason this tape conducts less in the six probe measurements.

This observation is consistent with the infrared thermography results, where Hybrid tapes are shown to exhibit strongly localised current pathways. Such behaviour indicates limited fibre-fibre connectivity and the presence of discontinuities in the conductive network.

These characteristics are further explained by the microstructural features discussed in the following section, where the presence of isolated fibre bundles and extensive polymer rich regions contributes to the observed non uniform electrical response.

Overall, eddy current testing provides a useful means of visualising the relationship between microstructure and electrical behaviour of UD TPC tapes. The results show qualitative agreement with six probe measurements and infrared thermography, suggesting that variations in conductivity between samples may be linked to differences in fibre distribution, contact, and network continuity.

Furthermore, the measurements highlight the pronounced anisotropy of these materials, with current flow primarily aligned along the fibre direction and significant local variability across the tape width. This reinforces the conclusion that electrical performance is not uniform but governed by microstructural features.

The combination of eddy current testing with electrical and microstructural analysis provides a comprehensive understanding of how manufacturing routes influence conductive behaviour. A more detailed investigation of these microstructural features is presented in the following section.

4.2. Microstructural Characterisation

This section presents the results of the microstructural characterisation of the UD TPC tapes investigated in this study. The primary objective is to analyse the cross sectional microstructure of the four material systems and identify the key architecture features that distinguish them. Particular attention is given to fibre distribution and arrangement, resin rich regions, and the presence of voids, as these features are indicative of the manufacturing route and its influence on material properties.

These microstructural characteristics are directly linked to the electrical behaviour observed in the conductivity study, as they govern the formation and continuity of conductive pathways within the tapes. Optical microscopy is employed to provide a qualitative assessment of the cross sections, enabling the evaluation of the fibre packing, defect distribution, and thickness variation. Furthermore, the analysis of thickness variance variations allows for a more accurate interpretation of the measured conductivity values.

The microstructural observations are finally correlated with results obtained from eddy current sensing and infrared thermography, enabling a comprehensive comparison between physical architecture, local conductivity variations, and current distribution behaviour.

4.2.1. Microstructural Features of UD Tapes

Optical microscopy is performed on all four investigated tape systems (TC 1225, DPR, TPR, and Hybrid) in order to visualise and compare their cross sectional microstructures. The analysis focuses on fibre volume fraction, fibre distribution, resin rich regions, void content, and thickness variations, as these features are directly linked to the electrical behaviour discussed previously.

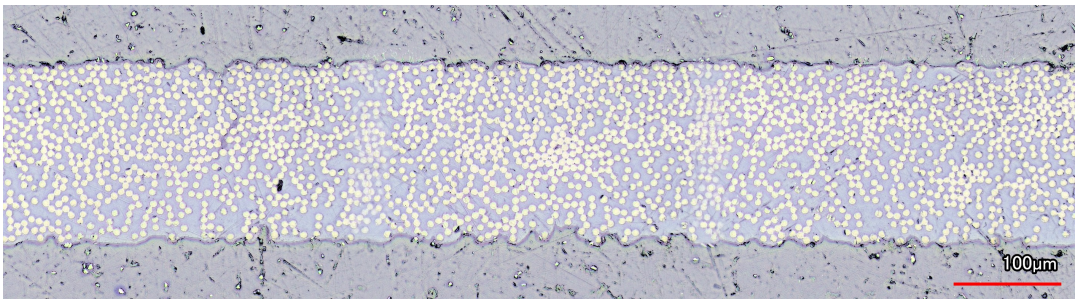

Figure 4.14: Micrography of TC 1225 tape

Figure 4.14 presents the cross sectional microstructure of the TC 1225 tape. No significant defects such as voids are observed, indicating a high quality manufacturing process. The fibre volume fraction, estimated from the analysis Section 4.1.2, lies between $46 - 48\ \%$.

The fibre distribution is generally uniform; however, locations of higher fibre concentration are visible, interspersed with polymer rich regions. These resin rich areas slightly reduce the overall FVF and appear to slightly disrupt fibre connectivity when comparing the conductivity values from the ROM method. The tape surface is not perfectly flat, although thickness variations remain relatively limited and consistent across the section.

Overall, the TC 1225 tape exhibit a well balanced microstructure with good fibre dispersion and minimal defects. This homogeneous architecture supports the formation of continuous conductive pathways, which is consistent with the relatively high and stable conductivity measured using the six probe method.

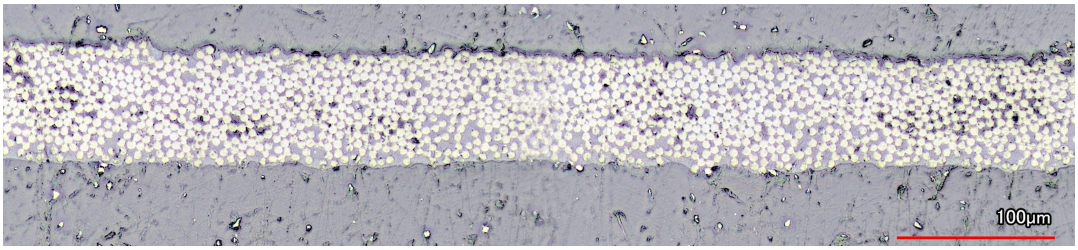

Figure 4.15: Micrography of DPR tape

The microstructure of the DPR tape, shown in Figure 4.15, is characterised by a noticeably smaller thickness compared to the TC 1225 and a significantly higher fibre packing density. The fibres are densely distributed throughout the cross section, with fewer polymer rich regions, resulting in an estimated FVF of $61 - 63\ \%$.

Although a higher void content is observed compared to TC 1225, the effect of voids on electrical conductivity has not been explicitly analysed in this study. However, it may partially contribute to the deviation between the experimentally measured conductivity and the ideal ROM predictions. Nevertheless, the relatively high FVF ensures sufficient fibre-fibre contact, supporting efficient electrical conduction despite the presence of such defects. It should also be noted that these voids may still have implications for mechanical performance, even if their influence on electrical behaviour remains uncertain within the scope of this work.

A key feature of this tape is the high fibre concentration near the surfaces, where no distinct polymer rich layer is observed. This facilitates efficient current injection, as also indicated by IR thermography results showing more distributed current pathways. This microstructural characteristic directly supports high conductivity value obtained from the six probe measurements.

However, the DPR tape exhibits more pronounced thickness variations than TC 1225. These geometric inconsistencies introduce uncertainty in cross sectional area estimation, potentially affecting the accuracy of calculated resistivity values.

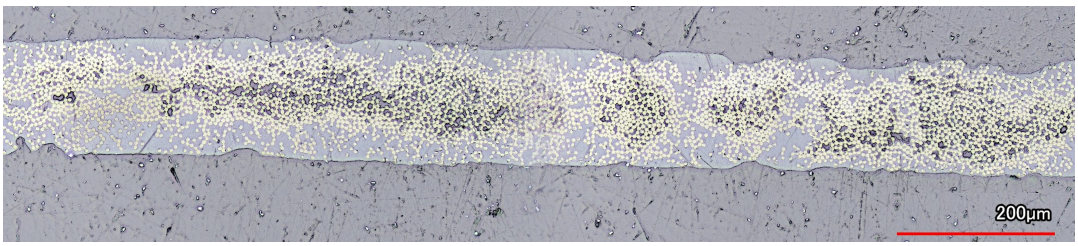

Figure 4.16: Micrography of TPR tape

Figure 4.16 shows the cross sectional microstructure of the TPR tape, which is thicker than the DPR tape and exhibits a heterogeneous fibre distribution. Fibres are highly concentrated in the central region, while significant polymer rich layers are present close to the surfaces.

The fibre arrangement appears discontinuous, while bundles of densely packed fibres separated by resin rich zones. This non uniform distribution disrupts the continuity of conductive pathways. Additionally, a relatively high void content is observed, particularly within the region where the fibres are most densely packed.

The estimated FVF ranges between $38 - 44\ \%$, significantly lower than that of TC 1225 and DPR. This combination of lower fibre content, poor distribution and increased void content leads to a less efficient conductive network.

These microstructural features explain the reduced conductivity and increased instability observed in electrical measurements. In addition, the presence of surface polymer rich regions is likely to increase

contact resistance, which can restrict current flow to more confined pathways. This behaviour is consistent with the localised current distribution observed in the infrared thermography, where heating is concentrated in specific regions rather than being uniformly distributed.

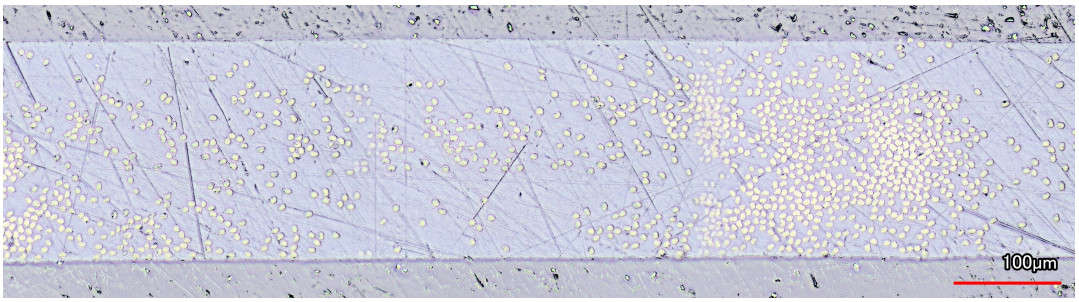

Figure 4.17: Micrography of Hybrid tape

The Hybrid tape, shown in Figure 4.17, exhibits the lowest fibre volume fraction, estimated $28 - 29\ \%$. The microstructure is highly heterogeneous, with isolated bundles of fibres surrounded by extensive polymer rich regions. In some areas, the full thickness of the tape consist almost entirely of polymer, indicating poor fibre distribution.

The fibres are not uniformly dispersed but instead appear segregated, likely due to differences in fibre type and challenges associated with impregnation. This results in a highly discontinuous conductive network, where fibre distribution is limited to isolated regions.

This microstructural configuration directly explains the very low electrical conductivity measured for this material. IR thermography further supports this observation, showing that current flow is confined to individual fibre bundles rather than being distributed across the tape.

Overall, the Hybrid tape demonstrates that the manufacturing process for mixed fibre systems requires further optimisation. The lack of homogeneous fibre mixing leads to a highly anisotropic and non uniform microstructure, which severely limits electrical performance.

4.2.2. Thickness Variations of UD Tapes

Infrared thermography results have shown that the different material systems exhibit distinct current distribution behaviour under varying clamping pressure. In particular, TC 1225 and DPR tapes display relatively homogeneous current pathways, whereas TPR and Hybrid tapes exhibit highly localised current pathways. One hypothesis for this behaviour is the presence of polymer rich surface layers, which can act as insulating barriers and influence how current is injected into the material. In addition, the applied pressure affects the resistance of electrical contact, thereby impacting both current injection and the measured response in six probe measuring.

Accurate determination of electrical resistivity using the six probe method required precise knowledge of the tape cross sectional area, and therefore its thickness. However, as observed in the microstructural analysis, each material system exhibits different thickness characteristics based on the manufacturing route. In particular, some tapes show significant thickness variations across their width, which introduces uncertainty in conductivity calculations.

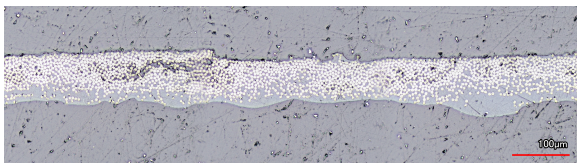

Figure 4.18: Micrograph of DPR tape used for thickness variation

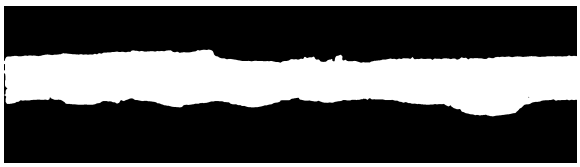

Figure 4.19: Thickness variance mask of DPR tape

This section evaluates the thickness variation of the four investigated tapes to assess its influence on

the measured electrical conductivity. The analysis is performed using optical micrographs of the tape cross sections. As shown in Figure 4.19, a masking technique based on image contrast, following the approach of *S. Upadhyay*, is applied to isolate the tape cross section from the surrounding resin and enable pixel wise thickness measurements.

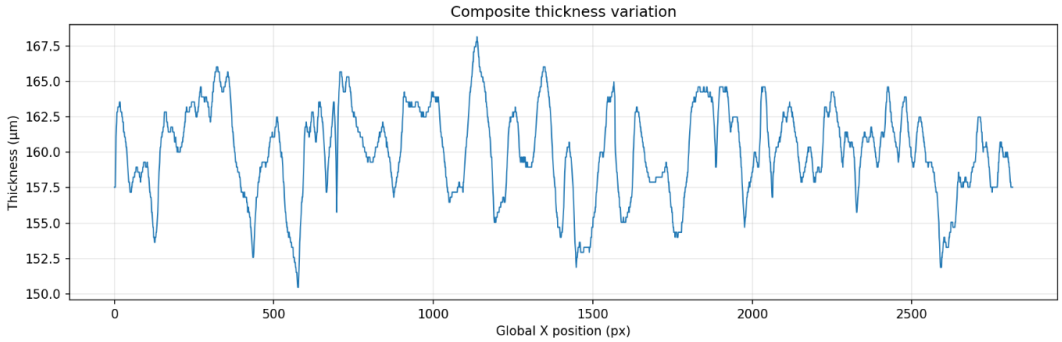

Figure 4.20: Thickness variance of TC 1225 tape

Figure 4.20 shows the thickness profile of the TC 1225 tape as a function of pixel position. The thickness is relatively uniform, ranging between 150 and $167\ \mu m$. This limited variation supports a reliable estimation of cross sectional area and contributes to the consistency observed in the corresponding conductivity measurements.

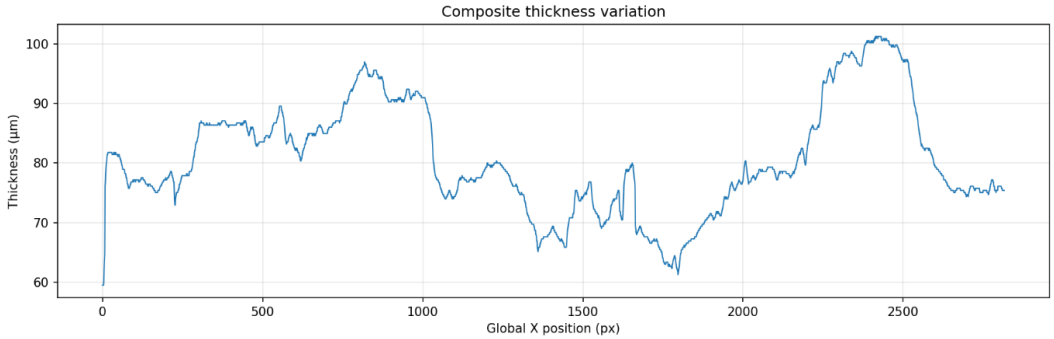

Figure 4.21: Thickness variance of DPR tape

Figure 4.21 presents the thickness distribution for the DPR tape, which is the thinnest material investigated, with values ranging from approximately 60 to $104\ \mu m$. In contrast to TC 1225, the DPR tape exhibits significantly larger thickness variations, with pronounced local differences along the cross section. This non uniformity introduces uncertainty in the selection of a representative thickness value, which may contribute to deviations between the experimentally measured conductivity and the values predicted by the Rule of Mixtures.

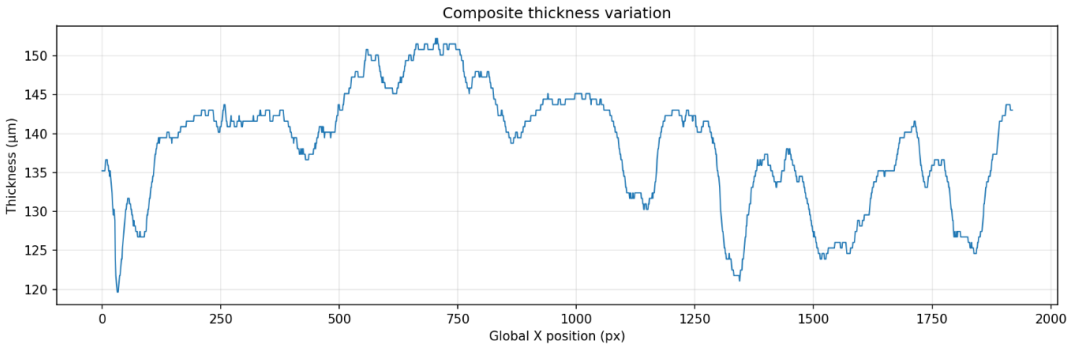

Figure 4.22: Thickness variance of TPR tape

Figure 4.22 shows the thickness variation for the TPR tape, ranging between approximately 120 and $150\ \mu m$. Although the variation is moderate, the presence of polymer rich surface layers suggests that part of the measured thickness may not contribute effectively to electrical conduction. A more detailed analysis separating structural thickness from polymer rich layers would provide further insight into their influence on current injection and voltage measurements in six probe testing.

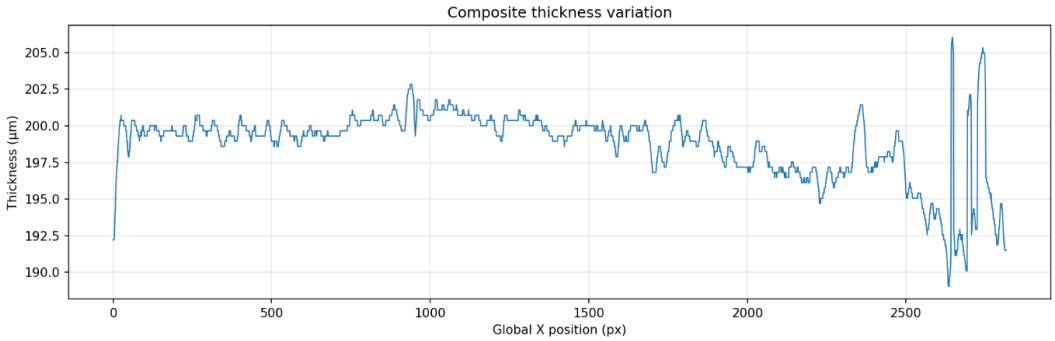

Figure 4.23: Thickness variance of Hybrid tape

Figure 4.23 presents the thickness profile of the Hybrid tape, with values ranging from approximately 192 to $205\ \mu m$. Compared to the other materials, this tape exhibits the smallest thickness variation across its width, making it the most uniform tape out of the four material systems. This consistency is likely associated with its high polymer content, which facilitates the formation of a more regular and stable cross sectional geometry during manufacturing.

A summary of the thickness variation for all material systems is provided in Table 4.5.

Table 4.5: Thickness variance results from cross section analysis

Manufacturing Route	**Thickness variance** $[\mu m]$
Toray TC 1225	$150 - 167$
DPR	$60 - 104$
TPR	$120 - 150$
Hybrid	$192 - 205$

Overall, this analysis highlights the challenge of accurately defining the cross sectional area for resistivity calculations of UD TPC tapes. Thickness variations, particularly in materials such as DPR, can lead to significant uncertainty in conductivity values obtained from six probe measurements. These findings further emphasise that geometric factors, in addition to microstructural features, play a critical role in the interpretation of electrical characterisation results in anisotropic uni directional composites.

Correlation Between Thickness Variance, Fibre Volume Fraction and Electrical Behaviour

As discussed in the previous sections, the four systems investigated in this study exhibit distinct microstructural features that influence their electrical behaviour. Among these, thickness variation plays a critical role in the accuracy of conductivity measurements obtained using the six probe method. The calculation of electrical conductivity requires an estimation of the tape cross sectional area, for which thickness is a key parameter. However, microstructural analysis shows that thickness is not uniform within a given tape and can vary significantly across material systems.

In the current approach, an average thickness value is used to approximate the cross section for conductivity calculations. While this simplification enables comparison between materials, it introduces a source of uncertainty, particularly for thin tapes exhibiting large thickness variations. This effect is especially pronounced in the DPR material, where the thickness ranges from approximately 60 to $100\ \mu m$. The use of a single representative value (closer to the upper bound of this range), results in an overestimation of the cross sectional area and, consequently, an underestimation of the calculated conductivity. This explains the significant deviation observed between the experimentally measured conductivity and the value predicted by the Rule of Mixtures.

To reduce the influence of this uncertainty, an alternative approach is considered in which the conductivity is recalculated using a normalised thickness. In this case, the thickness term is removed from the calculation, resulting in a parameter proportional to conductivity but expressed in units of S/m^2 rather than the conventional S/m. Although this normalised quantity does not represent a physical conductivity value, it provides a useful basis for comparing the relative electrical performance of the different material while minimising the impact of thickness variability.

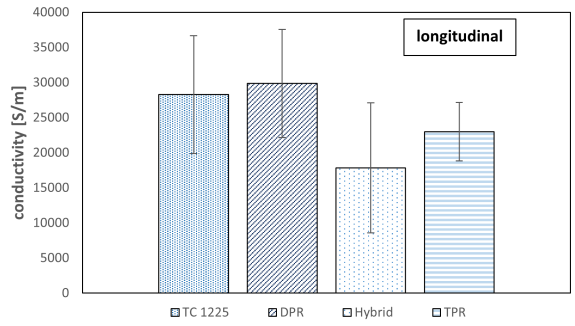

Figure 4.24: Longitudinal electrical conductivity of 4 UD tapes

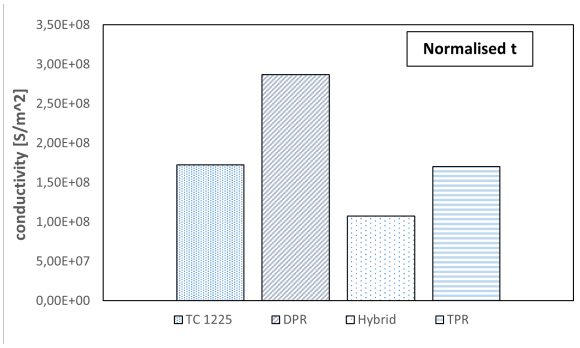

Figure 4.25: Longitudinal electrical conductivity of 4 UD tapes with normalised thickness

The comparison between the original and normalised results, shown in Figures 4.24 and 4.25, indicates that the overall ranking of the materials remains consistent. However, notable differences emerge when the effect of thickness uncertainty is reduced. In particular, the DPR tape exhibits a significant increase in relative conductivity, nearly doubling compared to its uncorrected value. This behaviour confirms that its electrical performance was previously underestimated due to the use of a non representative thickness value. Given its high FVF, this corrected trend is more consistent with expectations based on microstructural considerations.

In contrast, the Hybrid tape shows a relative decrease in performance under normalised conditions, suggesting that its low conductivity is primarily governed by its microstructural characteristics, namely, extensive polymer rich regions ad poor fibre connectivity, rather than geometric uncertainties. The TPR tape, when corrected for thickness variation, shows improved performance and approaches that of TC 1225, indicating that thickness effects contribute significantly to the initial discrepancy observed between these materials.

Furthermore, after correcting the measured conductivity for thickness uncertainty, the fibre volume fraction can also be normalised to enable comparison with the corresponding dry fibre conductivities used in the Rule of Mixtures in Table 4.2.

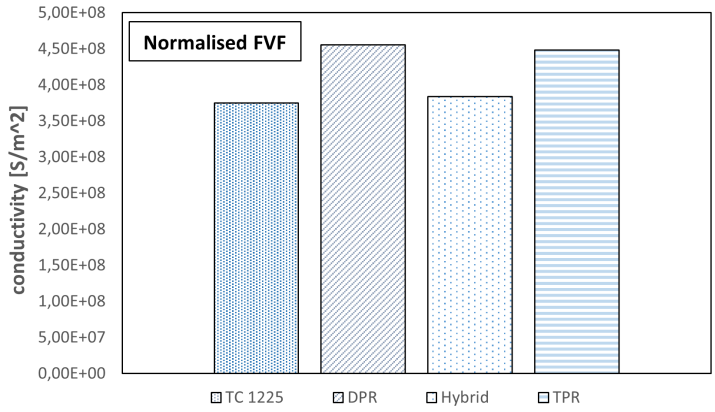

Figure 4.26: Longitudinal electrical conductivity of 4 UD tapes with normalised FVF

As shown in Figure 4.26, this normalisation yields consistent trends: DPR and TPR exhibit similar behaviour, as both use T800 carbon fibres ($77,000\ S/m$), while TC 1225 shows slightly lower conductivity ($67,000\ S/m$). Although the values are expressed in S/m^2 and are not directly comparable in magnitude, their relative behaviour is consistent. For instance, the ratio between TC 1225 and DPR dry fibre conductivity ($67,000/77,000\ =\ 0.87$) closely matches the ratio obtained from the normalised data ($=\ 0.83$), supporting the validity of the FVF and conductivity estimations.

In contrast, the Hybrid tape, despite combining T800 and M40J fibres and an expected higher average conductivity ($88,500\ S/m$), does not follow this trend. Its measured normalised conductivity remains below that of DPR and TPR. This discrepancy is attributed to its low FVF ($\approx 29\%$) and microstructural characteristics, where polymer rich regions and increased contact resistance hinder effective current flow, leading to an underestimation of conductivity in the six probe measurements.

Overall, this analysis highlights the importance of accurately accounting for geometric parameters in electrical characterisation. Thickness variations can introduce significant errors in conductivity calculations, particularly when simplified assumptions are applied. The normalisation approach shows that part of the observed electrical behaviour arises from measurement uncertainty rather than intrinsic material properties. Therefore, a more representative definition of the cross sectional area is needed, for example through spatially resolved thickness measurements or local conductivity mapping. Such approaches would improve accuracy and strengthen the link between manufacturing, microstructure, and electrical performance.

Finally, while fibre volume fraction and dry fibre conductivity are the primary drivers of electrical performance in UD TPC tapes, the results indicate that microstructure also plays a critical role, influencing both the measured response and the effectiveness of current transport.

4.3. Influence of Manufacturing Route on Microstructure and Electrical Behaviour

While the primary focus of this study is on the relationship between microstructure and electrical performance, the results also provide indirect insight into the influence of manufacturing routes on the final properties of UD TPC tapes. Although the tapes investigated were not manufactured within this work, the combination of electrical characterisation and microstructural analysis enables a qualitative comparison between industrially produced and in-house developed materials.

The industrial reference material, TC 1225, exhibits a well controlled microstructure characterised by relatively uniform fibre distribution, limited thickness variation, and moderate fibre volume fraction ($\approx 48\%$). Despite not having the highest FVF or the most conductive fibres, its electrical performance is comparable to that of higher FVF systems. This indicates a high level of manufacturing consistency and efficient fibre connectivity, reflecting the maturity of industrial processing routes.

In contrast, the in-house manufactured tapes show a stronger dependence of electrical behaviour on the specific impregnation technique. The DPR (dispersion based impregnation) tapes exhibit the highest FVF ($\approx 63\%$) and the smallest thickness, together with a relatively homogeneous microstructure and limited presence of polymer rich surface regions. This can be attributed to the nature of the dispersion process, in which fibres are passed through a slurry bath, allowing for more uniform wetting and polymer pickup prior to consolidation. As a result, DPR tapes demonstrate the highest acquired electrical conductivity, indicating efficient formation of conductive pathways.

Conversely, the TPR (thermoplastic extrusion impregnation) tapes show a lower FVF ($\approx 44\%$) and a heterogeneous microstructure, characterised by fibre concentration in the core and pronounced polymer rich regions at the surfaces. This behaviour is likely related to the impregnation mechanism, where molten polymer is introduced from the exterior and forced through the fibre tows. Such a process may limit complete and uniform impregnation, leading to non-uniform fibre distribution and reduced inter fibre contact. These features directly contribute to the lower and less stable electrical conductivity observed experimentally.

The limitations of the DPR process become evident in the Hybrid tape, where a combination of T800 and M40J fibres was used. Despite being manufactured using the same dispersion-based approach, this system exhibits the lowest FVF ($\approx 29\%$) and significant fibre segregation, with distinct bundles remaining poorly connected. This results in a substantial reduction in electrical performance, demonstrating that the effectiveness of a manufacturing route is strongly dependent on fibre type and compatibility.

Overall, these observations suggest that manufacturing route influences microstructural features such as fibre distribution, bundle connectivity, and the presence of polymer rich regions, which in turn affect electrical behaviour. However, no direct conclusions can be drawn regarding the superiority of one process over another. Instead, the results indicate that both processing route and parameters selection play an important role, and that further dedicated studies are required to isolate and quantify these effects.

To better account for these effects, an extension to the conventional Rule of Mixtures (ROM) can be proposed through the introduction of an impregnation efficiency coefficient:

$$\sigma \approx v_f \, \sigma_f \, \delta_{imp} \tag{4.2}$$

where δ_{imp} represents the effectiveness of the impregnation process in establishing conductive pathways. This coefficient can be interpreted as a function of microstructural quality, incorporating factors such as fibre contact, homogeneity, and interfacial polymer rich regions and resistance.

This modified formulation provides a more realistic framework for interpreting conductivity in UD TPC tapes, linking manufacturing process, microstructure, and electrical performance. It also highlights the potential for process optimisation to improve electrical behaviour, particularly for applications such as induction welding where efficient current transport is required.

4.4. Induction Welding Outlook

This section examines the implications of the electrical characterisation for induction welding of TPC structures. Although promising for aerospace assembly, induction welding remains a developing process, with heat generation and weld quality strongly dependent on processing parameters and current distribution.

To improve understanding, finite element method (FEM) simulations are commonly combined with experiments, requiring accurate input of anisotropic material properties. In this context, this study provides detailed conductivity data for UD TPC tapes, which are implemented into an FEM model.

A TC 1225 UD tape is modelled under static inductive heating conditions using the measured anisotropic conductivities, with the aim of reproducing the experimentally observed behaviour.

The results presented in this section therefore provide insight into the applicability of experimentally derived conductivity values for modelling purposes, and highlight potential pathways for improving the FEM based analysis of induction welding in UD TPC composites.

4.4.1. FEM Simulation of Static Induction Heating

A finite element method (FEM) model is developed to validate the electrical conductivity values obtained from the six probe measurements and to assess their ability to accurately reproduce the experimentally observed behaviour under inductive heating conditions. For this purpose, a TC 1225 UD tape is modelled to replicate the experimental setup used for static inductive heating of UD TPC tapes.

The simulation results are directly compared with the electrical characterisation data, as the measured conductivity values are used as input parameters in the model. Table 4.6 summarises the electrical conductivities assigned to each principal material direction, namely the longitudinal x, transverse y, and through thickness z directions, based on the six probe analysis.

While the transverse conductivity in the y directions was not directly measured, it is assumed, based on literature, that it is of the same order of magnitude as the though thickness conductivity. This assumption is justified by the unidirectional architecture of the tape, in which transverse electrical transport is similar to the through thickness direction.

Table 4.6: Electrical conductivity properties of UD TC 1225 tape input for FEM model

Orientation	**Electrical conductivity** $[S/m]$
σ_x	2.8×10^4
σ_y	0.4
σ_z	0.4

Table 4.6 summarises the electrical conductivity values used in the FEM model. As expected, the longitudinal conductivity σ_x is the highest, reflecting the dominant contribution of the aligned fibres on current transport in UD TPC tapes. This behaviour is characteristic of the strong anisotropy of these materials, where conductivity along the fibre direction is significantly higher than in the transverse and through thickness directions.

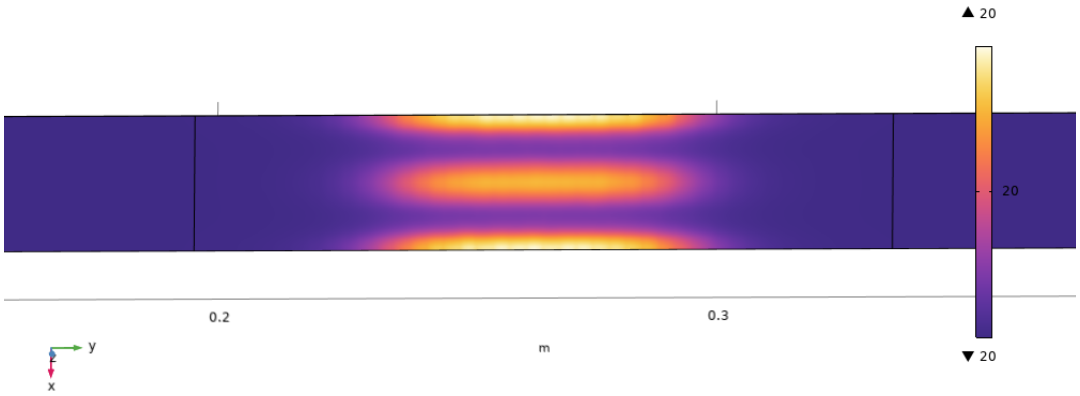

Figure 4.27: Top view heat map of simulated temperature distribution of TC 1225 tape after 1 second

Figure 4.27 presents a top view heat map of the simulated temperature distribution in the UD TPC tape following the application of an alternating current of $300\ A$ in the excitation coil. The results correspond to a time interval of 1 second after the magnetic field is introduced. The heat distribution follows the geometry of the pancake coil, reflecting the spatial profile of the induced magnetic field. However, no measurable temperature increase is observed, with the maximum temperature remaining equal to the initial room temperature. This indicates that the induced eddy currents are insufficient to generate significant Joule heating within the material under these conditions.

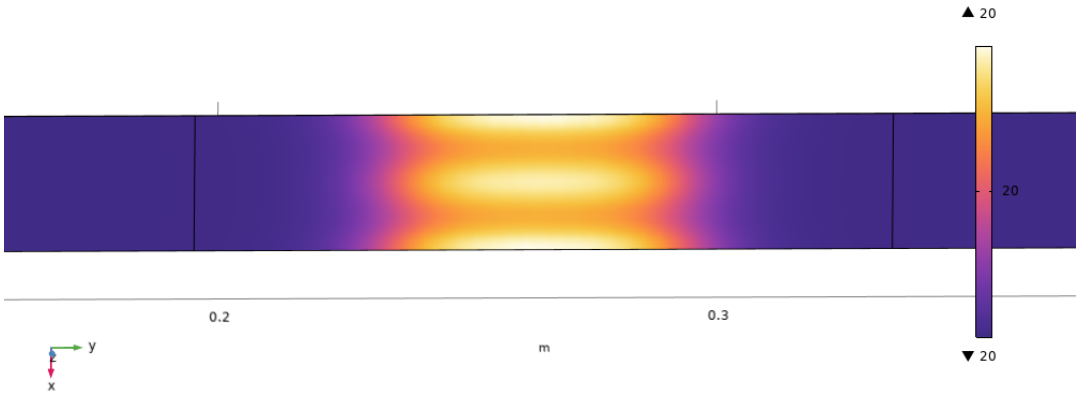

Figure 4.28: Top view heat map of simulated temperature distribution of TC 1225 tape after 10 second

Figure 4.28 shows the temperature distribution after 10 seconds of excitation. While the heat pattern becomes more homogeneous under the coil, the overall temperature remains unchanged, confirming that even over a longer time period, the induced currents do not lead to meaningful heat generation.

It is important to mention that, in experimental induction heating of TPC composites, temperature increases are typically observed within a few seconds. Therefore, simulation times are limited to a maximum of 10 seconds in order to capture the relevant thermal response while maintaining reasonable computational cost.

The FEM results suggest that, under the simulated conditions, UD TPC tapes are not able to generate sufficient eddy currents at the relatively low frequencies associated with the applied excitation. This behaviour can be attributed to the pronounced anisotropy in electrical conductivity, particularly the large difference between longitudinal and through thickness conductive pathways. As a result, current flow is constrained, limiting the formation of eddy current loops required for efficient inductive heating.

These findings highlight the challenges associated with controlling current distribution and heat generation in UD TPC materials, and emphasises the critical role of anisotropic electrical properties in determining their response to induction processes.

4.4.2. Experimental Induction Heating Validation

To validate the FEM results presented above, a static inductive heating experiment is conducted at SAM XL. Due to technical issues with the infrared thermography system, it was not possible to record images for the UD TPC tape during testing.

Nevertheless, qualitative observations from the experiment indicate that the TC 1225 UD tape did not exhibit any measurable temperature increase and remained at approximately room temperature throughout the test. This behaviour is consistent with the FEM predictions, confirming that the model is appropriately defined and that the electrical conductivity values obtained from the characterisation study provide a realistic representation of the material response under given conditions.

As the UD tape did not show significant eating, an additional experiment is performed using an eight layer woven laminate in order to further investigate the inductive heating behaviour.

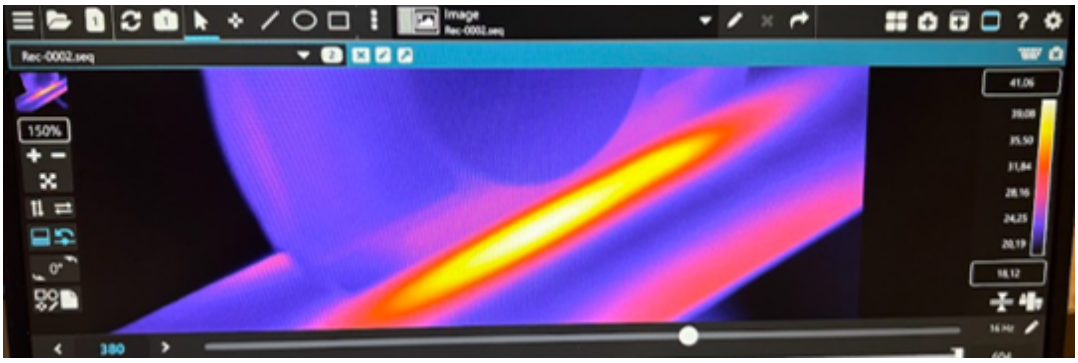

Figure 4.29: IR thermography results for woven laminate under $300\ A$ coil excitation

Figure 4.29 presents the infrared thermography results for this laminate. In contrast to the UD tape, the woven laminate exhibits a rapid temperature increase, reaching approximately $41°\mathrm{C}$ within a few seconds. A qualitative comparison suggests that the resulting heat distribution shares some similarities with the spatial pattern indicated by the FEM model.

To further explore this behaviour, the woven laminate is also simulated using the FEM model. Given its woven architecture, the material is expected to exhibit a more isotropic electrical response than the UD tape, as fibre interlacing promotes conductive pathways in multiple directions. For the purpose of this study, and to enable a first order comparison, a simplified conductivity assumption is adopted in which the same conductivity value is assigned to all principal directions (x, y, and z), as summarised in Table 4.7.

This approximation is based on the modelling framework proposed by *Han et al.* [59], which, through a percolation based approach described in Section 2.2.4, suggests that $\sigma_y \simeq \sigma_z$ for textile based composites. Extending this assumption to woven architectures, it is assumed here that $\sigma_x \simeq \sigma_y$, resulting in an effectively isotropic conductivity tensor. The laminate is also assumed to consist of T800 carbon fibres. It should be emphasised that this represents a strong simplification adopted solely for the purpose of enabling the numerical study and qualitative comparison, rather than a fully representative material description.

Table 4.7: Electrical conductivity properties of woven laminate input for FEM model

Orientation	**Electrical conductivity** $[S/m]$
σ_x	2.8×10^4
σ_y	2.8×10^4
σ_z	2.8×10^4

These properties are then implemented in the model to simulate the inductive response of the laminate.

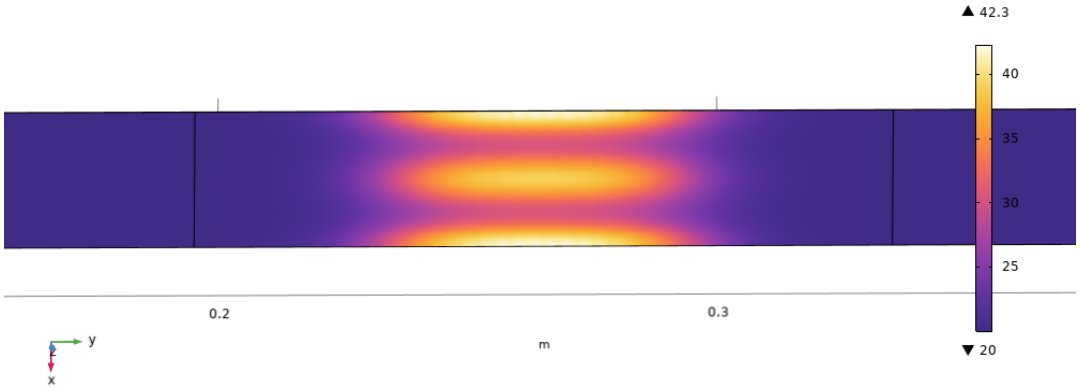

Figure 4.30: Top view heat map of simulated temperature distribution of woven laminate after 3 second

The resulting temperature distribution, shown in Figure 4.30, indicates a rapid increase in temperature over a short time interval, with a spatial pattern and peak temperature that show qualitative similarity to the experimental thermography results. However, given the simplified and highly idealised material assumptions used in the model, particularly the isotropic conductivity approximation and the assumed fibre properties, the agreement should be interpreted cautiously and primarily in a qualitative sense rather than as a quantitative validation.

These findings provide qualitative support for the FEM model while also highlighting the strong influence of material architecture on inductive heating behaviour. In particular, the comparison between the UD tape and the woven laminate illustrates the role of electrical anisotropy in governing eddy current development and the resulting heat generation. While the observed agreement is encouraging, it should be interpreted in the context of the simplified modelling assumptions. Nevertheless, the results underline the importance of considering material architecture when designing and optimising induction welding processes for thermoplastic composites.

4.4.3. FEM Modelling and Microstructural Features

As discussed in the infrared thermography results, the surface condition of each material system plays a significant role in determining how current pathways are established within UD TPC tapes. In particular, materials such as TPR and Hybrid tapes exhibit non uniform current injection, which can be attributed to the presence of polymer rich surface films. These regions increase local electrical resistivity and act as barriers to current injection, thereby influencing both the distribution and efficiency of conductive pathways.

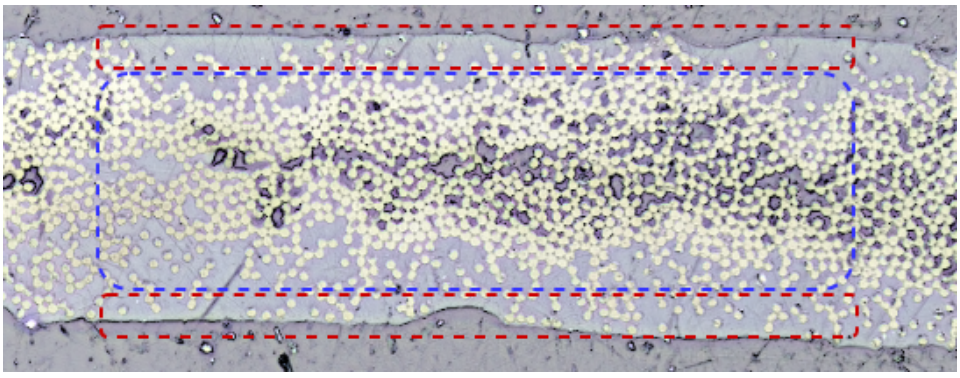

Figure 4.31: Cross section of TPR tape with polymer rich regions highlighted in red and bulk fibre concentration highlighted in blue

Figure 4.31 presents the micrograph of a TPR tape, where distinct polymer rich areas are visible at both surfaces. These regions, highlighted by red dotted rectangles, contrast with the central region of the tape (blue rectangle), where fibre concentration is highest and the primary conductive network

is established. This separation between the insulating regions and the conductive core suggests that electrical behaviour is governed not only by bulk properties but also by surface and interfacial effects.

Extending this observation to multi ply UD TPC laminates, it is reasonable to assume that similar polymer rich layers may form at the interfaces between adjacent plies during consolidation. The presence of such interfacial regions could significantly alter the three dimensional fibre network by reducing fibre-fibre contact through the thickness. As a result, both total longitudinal and through thickness conductivities may be further limited, affecting the formation of eddy current loops and the overall efficiency of inductive heating.

To improve the predictive capability of FEM simulations, it is therefore important to incorporate these microstructural features into the modelling framework. This could be achieved by explicitly defining interfacial regions with reduced FVF and correspondingly lower electrical conductivity. Such an approach would enable a more realistic representation of the anisotropic architecture and its effect on electrical performance.

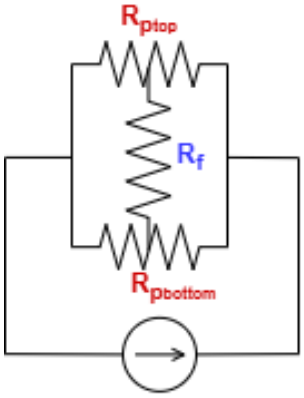

Figure 4.32: Top view heat map of simulated temperature distribution of woven laminate after 3 second

This concept can be related to the equivalent electrical circuit introduced in the six probe methodology and illustrated again in Figure 4.32, where the surface regions (highlighted in red) can be interpreted as resistive layers R_{ptop} and $R_{pbottom}$, while the bulk of the material (blue region of micrograph) represent the respective conductive pathway R_f. Including this layered behaviour into FEM models would allow for a more accurate simulation of current distribution and heat generation in UD TPC composites.

Overall, this analysis highlights the importance of considering microstructural heterogeneity, particularly surface and interfacial effects, in the modelling of electrical behaviour in UD TPC composites. Future FEM developments that include these features are expected to provide improved correlation with experimental observations and improve the reliability of simulations for the induction welding process.

4.5. In-situ Quality Control for Tape Manufacturing

This study established a direct relationship between the electrical conductivity of UD TPC tapes, their microstructural features, and the associated manufacturing routes. By combining six probe electrical measurements with infrared thermography, it has been shown that electrical behaviour can serve as a sensitive indicator of fibre architecture, polymer distribution, and overall material quality. Furthermore, these findings provide valuable input for improving FEM models of induction welding processes.

Beyond modelling applications, the results of this study can also highlight a significant opportunity for practical implementation in manufacturing. In particular, electrical characterisation can be utilised as a tool for in-situ quality control of UD TPC tapes during production. Since electrical conductivity and current pathway distribution are directly influenced by fibre volume fraction, fibre connectivity, and surface condition, they can be used as indirect but reliable indicators of microstructural quality.

In current in-line tape manufacturing processes, such as TPR and DPR routes, quality assessment is largely based on operator experience and post processing evaluation. The absence of real-time monitoring limits the ability to detect defects during production. Integrating an in-situ electrical characterisation step within the tape line could therefore provide immediate feedback on material quality, enabling more controlled and consistent manufacturing.

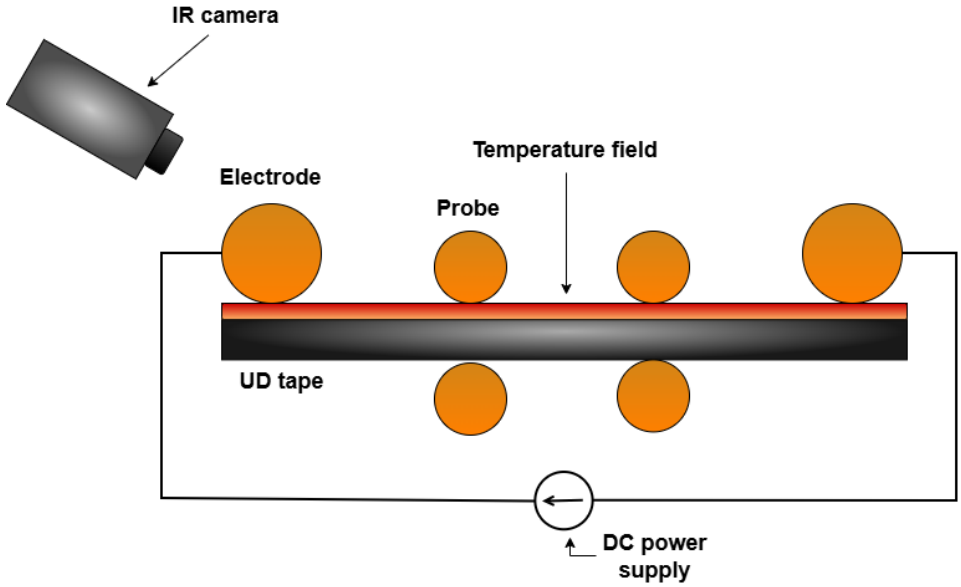

Figure 4.33: Schematic view of six probe and IR thermography for in-situ quality control for tape manufacturing

A potential implementation involves adapting the six probe measurement principle to a continuous production line. Instead of fixed electrodes, cylindrical probes could be used to maintain electrical injection with the moving tape while preserving the required tension and continuity of the process, as illustrated in Figure 4.33. By applying a low current, the longitudinal conductivity of the tape could be measured in real time without interfering with the manufacturing operation.

Based on the findings of this study, the measured conductivity values can be correlated with expected FVF and overall microstructural quality. For example, lower conductivity or significant deviations from expected ranges may indicate poor fibre distribution, increased resin rich regions, or inadequate consolidation. In addition, unstable or noisy voltage signals can serve as an indicator for poor surface quality, such as the presence of insulating polymer rich films that affect electrical contact.

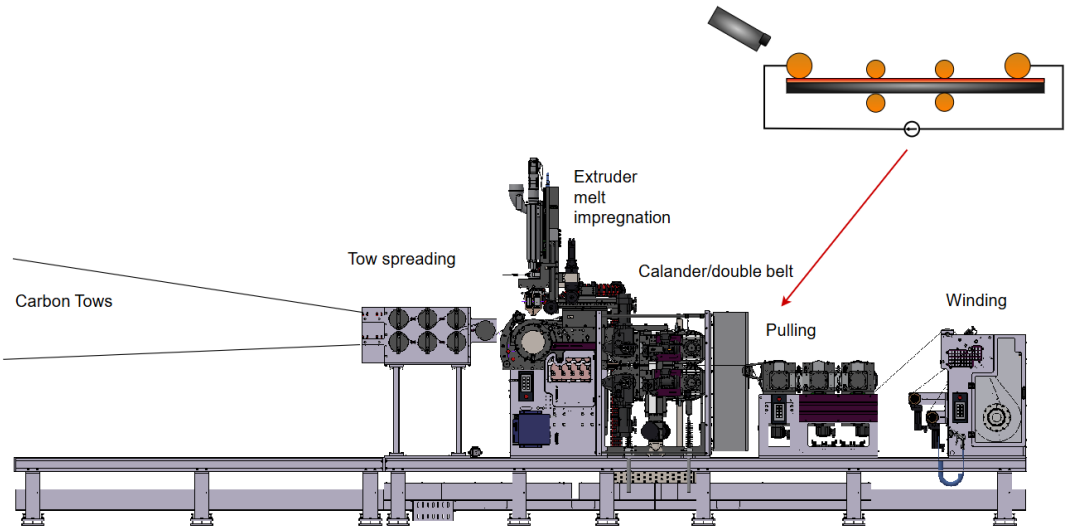

Figure 4.34: Schematic view of in-situ placement in TPR tape production line

As shown schematically in Figure 4.34, such a system could be implemented at the end of the tape production line, after consolidation and cooling where the calander is placed, and before winding onto a bobbin. Complementing this setup with infrared thermography would provide further insight into current pathway distribution. A homogeneous thermal response would indicate efficient fibre-electrode contact and well distributed conductive pathways, whereas localised heating patterns would suggest microstructural heterogeneity or local defects.

The integration of this approach would enable real-time monitoring and process optimisation. By adjusting manufacturing parameters during production and immediately observing their effect on electrical behaviour, it becomes possible to establish a more robust and efficient manufacturing process.

Overall, this work demonstrates that electrical characterisation techniques, when combined with thermal imaging, offer a powerful and practical solution for in-situ quality control of UD TPC tape manufacturing. This approach has the potential to significantly improve process reliability, reduce defects, and enhance the performance consistency of composites.

5

Conclusion

This study investigated the relationship between manufacturing route, microstructure, and electrical behaviour of unidirectional thermoplastic composite tapes, with an outlook on their applicability in induction welding process.

The work was guided by the main research question: *How do microstructural features and manufacturing routes of unidirectional thermoplastic composite (UD TPC) tapes influence their electrical conductivity and current pathway formation, and how can these relationship be utilised for improved characterisation and process application?*.

To address this, a structured experimental and analytical methodology was developed, combining electrical characterisation, infrared thermography, eddy current testing, microstructural analysis, and static inductive simulations and experiments.

The results demonstrate that the electrical behaviour of UD TPC tapes is strongly governed by both microstructural features and manufacturing route.

Firstly, electrical conductivity measurements obtained using the six probe method were found to be consistent with literature values, confirming the validity of the approach. However, significant deviations from the idealised Rule of Mixtures were observed. These deviations highlight that electrical conductivity in UD TPC tapes can not be described solely by fibre volume fraction, but is strongly influenced by local microstructural variations.

Among the investigated materials, DPR tapes exhibited the highest conductivity, followed by TC 1225, TPR and Hybrid tapes. This trend correlates directly with the measured fibre volume fraction, confirming that increased fibre content enhances conductive pathway formation. Nevertheless, FVF alone does not fully explain the observed behaviour, as local features such as fibre distribution, defects, and polymer rich regions significantly alter the effective conductivity.

Microstructural analysis revealed clear differences between manufacturing routes. DPR tapes exhibited high FVF and relatively uniform fibre distribution, resulting in efficient conductive networks. TC 1225 tapes showed stable and homogeneous behaviour with moderate FVF and limited thickness variation. In contrast, TPR and Hybrid tapes displayed heterogeneous fibre architectures, with significant resin rich regions particularly at the surfaces, and higher defect content. These features resulted in reduced conductivity and increased measurement instability.

Infrared thermography and eddy current testing further confirmed the influence of microstructure on current pathway formation. Materials with more homogeneous fibre networks (TC1225 and DPR) exhibited distributed current pathways, while TPR and Hybrid tapes showed highly localised conduction. These observations demonstrate that electrical transport in UD TPC tapes is governed by the connectivity of fibre network rather than by bulk material properties alone.

The study also highlighted important limitations and considerations in electrical characterisation. The six probe method, while effective, relies on simplified geometric assumptions, particularly regarding

cross sectional area. Microstructural analysis showed that tape thickness varies significantly, introducing uncertainty in conductivity calculations. This effect was particularly evident for DPR tapes, where large thickness variations led to underestimation of conductivity when using averaged thickness values.

To address this, a normalised approach was introduced to reduce the influence of thickness uncertainty. This revealed that DPR tapes exhibit significantly higher intrinsic conductivity than initially calculated, reinforcing the importance of accurate geometric representation in electrical measurements.

Additionally, the results demonstrated that contact conditions between electrodes and the material surface play a critical role. Polymer rich surface layers were found to increase contact resistance, leading to localised current injection and unstable measurements. This was further confirmed through experiments on an 8 layer laminate, where removal of surface polymer layers restored expected conductivity values and improved current distribution.

The findings of this study have implications for induction based processing of composite structures. Due to their strong electrical anisotropy, UD TPC tapes exhibit limited current flow in the transverse and through thickness directions, which restricts their ability to generate heat under inductive excitation when considered in isolation. This was observed experimentally, where UD tapes showed minimal heating compared to woven laminates, which heated more rapidly due to their more isotropic conductive network.While individual UD tapes are not typically heated directly in practical applications, these results highlight the importance of material architecture in governing heat generation during induction welding of composite structures.

A finite element method (FEM) model was developed to simulate this behaviour and validated against experimental results. The model confirmed that sufficient transverse conductivity is required to enable efficient inductive heating. Furthermore, the results suggest that microstructural features such as polymer rich interfacial layers may further limit current transfer between plies, highlighting the need to incorporate such features in future modelling effort.

Beyond fundamental understanding, this work demonstrates the potential of electrical characterisation as a tool for manufacturing quality control. The correlation between electrical conductivity, current pathway distribution, and microstructural quality enables indirect assessment of fibre architecture, impregnation and consolidation quality.

This opens the possibility for in-situ monitoring of tape manufacturing processes. By measuring conductivity and analysing signal stability in real time, it would be possible to detect defects such as polymer rich surfaces or poor fibre distribution during production. Such an approach could significantly improve process control and material consistency.

Overall, this study demonstrates that the electrical behaviour of UD TPC tapes is governed by a complex interplay between fibre content, microstructural organisation, and manufacturing induced variability. It highlights the limitations of idealised models and emphasises the importance of multi-scale characterisation in understanding and predicting composite material behaviour.

This work provides insight into the relationship between manufacturing route, microstructure, and electrical performance, and offers useful considerations for the characterisation and development of composite materials.

To further advance this research, the following developments are recommended:

- Implementation of spatially resolved conductivity measurements to capture local variations more accurately
- Improved modelling of cross sectional geometry and thickness variation in electrical calculations
- Integration of microstructural features, such as polymer rich interfacial layers, into FEM simulations
- Implementation of the six probe measurement to a structure that supports in-situ quality control for the tape line production

References

[1] Yongxian Huang et al. “Friction spot welding of carbon fiber-reinforced polyetherimide laminate”. In: *Composite Structures* 189 (Apr. 2018), pp. 627–634. issn: 02638223. doi: 10.1016/j.compstruct.2018.02.004.

[2] Wenjie Ni et al. “Effect of Carbon Fiber Fabric Areal Density on Resistance Welded Joint of Thermoplastic Composites”. In: *Polymer Composites* (July 2025). issn: 0272-8397. doi: 10.1002/pc.70162.

[3] Sebastiaan van den Berg et al. “Thermal response of an induction-heated fabric reinforced thermoplastic composite with anisotropic electrical conductivity: An experimental study”. In: *Journal of Thermoplastic Composite Materials* 37 (5 May 2024), pp. 1877–1892. issn: 0892-7057. doi: 10.1177/08927057231201353.

[4] M. Dubé et al. “Resistance welding of thermoplastic composites skin/stringer joints”. In: *Composites Part A: Applied Science and Manufacturing* 38 (12 Dec. 2007), pp. 2541–2552. issn: 1359835X. doi: 10.1016/j.compositesa.2007.07.014.

[5] C. Ageorges, L. Ye, and M. Hou. “Advances in fusion bonding techniques for joining thermoplastic matrix composites: a review”. In: *Composites Part A: Applied Science and Manufacturing* 32 (6 June 2001), pp. 839–857. issn: 1359835X. doi: 10.1016/S1359-835X(00)00166-4.

[6] Christian Hopmann et al. “Investigation of the influence of melt-impregnation parameters on the morphology of thermoplastic UD-tapes and a method for quantifying the same”. In: *Journal of Thermoplastic Composite Materials* 34 (9 Sept. 2021), pp. 1299–1312. issn: 0892-7057. doi: 10.1177/0892705719864624.

[7] K K C Ho et al. “Wet impregnation as route to unidirectional carbon fibre reinforced thermoplastic composites manufacturing”. In: *Plastics, Rubber and Composites* 40 (2 Mar. 2011), pp. 100–107. issn: 1465-8011. doi: 10.1179/174328911X12988622801098.

[8] {Yannick Martijn} Buser. “Predicting induction heating of tape-based thermoplastic composites: The role of orthotropic electrical conductivity”. English. PhD Thesis - Research UT, graduation UT. Netherlands: University of Twente, Feb. 2025. isbn: 978-90-365-6469-4. doi: 10.3990/1.9789036564700.

[9] K.W. Tse, C.A. Moyer, and S. Arajs. “Electrical conductivity of graphite fiber-epoxy resin composites”. In: *Materials Science and Engineering* 49 (1 June 1981), pp. 41–46. issn: 00255416. doi: 10.1016/0025-5416(81)90131-2.

[10] Wouter J. B. Grouve et al. “Simulating the induction heating of cross-ply C/PEKK laminates – sensitivity and effect of material variability”. In: *Advanced Composite Materials* 30 (5 Sept. 2021), pp. 409–430. issn: 0924-3046. doi: 10.1080/09243046.2020.1783078.

[11] Fredrik Lundström, Kenneth Frogner, and Mats Andersson. “A numerical model to analyse the temperature distribution in cross-ply CFRP during induction heating”. In: *Composites Part B: Engineering* 202 (Dec. 2020), p. 108419. issn: 13598368. doi: 10.1016/j.compositesb.2020.108419.

[12] van Hoorn. N et al. *Machine Learning Assisted Induction Welding Simulations of Thick Unidirectional Carbon Fibre Reinforced Thermoplastic Polymer Laminates*. Tech. rep. May 2025. url: https://www.linkedin.com/company/nafems/.

[13] Patrice Gouin O’Shaughnessey, Martine Dubé, and Irene Fernandez Villegas. “Modeling and experimental investigation of induction welding of thermoplastic composites and comparison with other welding processes”. In: *Journal of Composite Materials* 50 (21 Sept. 2016), pp. 2895–2910. issn: 0021-9983. doi: 10.1177/0021998315614991.

[14] G. Gardiner. *Welding thermoplastic composites*. 2018. url: https://www.compositesworld.com/articles/welding-thermoplastic-composites.

[15] M. Labordus et al. “Induction welding of carbon fibre reinforced additive manufactured parts, in: Proceedings of the SAMPE Europe Conference 2019, Nantes, France”. In: (2019), pp. 251–259.

[16] Pratik Koirala et al. “Investigating interfacial properties vs interphase thickness in a thermoplastic composite”. In: *Composites Part B: Engineering* 299 (June 2025), p. 112444. issn: 13598368. doi: 10.1016/j.compositesb.2025.112444.

[17] Hui Quan et al. “On transcrystallinity in semi-crystalline polymer composites”. In: *Composites Science and Technology* 65 (7-8 June 2005), pp. 999–1021. issn: 02663538. doi: 10.1016/j.compscitech.2004.11.015.

[18] J. L. Thomason and A. A. Van Rooyen. “Transcrystallized interphase in thermoplastic composites”. In: *Journal of Materials Science* 27 (4 Feb. 1992), pp. 889–896. issn: 0022-2461. doi: 10.1007/BF01197638.

[19] J. Jäger et al. “Influence of plastic deformation on single-fiber push-out tests of carbon fiber reinforced epoxy resin”. In: *Composites Part A: Applied Science and Manufacturing* 71 (Apr. 2015), pp. 157–167. issn: 1359835X. doi: 10.1016/j.compositesa.2015.01.011.

[20] Helena Pérez-Martín et al. “Crystallinity studies of PEKK and carbon fibre/PEKK composites: A review”. In: *Composites Part B: Engineering* 223 (Oct. 2021), p. 109127. issn: 13598368. doi: 10.1016/j.compositesb.2021.109127.

[21] T.K. Slange et al. “Rapid Manufacturing of a Tailored Spar by AFP and Stamp Forming”. English. In: *ITHEC 2018*. Ed. by Hubert Borgmann. 4th International Conference and Exhibition on Thermoplastic Composites, ITHEC 2018, ITHEC ; Conference date: 30-10-2018 Through 31-10-2018. Germany: Messe Bremen GmbH, Oct. 2018. isbn: 9783933339317. url: https://www.ithec.de.

[22] F. Fischer et al. “How to produce a thermoplastic fuselage”. In: *Proceedings of the 6th International Conference & Exhibition on Thermoplastic Composites, ITHEC 2022*. Bremen, Germany, 2022, pp. 50–54.

[23] Arnt R. Offringa. “Thermoplastic composites—rapid processing applications”. In: *Composites Part A: Applied Science and Manufacturing* 27.4 (1996). 4th International Conference on Automated Composites, pp. 329–336. issn: 1359-835X. doi: https://doi.org/10.1016/1359-835X(95)00048-7. url: https://www.sciencedirect.com/science/article/pii/1359835X95000487.

[24] P. Peltonen et al. “The Influence of Melt Impregnation Parameters on the Degree of Impregnation of a Polypropylene/Glass Fibre Prepreg”. In: *Journal of Thermoplastic Composite Materials* 5 (4 Oct. 1992), pp. 318–343. issn: 0892-7057. doi: 10.1177/089270579200500404.

[25] S. P. Neuman. “Theoretical derivation of Darcy’s law”. In: *Acta Mechanica* 25 (3-4 Sept. 1977), pp. 153–170. issn: 0001-5970. doi: 10.1007/BF01376989.

[26] Per Nygard and Claes-Goran Gustafson. “Continuous Glass Fiber–Polypropylene Composites Made by Melt Impregnation: Influence of Processing Method”. In: *Journal of Thermoplastic Composite Materials* 17 (2 Mar. 2004), pp. 167–184. issn: 0892-7057. doi: 10.1177/0892705704035406.

[27] R Cano, H Belvin, B Hulcher, et al. “Studies on automated manufacturing of high performance composites”. In: *Proceedings of the Structure Specialist Meeting*. Williamsburg, USA, Nov. 2001.

[28] Peter J. Joyce, Danielle Kugler, and Tess J. Moon. “A Technique for Characterizing Process-Induced Fiber Waviness in Unidirectional Composite Laminates-Using Optical Microscopy”. In: *Journal of Composite Materials* 31 (17 Sept. 1997), pp. 1694–1727. issn: 0021-9983. doi: 10.1177/002199839703101702.

[29] Karthik Ramani and Chris Hoyle. “Processing of Thermoplastic Composites Using a Powder Slurry Technique. I. Impregnation and Preheating”. In: *Materials and Manufacturing Processes* 10 (6 Nov. 1995), pp. 1169–1182. issn: 1042-6914. doi: 10.1080/10426919508935100.

[30] Karthik Ramani, Daniel E. Woolard, and Mark S. Duvall. “An electrostatic powder spray process for manufacturing thermoplastic composites”. In: *Polymer Composites* 16 (6 Dec. 1995), pp. 459–469. issn: 0272-8397. doi: 10.1002/pc.750160604.

[31] J. C. Maxwell. *Electricity and Magnetism*. Oxford, U.K.: Claredon Press, 1973.

[32] S. Mahdi et al. “A Comparison of Oven-cured and Induction-cured Adhesively Bonded Composite Joints”. In: *Journal of Composite Materials* 37 (6 Mar. 2003), pp. 519–542. issn: 0021-9983. doi: 10.1177/0021998303037006776.

[33] Bruce K. Fink, Roy L. McCullough, and John W. Gillespie. “A local theory of heating in cross□ply carbon fiber thermoplastic composites by magnetic induction”. In: *Polymer Engineering & Science* 32 (5 Mar. 1992), pp. 357–369. issn: 0032-3888. doi: 10.1002/pen.760320509.

[34] Shridhar Yarlagadda et al. “A Study on the Induction Heating of Conductive Fiber Reinforced Composites”. In: *Journal of Composite Materials* 36 (4 Feb. 2002), pp. 401–421. issn: 0021-9983. doi: 10.1177/0021998302036004171.

[35] Darun Barazanchy and Michel van Tooren. “Heating mechanisms in induction welding of thermoplastic composites”. In: *Journal of Thermoplastic Composite Materials* 36 (2 Feb. 2023), pp. 473–492. issn: 0892-7057. doi: 10.1177/08927057211011621.

[36] Heejune Kim et al. “A study on the induction heating of carbon fiber reinforced thermoplastic composites”. In: *Advanced Composite Materials* 11 (1 Jan. 2002), pp. 71–80. issn: 0924-3046. doi: 10.1163/156855102753613309.

[37] Xiaojuan Xu et al. “Interlaminar contact resistivity and its influence on eddy currents in carbon fiber reinforced polymer laminates”. In: *NDT & E International* 94 (Mar. 2018), pp. 79–91. issn: 09638695. doi: 10.1016/j.ndteint.2017.12.003.

[38] A.J de Wit, N van Hoorn, and W.J Vankan. *Numerical simulation of eddy current generation in uni-directional thermoplastic composites*. Tech. rep. Netherlands Aerospace Centre NLR, 2023.

[39] Florian H. Gojny et al. “Evaluation and identification of electrical and thermal conduction mechanisms in carbon nanotube/epoxy composites”. In: *Polymer* 47 (6 Mar. 2006), pp. 2036–2045. issn: 00323861. doi: 10.1016/j.polymer.2006.01.029.

[40] Seung Hwan Lee et al. “Rheological and electrical properties of polypropylene composites containing functionalized multi-walled carbon nanotubes and compatibilizers”. In: *Carbon* 45 (14 Nov. 2007), pp. 2810–2822. issn: 00086223. doi: 10.1016/j.carbon.2007.08.042.

[41] Tapas Kuilla et al. “Recent advances in graphene based polymer composites”. In: *Progress in Polymer Science* 35 (11 Nov. 2010), pp. 1350–1375. issn: 00796700. doi: 10.1016/j.progpolymsci.2010.07.005.

[42] Jiahua Zhu et al. “Magnetic Epoxy Resin Nanocomposites Reinforced with Core−Shell Structured Fe@FeO Nanoparticles: Fabrication and Property Analysis”. In: *ACS Applied Materials & Interfaces* 2 (7 July 2010), pp. 2100–2107. issn: 1944-8244. doi: 10.1021/am100361h.

[43] Mohammad Moniruzzaman and Karen I. Winey. “Polymer Nanocomposites Containing Carbon Nanotubes”. In: *Macromolecules* 39 (16 Aug. 2006), pp. 5194–5205. issn: 0024-9297. doi: 10.1021/ma060733p.

[44] Jiahua Zhu et al. “Rheological behaviors and electrical conductivity of epoxy resin nanocomposites suspended with in-situ stabilized carbon nanofibers”. In: *Polymer* 51 (12 May 2010), pp. 2643–2651. issn: 00323861. doi: 10.1016/j.polymer.2010.04.019.

[45] Jiahua Zhu et al. “Surfactant-Free Synthesized Magnetic Polypropylene Nanocomposites: Rheological, Electrical, Magnetic, and Thermal Properties”. In: *Macromolecules* 44 (11 June 2011), pp. 4382–4391. issn: 0024-9297. doi: 10.1021/ma102684f.

[46] Marjan Alsadat Kashfipour, Nitin Mehra, and Jiahua Zhu. “A review on the role of interface in mechanical, thermal, and electrical properties of polymer composites”. In: *Advanced Composites and Hybrid Materials* 1 (3 Sept. 2018), pp. 415–439. issn: 2522-0128. doi: 10.1007/s42114-018-0022-9.

[47] Sasha Stankovich et al. “Graphene-based composite materials”. In: *Nature* 442 (7100 July 2006), pp. 282–286. issn: 0028-0836. doi: 10.1038/nature04969.

[48] Young Seok Song and Jae Ryoun Youn. “Influence of dispersion states of carbon nanotubes on physical properties of epoxy nanocomposites”. In: *Carbon* 43 (7 June 2005), pp. 1378–1385. issn: 00086223. doi: 10.1016/j.carbon.2005.01.007.

[49] J.K.W. Sandler et al. “Ultra-low electrical percolation threshold in carbon-nanotube-epoxy composites”. In: *Polymer* 44 (19 Sept. 2003), pp. 5893–5899. issn: 00323861. doi: 10.1016/S0032-3861(03)00539-1.

[50] Aiping Yu et al. “Enhanced Thermal Conductivity in a Hybrid Graphite Nanoplatelet – Carbon Nanotube Filler for Epoxy Composites”. In: *Advanced Materials* 20 (24 Dec. 2008), pp. 4740–4744. issn: 0935-9648. doi: 10.1002/adma.200800401.

[51] Hun-Sik Kim et al. “Nylon 610/functionalized multiwalled carbon nanotubes composites by in situ interfacial polymerization”. In: *Materials Letters* 61 (11-12 May 2007), pp. 2251–2254. issn: 0167577X. doi: 10.1016/j.matlet.2006.08.057.

[52] Rajagopal Ramasubramaniam, Jian Chen, and Haiying Liu. “Homogeneous carbon nanotube/polymer composites for electrical applications”. In: *Applied Physics Letters* 83 (14 Oct. 2003), pp. 2928–2930. issn: 0003-6951. doi: 10.1063/1.1616976.

[53] Li-Feng Ma et al. “Conductive thermoplastic vulcanizates (TPVs) based on polypropylene (PP)/ethylene-propylene-diene rubber (EPDM) blend: From strain sensor to highly stretchable conductor”. In: *Composites Science and Technology* 128 (May 2016), pp. 176–184. issn: 02663538. doi: 10.1016/j.compscitech.2016.04.001.

[54] V. Šafářová and J. Grégr. “Electrical conductivity measurement of fibers and yarns”. In: *Proceedings of the 7th International Conference on Textile Science, TEXSCI 2010*. Liberec, Czech Republic, 2010.

[55] Bradley A. Newcomb. “Processing, structure, and properties of carbon fibers”. In: *Composites Part A: Applied Science and Manufacturing* 91 (Dec. 2016), pp. 262–282. issn: 1359835X. doi: 10.1016/j.compositesa.2016.10.018.

[56] J Abry. “In situ detection of damage in CFRP laminates by electrical resistance measurements”. In: *Composites Science and Technology* 59 (6 May 1999), pp. 925–935. issn: 02663538. doi: 10.1016/S0266-3538(98)00132-8.

[57] Yelda Akcin, Sukru Karakaya, Omer Soykasap, et al. “Electrical, thermal and mechanical properties of CNT treated prepreg CFRP composites”. In: *Materials Sciences and Applications* 7.09 (2016), p. 465.

[58] J H Greenwood, S Lebeda, and J Bernasconi. “The anisotropic electrical resistivity of a carbon fibre reinforced plastic disc and its use as a transducer”. In: *Journal of Physics E: Scientific Instruments* 8 (5 May 1975), pp. 369–370. issn: 0022-3735. doi: 10.1088/0022-3735/8/5/010.

[59] Chaofeng Han, Baozhong Sun, and Bohong Gu. “Electric conductivity and surface potential distributions in carbon fiber reinforced composites with different ply orientations”. In: *Textile Research Journal* 92 (7-8 Apr. 2022), pp. 1147–1160. issn: 0040-5175. doi: 10.1177/00405175211048160.

[60] Robert J Hart and OI Zhupanska. “The role of electrical anisotropy and effective conducting thickness in understanding and interpreting static resistance measurements in CFRP composite laminates”. In: *Journal of Composite Materials* 54 (7 Mar. 2020), pp. 867–882. issn: 0021-9983. doi: 10.1177/0021998319870860.

[61] Yoshiyasu Hirano, Takuya Yamane, and Akira Todoroki. “Through-thickness electric conductivity of toughened carbon-fibre-reinforced polymer laminates with resin-rich layers”. In: *Composites Science and Technology* 122 (Jan. 2016), pp. 67–72. issn: 02663538. doi: 10.1016/j.compscitech.2015.11.018.

[62] H C Kim and S K See. “Electrical properties of unidirectional carbon-epoxy composites in wide frequency band”. In: *Journal of Physics D: Applied Physics* 23 (7 July 1990), pp. 916–921. issn: 0022-3727. doi: 10.1088/0022-3727/23/7/026.

[63] J B Park et al. “Experimental and numerical study of the electrical anisotropy in unidirectional carbon-fiber-reinforced polymer composites”. In: *Smart Materials and Structures* 16 (1 Feb. 2007), pp. 57–66. issn: 0964-1726. doi: 10.1088/0964-1726/16/1/006.

[64] Jin□Na Zhang et al. “Prediction on electrical resistivity of thin□ply unidirectional composites considering electric tunnel effect”. In: *Polymer Composites* 41 (10 Oct. 2020), pp. 4318–4328. issn: 0272-8397. doi: 10.1002/pc.25714.

[65] Hexcel. *Product Datasheet of Hexcel HexTow AS4*. https://www.hexcel.com/user_area/content_media/raw/AS4_HexTow_DataSheet.pdf. [cited 2023-08-10]. 2023.

[66] Hexcel. *Product Datasheet of Hexcel HexTow IM7*. https://www.hexcel.com/user_area/content_media/raw/IM7_HexTow_DataSheet.pdf. [cited 2023-08-10]. 2023.

[67] Toray Advanced Composites. *Product Datasheet of Toray T700S*. https://www.toraycma.com/wp-content/uploads/T700S-Technical-Data-Sheet-1.pdf. [cited 2023-08-10]. 2018.

[68] Toray Advanced Composites. *Product Datasheet of Toray T700G*. https://www.toraycma.com/wp-content/uploads/T700G-Technical-Data-Sheet-1.pdf. [cited 2023-08-10]. 2018.

[69] Sebastiaan Van den Berg et al. "Determination of the anisotropic electrical conductivity of carbon fabric reinforced composites by the six-probe method". In: *Journal of Thermoplastic Composite Materials* 36 (11 Nov. 2023), pp. 4257–4283. issn: 0892-7057. doi: 10.1177/08927057231154546.

[70] K. Schulte and Ch. Baron. "Load and failure analyses of CFRP laminates by means of electrical resistivity measurements". In: *Composites Science and Technology* 36 (1 Jan. 1989), pp. 63–76. issn: 02663538. doi: 10.1016/0266-3538(89)90016-X.

[71] Akira Todoroki, Miho Tanaka, and Yoshinobu Shimamura. "Measurement of orthotropic electric conductance of CFRP laminates and analysis of the effect on delamination monitoring with an electric resistance change method". In: *Composites Science and Technology* 62 (5 Apr. 2002), pp. 619–628. issn: 02663538. doi: 10.1016/S0266-3538(02)00019-2.

[72] Koichi Mizukami and Yudai Watanabe. "A simple inverse analysis method for eddy current-based measurement of through-thickness conductivity of carbon fiber composites". In: *Polymer Testing* 69 (Aug. 2018), pp. 320–324. issn: 01429418. doi: 10.1016/j.polymertesting.2018.05.043.

[73] James R Gaier et al. "The electrical and thermal conductivity of woven pristine and intercalated graphite fiber–polymer composites". In: *Carbon* 41 (12 2003), pp. 2187–2193. issn: 00086223. doi: 10.1016/S0008-6223(03)00238-0.

[74] Akira TODOROKI and Jyunji YOSHIDA. "Electrical Resistance Change of Unidirectional CFRP Due to Applied Load". In: *JSME International Journal Series A* 47 (3 2004), pp. 357–364. issn: 1344-7912. doi: 10.1299/jsmea.47.357.

[75] Shoukai Wang and D. D. L. Chung. "Electrical behavior of carbon fiber polymer-matrix composites in the through-thickness direction". In: *Journal of Materials Science* 35 (1 Jan. 2000), pp. 91–100. issn: 0022-2461. doi: 10.1023/A:1004744600284.

[76] Victor H. Guerrero and D. D. L. Chung. "Interlaminar interface relaxation upon heating carbon fiber thermoplastic-matrix composite, studied by contact electrical resistivity measurement". In: *Composite Interfaces* 9 (6 Jan. 2002), pp. 557–563. issn: 0927-6440. doi: 10.1163/156855402 60494128.

[77] H. C. Montgomery. "Method for Measuring Electrical Resistivity of Anisotropic Materials". In: *Journal of Applied Physics* 42 (7 June 1971), pp. 2971–2975. issn: 0021-8979. doi: 10.1063/1.1660656.

[78] R. Busch et al. "New aspects of the mixed state from six-terminal measurements on Bi2Sr2CaCu2Ox single crystals". In: *Physical Review Letters* 69 (3 July 1992), pp. 522–525. issn: 0031-9007. doi: 10.1103/PhysRevLett.69.522.

[79] Luca Marini. *Conductivity characterization of thin multilayer composites. Bachelor's thesis*. Tech. rep. Haute Ecole d'Ingénierie, Hes so, Aug. 2024.

[80] Koichi Mizukami et al. "Analytical solutions to eddy current in carbon fiber-reinforced composites induced by line current". In: *Advanced Composite Materials* 25 (4 July 2016), pp. 385–401. issn: 0924-3046. doi: 10.1080/09243046.2015.1052132.

[81] A Sophian et al. "Electromagnetic and eddy current NDT: a review". In: *Insight* 43 (2001), pp. 302–306.

[82] Dario Jeronimo Pasadas et al. "Detection and Classification of Defects Using ECT and Multi-Level SVM Model". In: *IEEE Sensors Journal* 20 (5 Mar. 2020), pp. 2329–2338. issn: 1530-437X. doi: 10.1109/JSEN.2019.2951302.

[83] Ladislav Janousek, Andrea Stubendekova, and Milan Smetana. “Novel insight into swept frequency eddy-current non-destructive evaluation of material defects”. In: *Measurement* 116 (Feb. 2018), pp. 246–250. issn: 02632241. doi: 10.1016/j.measurement.2017.11.039.

[84] Andrea Stubendekova and Ladislav Janousek. “Impact of defect extent on swept frequency eddy current responses in non-destructive evaluation”. In: *Electrical Engineering* 99 (4 Dec. 2017), pp. 1275–1281. issn: 0948-7921. doi: 10.1007/s00202-017-0650-z.

[85] Ali Sophian, Guiyun Tian, and Mengbao Fan. “Pulsed Eddy Current Non-destructive Testing and Evaluation: A Review”. In: *Chinese Journal of Mechanical Engineering* 30 (3 May 2017), pp. 500–514. issn: 1000-9345. doi: 10.1007/s10033-017-0122-4.

[86] Lawal Umar Daura et al. “Wireless power transfer-based eddy current non-destructive testing using a flexible printed coil array”. In: *Philosophical Transactions of the Royal Society A: Mathematical, Physical and Engineering Sciences* 378 (2182 Oct. 2020), p. 20190579. issn: 1364-503X. doi: 10.1098/rsta.2019.0579.

[87] Runhong Huang et al. “Frequency Splitting Phenomena of Magnetic Resonant Coupling Wireless Power Transfer”. In: *IEEE Transactions on Magnetics* 50 (11 Nov. 2014), pp. 1–4. issn: 0018-9464. doi: 10.1109/TMAG.2014.2331143.

[88] Hoang Nguyen and Johnson I. Agbinya. “Splitting Frequency Diversity in Wireless Power Transmission”. In: *IEEE Transactions on Power Electronics* 30 (11 Nov. 2015), pp. 6088–6096. issn: 0885-8993. doi: 10.1109/TPEL.2015.2424312.

[89] Yuan Zhuang et al. “Range-Adaptive Wireless Power Transfer Based on Differential Coupling Using Multiple Bidirectional Coils”. In: *IEEE Transactions on Industrial Electronics* 67 (9 Sept. 2020), pp. 7519–7528. issn: 0278-0046. doi: 10.1109/TIE.2019.2945304.

[90] Toray Composite Materials America, Inc. *Torayca M40J Carbon Fiber Data Sheet*. https://www.toraycma.com/wp-content/uploads/M40J-Data-Sheet.pdf. Accessed: 2026-04-16. 2024.

[91] Toray Composite Materials America, Inc. *Torayca T800S Carbon Fiber Technical Data Sheet*. Tech. rep. Accessed: 2026-04-16. Toray Composite Materials America, Inc., 2018. url: https://www.toraycma.com/wp-content/uploads/T800S-Data-Sheet.pdf.

[92] E. ul-Haq. “Carbon Fiber Tow Spreading: Experimental Machine Design, Friction Behaviour, and Novel Monitoring Concepts”. MA thesis. Delft University of Technology, 2023.

A

Material Preparation

A.0.1. Tape preparation

For this research, in order to ensure measurement accuracy and repeatability, each experimental technique requires specific specimen geometrical characteristics. Therefore, the UD tapes were cut and prepared to ensure tailored dimension to each test configuration. For general application, the tapes were prepared with a width of $30\ mm$ and a length of $200\ mm$. These dimensions were selected to ensure that the sample would fit within the electrodes of the six-probes setup. A minimum length of $150\ mm$ is necessary to ensure the tape is in full contact between the outer electrodes during the test. Moreover, to reduce edge effects or current generations under the electrodes, a total length of $200\ mm$ is needed to ensure the edges of the tape are far enough from the electrodes. A narrow width of $3\ mm$ is chosen as the transversal conductivity is not of interest for this research, hence only the longitudinal conductivity of the tape is required to study the through-thickness behaviour for thin UD tapes. Hence, to reduce noise related to transverse features, using a narrow tape is preferred. In addition, the maximum width that can fit within the six-probes setup is $100\ mm$.

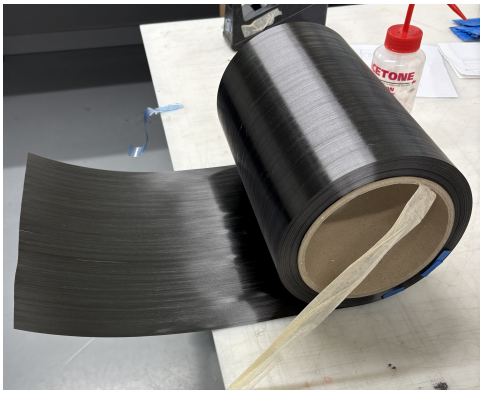

Figure A.1: Toray TC1225 tape

Figure A.2: Preparation of sample geometry

In order to investigate the influence of manufacturing processes on electrical conductivity of UD TPC tapes, as mentioned above, four different material are selected and prepared. These materials are chosen to represent different processing routes and reinforcement configuration. The investigated tapes are composed of: a commercial TC1225 Toray UD prepreg tape, a TPR-based PEEK matrix reinforced with T800SC-24k carbon fibres, a DPR-based PEEK matrix reinforced also by T800SC-24k, and a hybrid tape containing T800 and M40J high modulus carbon fibres. Shown in Figure A.1 and A.2 is the preparation of Toray TC1225 tapes.

A.0.2. Laminate preparation

In order to characterise the effect of sample thickness t on the acquired through-thickness conductivity of UD TPC, a different material than single layer tape is required. This can be achieved by staking multiple layers of UD tape and consolidating them into a thicker laminate. As the laminate is composed of the same material of the tapes, a direct comparison on the effect of thickness on conductivity can be observed. To manufacture the laminates a hot press is used, which applies pressure and temperature to melt and consolidate the polymer matrix in a controlled environment. For this experiment different geometrical configuration of the tapes is required, as the narrow $3\ mm$ tapes would potentially move during the hot press, as the pressure might squeeze them and allow polymer flow. To avoid squeezing, larger samples of $9\ mm$ width and $19\ mm$ of length are cut. Shown below are the samples being placed onto a flat metal mould prior to consolidation.

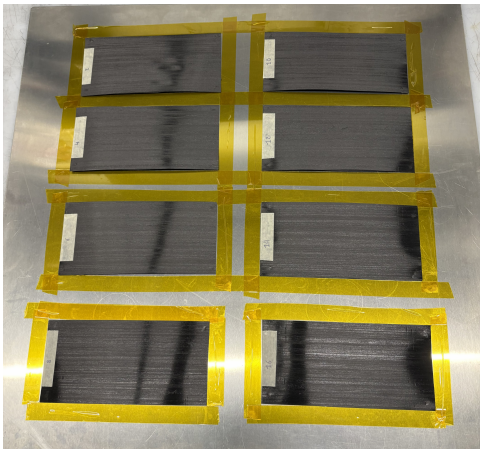

Figure A.3: 2 layer UD laminate stack

Figure A.4: Hot press

Shown in Figure A.3 is the stack preparation for eight thin UD laminates composed of two layers of Toray TC1225 tape. The idea of this experiment is to first test the single layer's conductivity in the six probes setup, and then calculate their conductivity after being consolidated into a thicker laminate. Starting from a single layer, up to a UD laminate of sixteen layers. Hence five different steps of calculating how conductivity increases between one layer up to sixteen. For the consolidation of these laminates no mould has been used. Hence, to avoid flow out of polymer due to pressure, Kapton tape has been placed around the samples to ensure the samples remain in place. After this step, a second flat metal plate is placed on top of the assembly and the material is placed in the hot press as shown in Figure A.4. Table A.1 lists the production parameters to consolidate the LM-PAEK laminates.

Table A.1: Hot Press Production Plan - Toray TC1225 laminate

Stage	Target Temperature (°C)	Rate (°C/min)	Time (min)	Pressure (MPa)
Heating	380	6	63.3	10
Dwell (Hold)	380	–	20	10
Cooling	Room Temperature	2	190	10

Once the consolidation cycle is done and the material is below its glass transition temperature T_g, the press can be opened and the samples de-moulded. Figure A.5 shows how the two layer UD laminates came out of the Joos hot press.

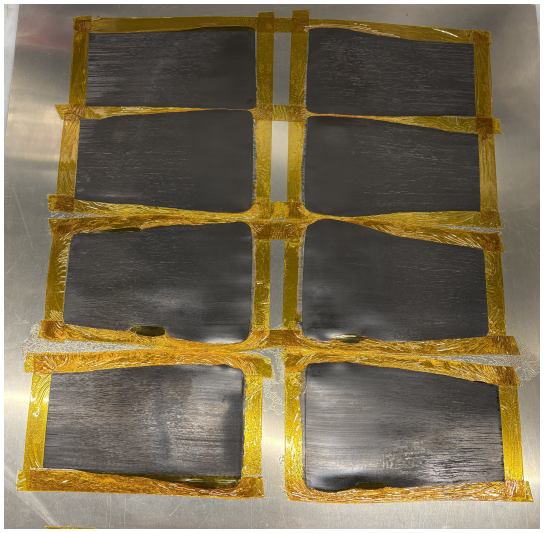

Figure A.5: De-moulding of 2 layer laminates

Unfortunately, as it can be seen from Figure A.5, the kapton tape is not sufficient to reduce excessive squeeze and polymer flow-out. Moreover, it can be observed that most of the flow-out occurred at the centre of the plate. This suggests that the metal mould sheet or the press plate are curved, causing application of uneven pressure on the material. Moreover, it can be observed that the laminates have regions in which there is a concentration of polymer and excessive fibre waviness. This can be observed in Figure A.6.

Figure A.6: Defects from hot press process

In spite of these manufacturing defects, it is still important to test the laminates, as characterising electrical conductivity dependence on defects is also fundamental knowledge. However, due to the excessive flow-out of polymer the laminates became wider than $100\ mm$, preventing the samples to fit within the electrodes of the six-probes setup. Therefore, the laminates have to be trimmed back to the original geometry to be compared. By doing so, a lot of material is lost from the samples, which is composed of polymer and conducting fibres. Due to the squeeze out of matrix material (or polymer, you choose) the microstructure of the original tape is directly modified and this may affect its electrical properties.

Figure A.7: Trimming of flow-out material

In order to address the change of microstructure due to polymer squeeze out, a larger laminate of $30 \times 30\ cm$ is manufactured to reduce flow-out of polymer during the hot press process. For this laminate eight UD layers are stacked and consolidated, and consequently trimmed with a saw, to the original intended geometry of $19 \times 9\ cm$. The idea is to use a larger laminate in order to reduce flow-out and only concentrate it on the edges. By doing so, the central part of the laminate should maintain a somewhat acceptable quality, with less spread-out and fibre waviness.

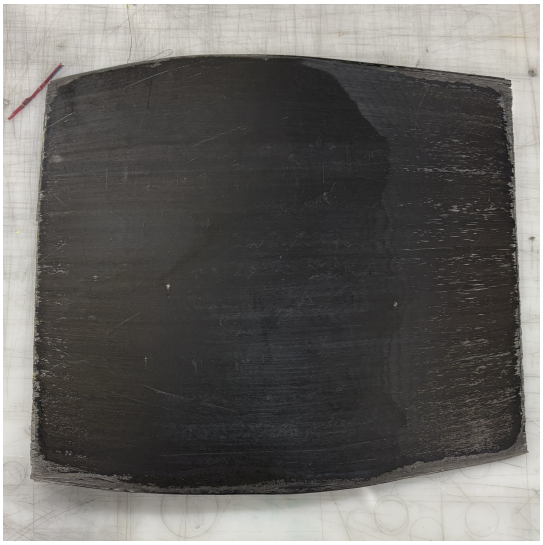

Figure A.8: 30x30cm 8 layer laminate

Figure A.9: Trimmed 8 layers laminate

This eight layer UD laminate is consolidated better than the previously consolidated two layer thin laminates. Significant reduction in material flow-out is observed, see Figure A.8. Nonetheless, although manufactured better, the eight layer laminate turned out to be very difficult to test and analyse in the six-probes setup. This is due to the resin rich surface which acts as an insulator, giving contact resistance problems with the electrodes when trying to inject direct current through the laminate. An intermediate solution was found to burn off with a gas torch the sides of the laminate where the electrodes are in contact. This has an interesting effect as discussed in the results section Section 4.

B

Six probes design and adjustments

B.1. set-up design & adjustments

As the setup was previously designed by *L. Marini* [79] and based on the design of *Y. Buser et al* [8], it had to be checked whether it would function and deliver the correct electrical data. To do so, instead of using highly anisotropic material such as UD TPC tapes, a t-bone sample of well known isotropic aluminium Al 2024 T3 is tested. As its electrical properties are well known from literature, it is straightforward to check whether the same properties can be calculated from this six-probes setup. The aluminium bar is placed within the electrodes and is clamped. A current of $1A$ is introduced by an RS PRO Digital bench power supply, and with a multimeter, the voltage drop between the longitudinal probes is acquired. The aluminium bar resulted in a resistivity of $5.42 \times 10^{-8}\,\Omega$m, which is very close to the value found in literature of $5.7 \times 10^{-8}\,\Omega$m. Moreover, a set of stainless steel strips with different thickness $(0.03, 0.07, 0.1\ mm)$ are tested to check whether material geometry would have an effect. In theory, electrical resistivity is a material property independent of the geometry of the sample, unlike its resistance. Hence three strips of different thickness should have the same resistivity if made of the same isotropic material. And indeed, the found resistivity of the three strips is essentially the same, with a minor difference probably due to imperfect contact pressure. This can be seen in Figure B.2. This is the required sanity check to ensure that the setup correctly introduces a current field along the conductor without losses or bad contacts. Shown below is the experiment with the aluminium t-bone in Figure B.1.

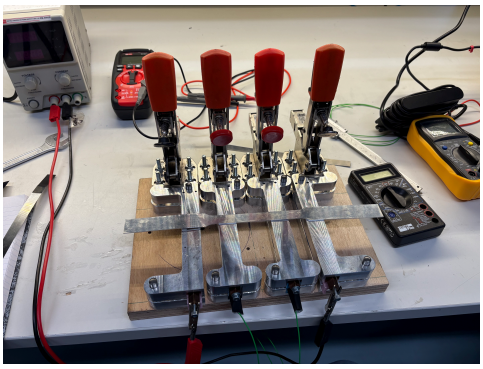

Figure B.1: Six-probe test of aluminium t-bone

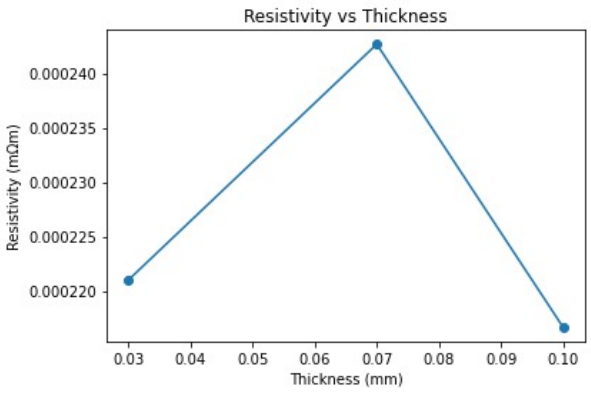

Figure B.2: Thickness effect on calculated resistivity of stainless steel strips

As can be seen in Figure B.2, the resistivity of three different thickness stainless steel strips is approximately the same. The difference observed is probably due to signal noise from the DAQ system. The units of resistivity are on the order of $2.3e-7$ which is extremely low resistivity and high conductivity.

Hence the variance between the three samples is negligible for these small values. Hence with this experiment it could be concluded that the six probe setup would accurately gather the correct conductivity range of a given sample.

Shown below is an illustration of the NI DAQ device used to acquire voltage drop signals from the six probe setup and directly connect it to a laptop via USB connection.

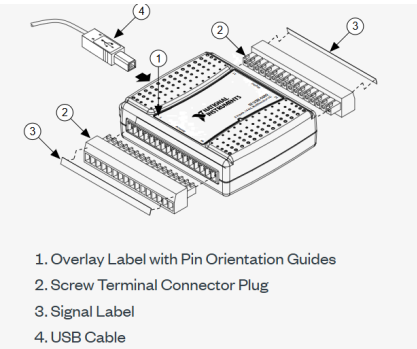

Figure B.3: NI USB-6009 DAQ

Shown in Figure B.3 is the interface of the Python application live results, when a DC current would be injected within the UD tapes. The python script generates two graphs: top and bottom surface resistivity, and calculated through thickness conductivity based on *Busch et al.* approach.

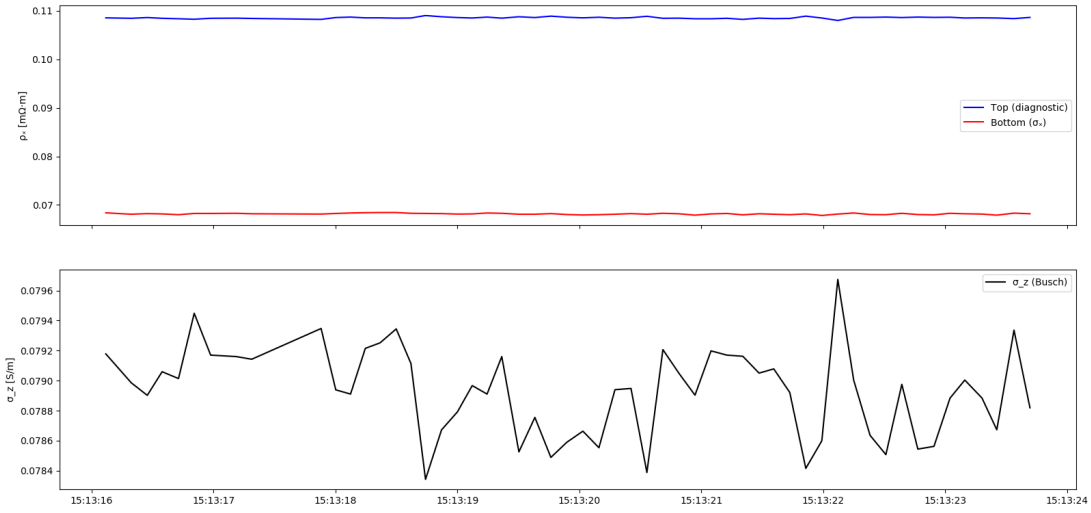

Figure B.4: Python live visualisation of top and bottom resistivity, and calculated through-thickness conductivity of the tape

As described from the Methodology of the six probe method, different electrodes geometries were tested.

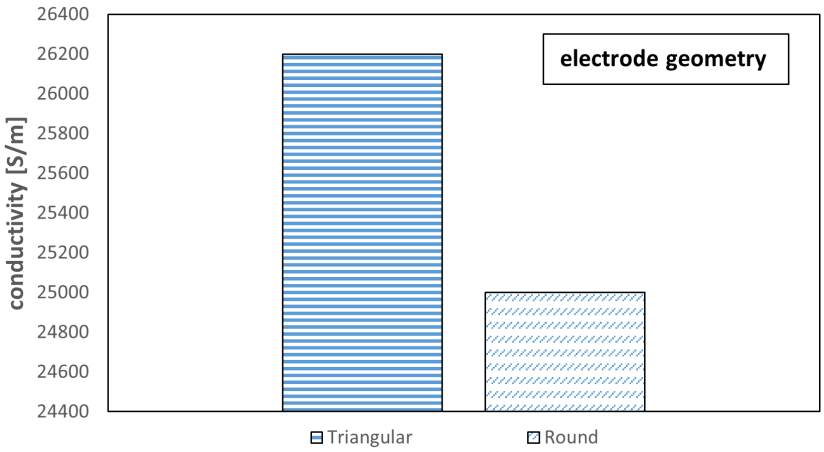

Figure B.5: Electrode geometry effect on acquired longitudinal conductivity

Figure B.5 shows the difference conductivity calculated by using triangular and round electrodes/probes. On average a variance of $1200\ S/m$ can be found between the two different geometries. This is given by a lower contact pressure achieved with the round electrodes. Anyway, this trade off was reasonable as the triangular electrodes would leave marks on the tape surface, damaging it.

Moreover, the effect of contact pressure on the acquired resistivity was calculated.

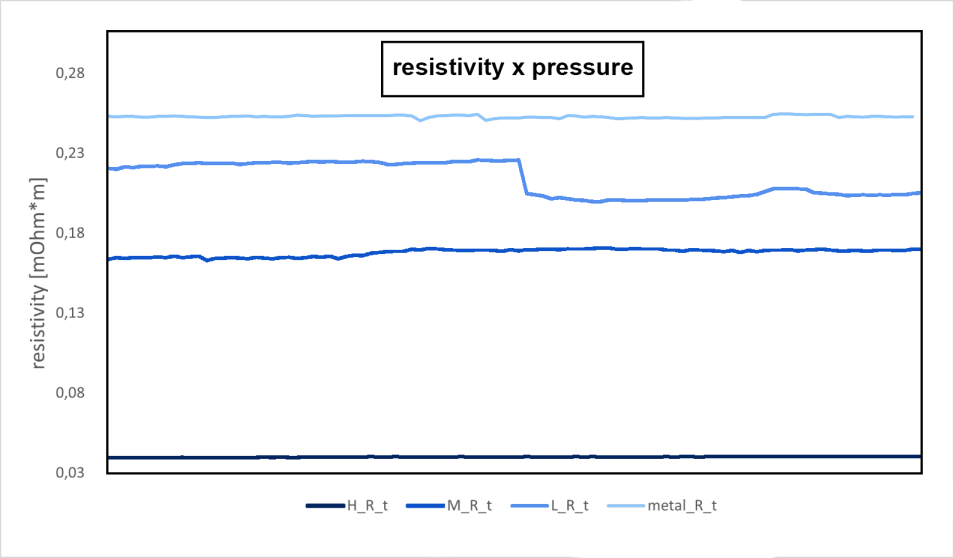

Figure B.6: Clamping pressure effect on acquired longitudinal resistivity

As shown in Figure B.6, by applying a higher pressure (blue line), a lower resistivity would be achieved. The blue line represents the full clamp pressure that was used for every test of characterising the four UD TPC tape systems in the results.

In addition, also the effect of injected current on acquired conductivity was analysed.

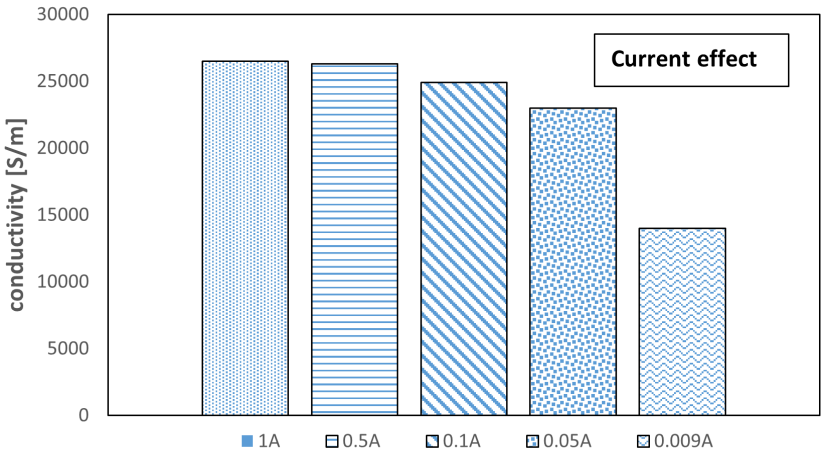

Figure B.7: Current effect on acquired longitudinal conductivity

Figure B.7 shows that by applying current values below $0.5\ A$, the acquired conductivity would decrease. Hence to acquire the most accurate value of conductivity of the UD TPC tapes, a value of $0.5\ A$ was chosen. This value seemed to reach a plateau, and over it the tape would experience joule heating which would make the test not isothermal.

Finally, also the effect of time and temperature on the six probe measurements was observed.

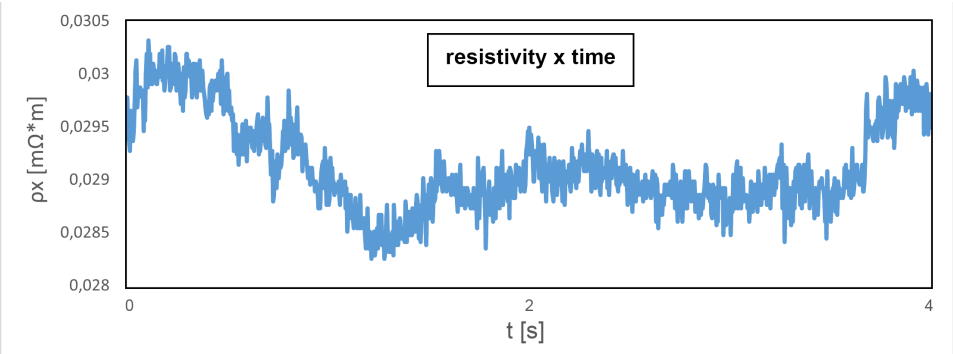

Figure B.8: Resistivity variance over a time frame of four minutes

As shown in Figure B.8, by applying a current of $0.5\ A$ for 4 minutes, the overall resistivity of the UD TPC tape seemed to lower and eventually stabilise again.

This results showed that longer period of times wouldn't really have a great impact on the material's resistivity at that current intensity.

This was a simple test to prove that when applying a current of $0.5\ A$ the material would remain isothermal and not experience great variance in resistivity. For more complete analysis, further work must be done on the time effect on calculated conductivity.

C

Six probe data acquisition code

Shown below is the initial Python code based on the work of *E. ul-Haq* [92], who used the same DAQ system to acquire electrical and mechanical data during the impregnation of TPC tapes. This code was initially used for the six probe measurements.

```
'Python'

import nidaqmx
import matplotlib.pyplot as plt
import keyboard
import numpy as np
import os
from datetime import datetime
import sys
import matplotlib
matplotlib.use('TkAgg')

i = 0
x = []
rholist1 = []
rholist2 = []
rholist3 = []
rholist4 = []
Flist1 = []
Flist2 = []

I = 0.5 #A
#L = 0.125 #m
L = 0.06
t = 0.000164
#t = 0.001
#W = 0.0285 m
#t = 0.189 mm 0.000250m
#A = 12000 * 0.25 * np.pi * 0.000007**2
#w_metal1 = 0.013
#t_metal1 = 0.00003 m
A_longitudinal = 0.000164*0.0285
A_throughthick = 0.0285*0.00057
factor1 = 1 *10
factor2 = 1 *10

plt.ion()
fig, (ax1, ax2) = plt.subplots(2, 1, sharex=True)


# Create a new file for writing data
save_path = r"C:\Users\col\OneDrive\Documents\TU␣Delft\Thesis"
filename = datetime.now().strftime('%Y-%m-%d_%H-%M-%S') + ".txt"
full_path = os.path.join(save_path, filename)
print("Saving␣file␣to:", full_path)
```

```
with open(full_path, 'w') as f:
# with open('output.txt', 'w') as f:
    f.write('Timestamp\tRho1\tRho2\tRho3\tRho4\n') # write header row
   # index = 0

    with nidaqmx.Task() as task1, nidaqmx.Task() as task2:
        task1.ai_channels.add_ai_voltage_chan("Dev1/ai0:1")
        task2.ai_channels.add_ai_voltage_chan("Dev1/ai1:2")

        while i < 500:
            data1 = task1.read(number_of_samples_per_channel=10)
            data2 = task2.read(number_of_samples_per_channel=10)


            x.append(datetime.now()) # Use current timestamp as x value

            floa1 = float(data1[1][0]) #Top longitudinal probes
            R1 = floa1 * (1/I)
            rho1 = A_longitudinal*R1/L
            rholist1.append(rho1*1000 )  #rholist1.append(rho1*1000*1.736)

            floa2 = float(data1[0][0]) # bottom longitudinal probes
            R2 = floa2 * (1/I)
            rho2 = A_longitudinal*R2/L
            rholist2.append(rho2*1000 )

            floa3 = float(data2[0][1]) # Left thorugh thickness probes
            #floa3 = np.mean(data2[1][0])
            R3 = floa3 * (1/I)
            rho3 = A_throughthick*R3/t
            rholist3.append(rho3*1000 )

            floa4 = float(data2[0][0]) # Right thorugh thickness probes
            R4 = floa4 * (1/I)
            rho4 = A_throughthick*R4/t
            rholist4.append(rho4*1000  )

           # floa3 = float(data2[1][0]) #Top longitudinal probes
           # F1 = floa3 * factor1
           # Flist1.append(F1)

           # floa4 = float(data2[0][0]) # bottom longitudinal probes
           # F2 = floa4 * factor2
           # Flist2.append(F2)

            ax1.plot(x, rholist1, c='b')
            ax1.plot(x, rholist2, c='r')
            ax1.set_ylabel('Effective resistivity [mOhm m]')
            ax1.legend(['Top longitudinal probes','Bottom longitudinal probes'])

            ax2.plot(x, rholist3, c='b')
            ax2.plot(x, rholist4, c='r')
            ax2.set_ylabel('Effective resistivity [mOhm m]')
            ax2.legend(['Left through thickness probes','Right through thickness probes'])

           # ax2.plot(x, Flist1, c='y')
           # ax2.plot(x, Flist2, c='k')
           # ax2.set_ylabel('Tension [N]')
           # ax2.set_xlabel('Timestamp')
           # ax2.legend(['One', 'Two'])

            plt.gcf().autofmt_xdate() # Format x-axis as dates
            plt.autoscale(enable=True, axis='y')
            # Write the data to the output file with the current timestamp as the index
            timestamp = datetime.now().strftime('%Y-%m-%d %H:%M:%S.%f')
            f.write(f'{timestamp}\t{rho1:.10e}\t{rho2:.10e}\t{rho3:.10e}\t{rho4:.10e}\n')
            f.flush #Make sure it write immediately

            i += 1
            plt.show()
            plt.pause(0.25)
```

```
            # Check for ESC key press and break out of loop
            if keyboard.is_pressed('esc'):
                print('Esc pressed, stopping acquisition')
                sys.exit()
                break
                # plt.close(fig)
                # break
```

Moreover, a second version of the code is implemented to improve automation, by directly calculating the formulas based on the work of *Busch et al.* [78]. The code takes data in live time, and for each time step the formulas are re-calculated for each voltage drop acquired, giving a complete information of the electrical behaviour of the conductor, and saving time in post processing. Once an end command is given, the program stops gathering and analysing data, and directly saves the information in a text file containing information on the top and bottom surface voltage drop, and longitudinal and transverse resistivity and conductivity of the UD TPC tape. These text files can then be imported again on another Python script, or onto Excel to gather qualitative and quantitative data of each material. In contrast, initially for the six-probe setup, all of these steps would have been done manually with a multimeter and pen and paper. The new approach is more reliable and robust over time, and is more efficient.

Shown below is the improved python code to acquire data from the NI USB-6009 for the six probes setup:

```

import nidaqmx
from nidaqmx.constants import TerminalConfiguration
import matplotlib.pyplot as plt
import keyboard
import numpy as np
import os
from datetime import datetime
import math
import matplotlib
matplotlib.use('TkAgg')

# =========================
# Busch inversion  (z only)
# =========================
def busch_sigma_z(Vt, Vb, I, L, l, w, t, sigma_x_ref):
    """
    Busch et al. six-probe inversion.
    Uses externally measured sigma_x_ref.
    Returns sigma_z, z_eff, t_eff.
    """

    if I <= 0 or Vt <= 0 or Vb <= 0:
        raise ValueError("Invalid current or voltage")

    ratio = Vt / Vb
    if ratio <= 1.0:
        raise ValueError("Vt/Vb<=1: no usable Busch asymmetry")

    arccosh = math.log(ratio + math.sqrt(ratio**2 - 1.0))
    z_eff = (L / math.pi) * arccosh
    t_eff = min(t, z_eff)

    rho_x_ref = 1.0 / sigma_x_ref

    numerator = (Vt * w * L) / (I * math.pi * l)
    rho_z = (numerator**2) / rho_x_ref

    if rho_z <= 0:
        raise ValueError("Computed rho_z <=0")

    sigma_z = 1.0 / rho_z
    return sigma_z, z_eff, t_eff


```

```
# ========================
# Geometry & material data
# ========================
I = 0.5               # Applied current [A]
w = 0.0298        # Tape width [m]
t = 0.000104        # Tape thickness [m]
l = 0.06              # Voltage probe spacing [m]
L = 0.1412            # Current electrode spacing [m]

A_longitudinal = w * t
A_throughthick = w * 0.00064   # contact spacing (diagnostic only)

# ========================
# Storage
# ========================
i = 0
x = []
rho_top_list = []
rho_bottom_list = []
sigma_x_list = []
sigma_z_list = []

# ========================
# Plot setup
# ========================
plt.ion()
fig, (ax1, ax2) = plt.subplots(2, 1, sharex=True)

# ========================
# File output
# ========================
save_path = r"C:\Users\colai\OneDrive\Documents\TU␣Delft\Thesis"
filename = datetime.now().strftime('%Y-%m-%d_%H-%M-%S') + ".txt"
full_path = os.path.join(save_path, filename)

with open(full_path, 'w') as f:
    f.write("Timestamp\tV_top\tV_bottom\tRho_top\tRho_bottom\tSigma_x\tSigma_z\n")

    # ========================
    # DAQ configuration
    # ========================
    with nidaqmx.Task() as task:
        task.ai_channels.add_ai_voltage_chan(
            "Dev1/ai0",
            terminal_config=TerminalConfiguration.DIFFERENTIAL,
            name_to_assign_to_channel="V_top"
        )
        task.ai_channels.add_ai_voltage_chan(
            "Dev1/ai1",
            terminal_config=TerminalConfiguration.DIFFERENTIAL,
            name_to_assign_to_channel="V_bottom"
        )
        task.ai_channels.add_ai_voltage_chan(
            "Dev1/ai2",
            terminal_config=TerminalConfiguration.DIFFERENTIAL,
            name_to_assign_to_channel="V_left"
        )
        task.ai_channels.add_ai_voltage_chan(
            "Dev1/ai3",
            terminal_config=TerminalConfiguration.DIFFERENTIAL,
            name_to_assign_to_channel="V_right"
        )

        print("DAQ␣channels:")
        for ch in task.ai_channels:
            print(f"␣␣{ch.name}␣->␣{ch.physical_channel}")

        # ========================
        # Acquisition loop
        # ========================
        while i < 500:
```

```
            data = task.read(number_of_samples_per_channel=10)

            V_top = float(np.mean(data[0]))
            V_bottom = float(np.mean(data[1]))

            # ---- Simple 4-probe (absolute  x) ----
            R_bottom = V_bottom / I
            rho_x_bottom = A_longitudinal * R_bottom / l
            sigma_x = 1.0 / rho_x_bottom

            # Diagnostic only
            R_top = V_top / I
            rho_x_top = A_longitudinal * R_top / l

            # ---- Busch  z (anchored by  x) ----
            try:
                sigma_z, z_eff, t_eff = busch_sigma_z(
                    Vt=V_top,
                    Vb=V_bottom,
                    I=I,
                    L=L,
                    l=l,
                    w=w,
                    t=t,
                    sigma_x_ref=sigma_x
                )
            except Exception as e:
                sigma_z = float('nan')

            # ---- Store ----
            rho_top_list.append(rho_x_top * 1000)
            rho_bottom_list.append(rho_x_bottom * 1000)
            sigma_x_list.append(sigma_x)
            sigma_z_list.append(sigma_z)
            x.append(datetime.now())

            # ---- Plot ----
            ax1.cla()
            ax2.cla()

            ax1.plot(x, rho_top_list, 'b', label='Top␣(diagnostic)')
            ax1.plot(x, rho_bottom_list, 'r', label='Bottom␣ ()')
            ax1.set_ylabel(' ␣[Ωm·m]')
            ax1.legend()

            ax2.plot(x, sigma_z_list, 'k', label=' _z␣(Busch)')
            ax2.set_ylabel(' _z␣[S/m]')
            ax2.legend()

            plt.pause(0.1)

            # ---- Save ----
            timestamp = datetime.now().strftime('%Y-%m-%d␣%H:%M:%S.%f')
            f.write(
                f"{timestamp}\t{V_top:.6e}\t{V_bottom:.6e}\t"
                f"{rho_x_top:.6e}\t{rho_x_bottom:.6e}\t"
                f"{sigma_x:.6e}\t{sigma_z:.6e}\n"
            )
            f.flush()

            i += 1
            if keyboard.is_pressed('esc'):
                print("Stopped␣by␣user")
                break
```

It is to be mentioned that the use of AI, was used to debug the code. Specifically with the DAQ packages to associate physical wirings and corresponding NI DAQ ports. Between lines 85 - 111. With prompts such as *"Change GND voltage acquisition to DIFFERENTIAL mode for the NI DAQ USB 6009 Python package"*.

D

Results

D.1. Electrical Conductivity

This appendix section illustrates the single conductivity values for the four investigated tapes and their different sections.

D.1.1. TC 1225 tape

Figure D.1 illustrates the longitudinal conductivity values calculated with the six probe measurement for the TC 1225 tape sections.

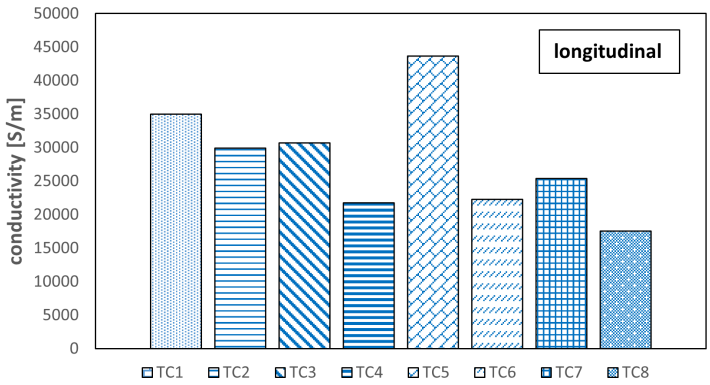

Figure D.1: Longitudinal conductivity of TC 1225 tape sections

Figure D.2 illustrates the through thickness conductivity values calculated with the six probe measurement for the TC 1225 tape sections.

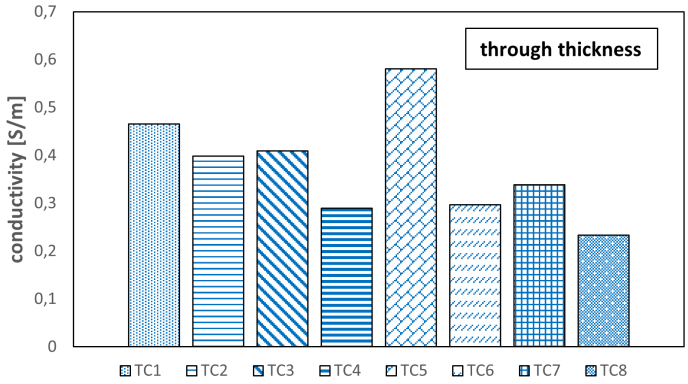

Figure D.2: Through thickness conductivity of TC 1225 tape sections

D.1.2. DPR tape

Figure D.3 illustrates the longitudinal conductivity values calculated with the six probe measurement for the DPR tape sections.

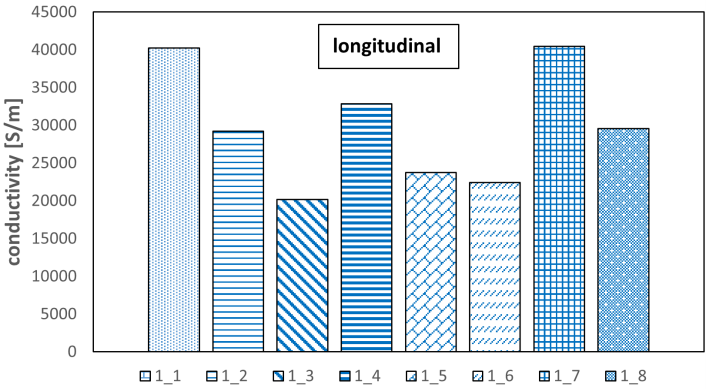

Figure D.3: Longitudinal conductivity of DPR tape sections

Figure D.4 illustrates the through thickness conductivity values calculated with the six probe measurement for the DPR tape sections.

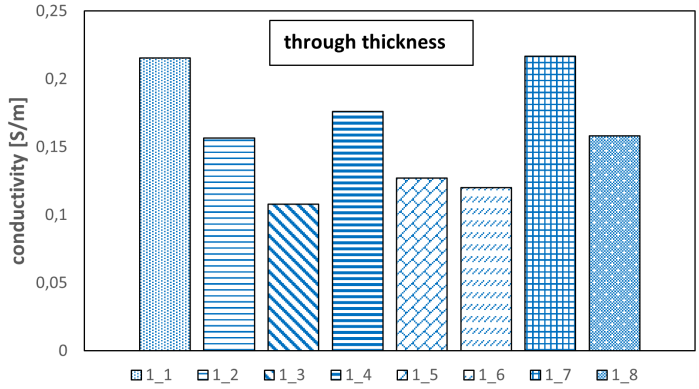

Figure D.4: Through thickness conductivity of DPR tape sections

D.1.3. TPR tape

Figure D.5 illustrates the longitudinal conductivity values calculated with the six probe measurement for the TPR tape sections.

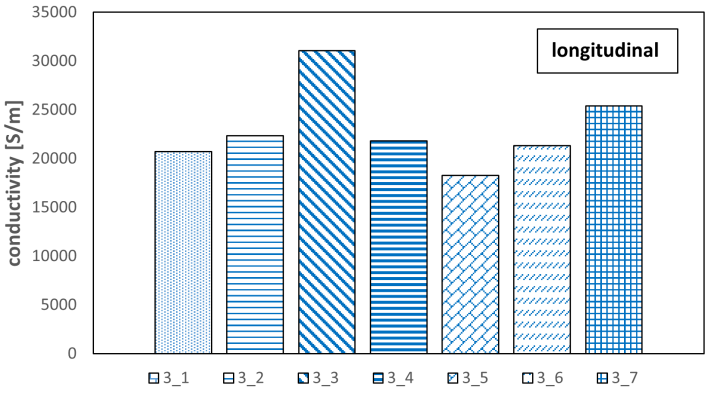

Figure D.5: Longitudinal conductivity of TPR tape sections

Figure D.6 illustrates the through thickness conductivity values calculated with the six probe measurement for the TPR tape sections.

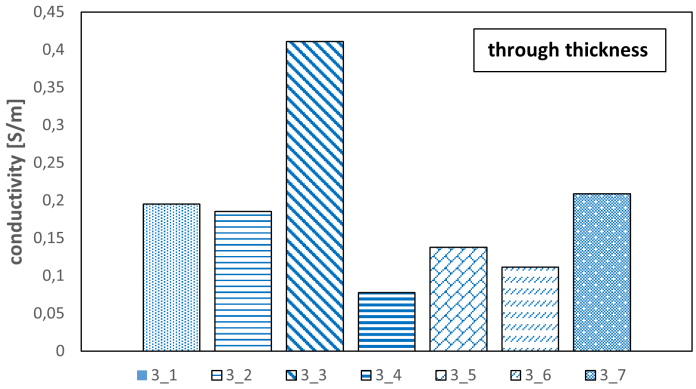

Figure D.6: Through thickness conductivity of TPR tape sections

D.1.4. Hybrid tape

Figure D.7 illustrates the longitudinal conductivity values calculated with the six probe measurement for the Hybrid tape sections.

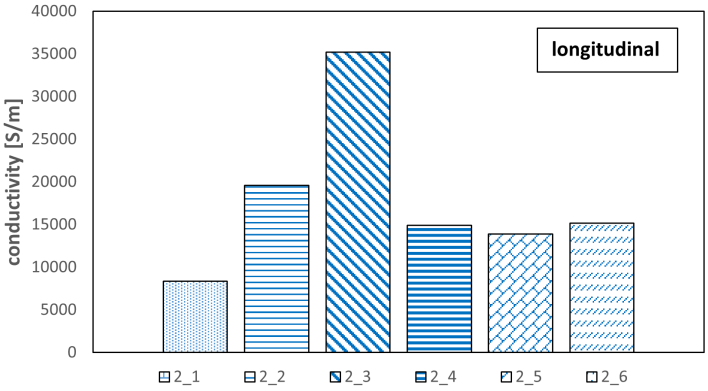

Figure D.7: Longitudinal conductivity of Hybrid tape sections

Figure D.8 illustrates the through thickness conductivity values calculated with the six probe measurement for the Hybrid tape sections.

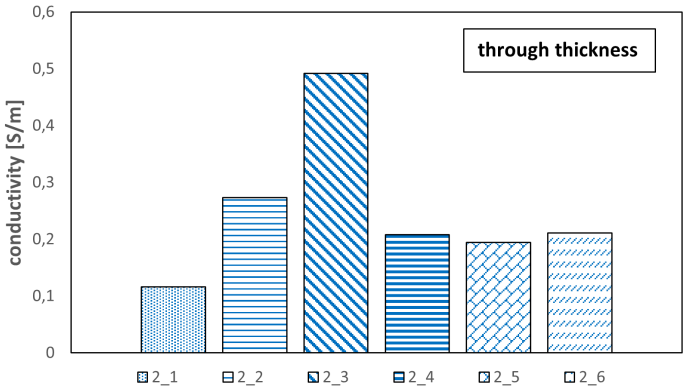

Figure D.8: Through thickness conductivity of Hybrid tape sections

D.2. Microscopy

This appendix section illustrates the micrograph of the four investigated tapes and their different sections.

D.2.1. TC 1225 tape

Least conductive

Figure D.9 and Figure D.10 illustrate the cross sectional micrographs of the TC 1225 tape sections of the least conductive TC_4 tape.

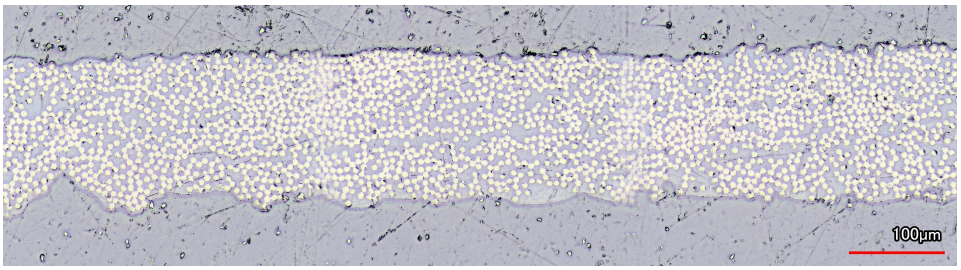

Figure D.9: Micrograph of TC1225 tape TC_4_1

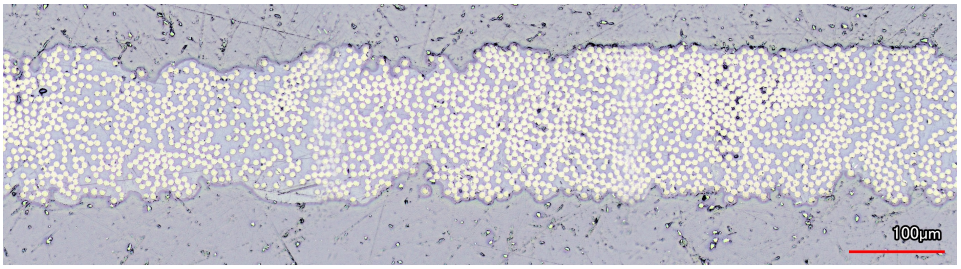

Figure D.10: Micrograph of TC1225 tape TC_4_2

Most conductive

Figure D.11 and Figure D.12 illustrate the cross sectional micrographs of the TC 1225 tape sections of the most conductive TC_5 tape.

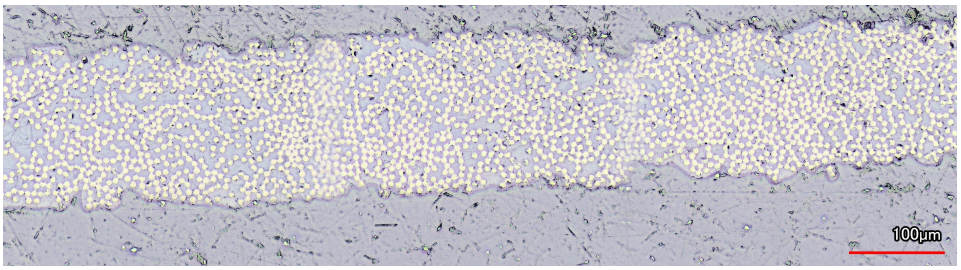

Figure D.11: Micrograph of TC1225 tape TC_5_1

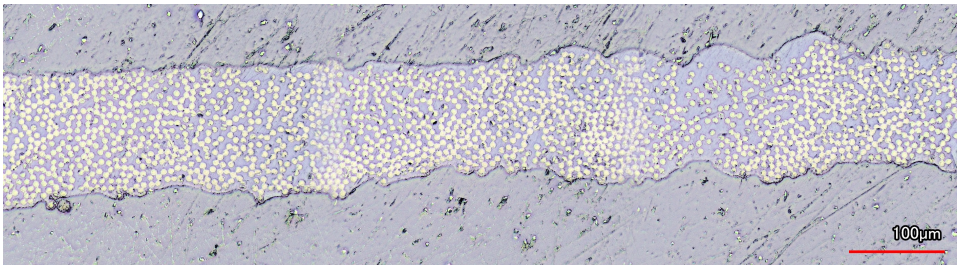

Figure D.12: Micrograph of TC1225 tape TC_5_2

D.2.2. DPR tape

Least conductive

Figure D.13 and Figure D.14 illustrate the cross sectional micrographs of the DPR tape sections of the least conductive 1_3 tape.

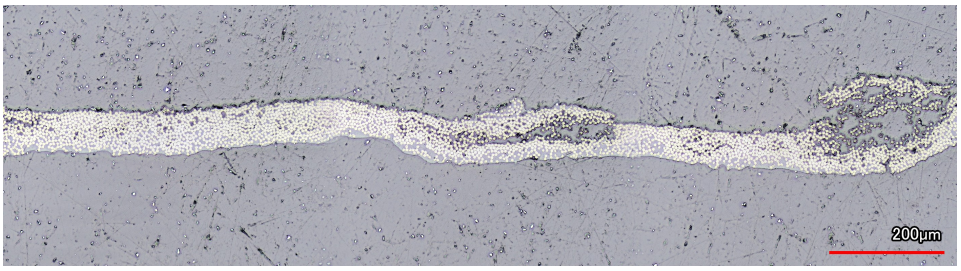

Figure D.13: Micrograph of DPR tape 1_3_1

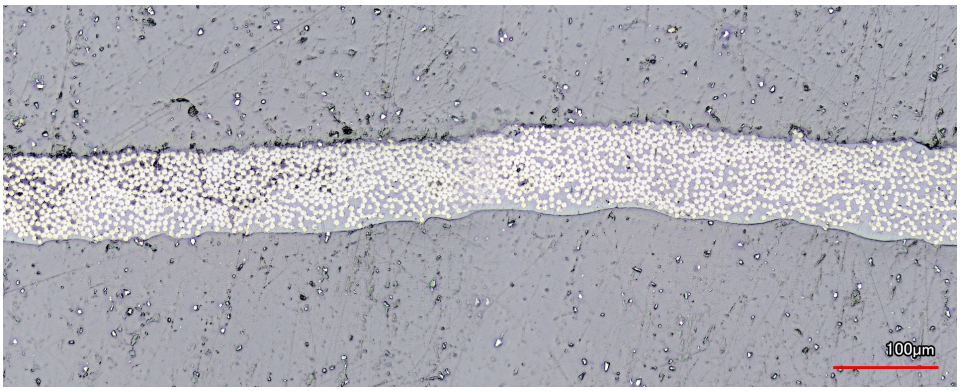

Figure D.14: Micrograph of DPR tape 1_3_2

Most conductive

Figure D.15 and Figure D.16 illustrate the cross sectional micrographs of the DPR tape sections of the most conductive 1_7 tape.

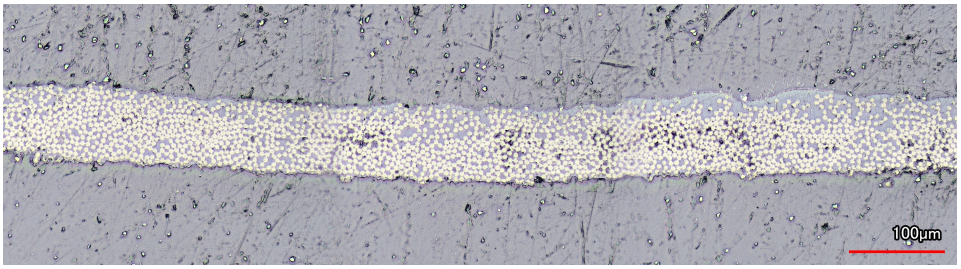

Figure D.15: Micrograph of DPR tape 1_7_1

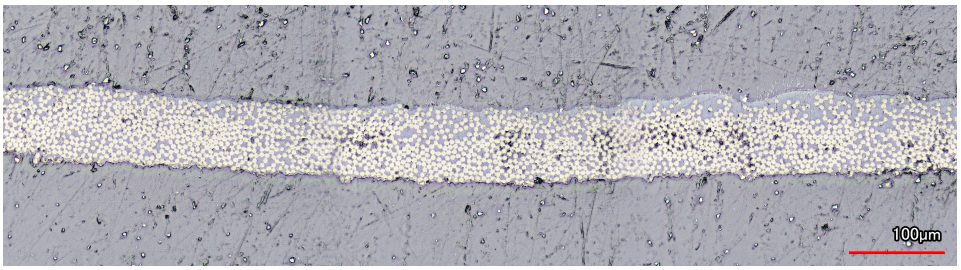

Figure D.16: Micrograph of DPR tape 1_7_2

D.2.3. TPR tape

Least conductive

Figure D.17 and Figure D.18 illustrate the cross sectional micrographs of the TPR tape sections of the least conductive 3_1 tape.

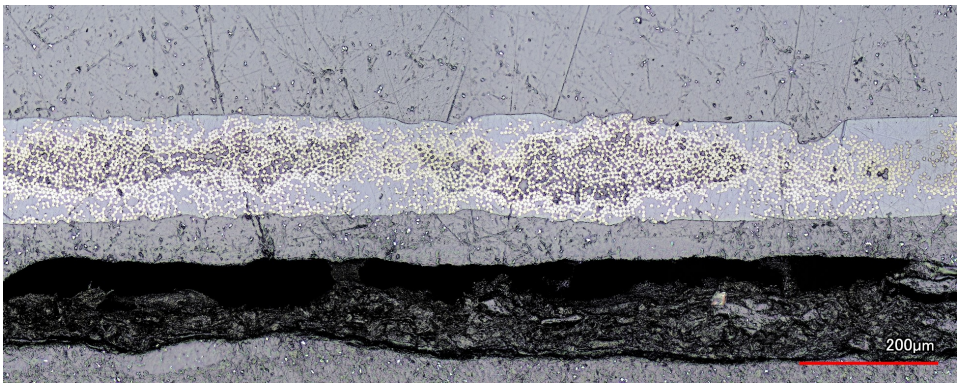

Figure D.17: Micrograph of TPR tape 3_1_1

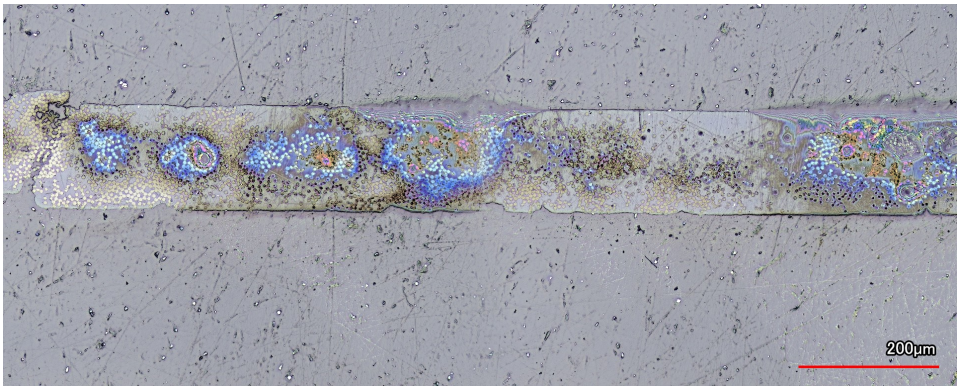

Figure D.18: Micrograph of TPR tape 3_1_2

Most conductive

Figure D.19 and Figure D.20 illustrate the cross sectional micrographs of the TPR tape sections of the most conductive 3_2 tape.

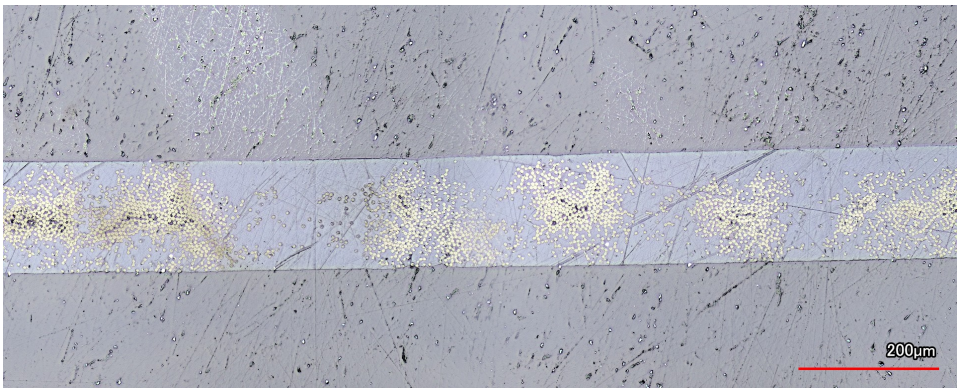

Figure D.19: Micrograph of TPR tape 3_2_1

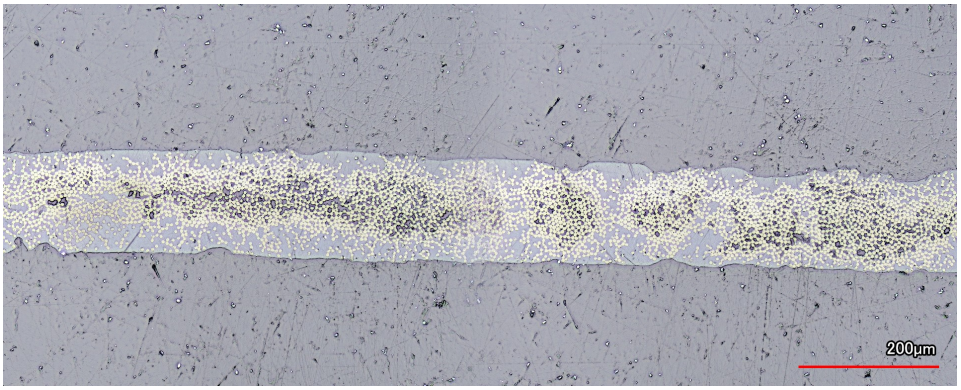

Figure D.20: Micrograph of TPR tape 3_2_2

D.2.4. Hybrid tape

Least conductive

Figure D.21 and Figure D.21 illustrate the cross sectional micrographs of the Hybrid tape sections of the least conductive 2_1 tape.

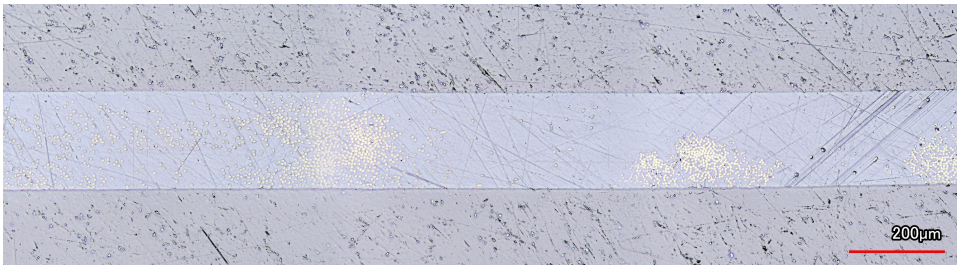

Figure D.21: Micrograph of Hybrid tape 2_1_1

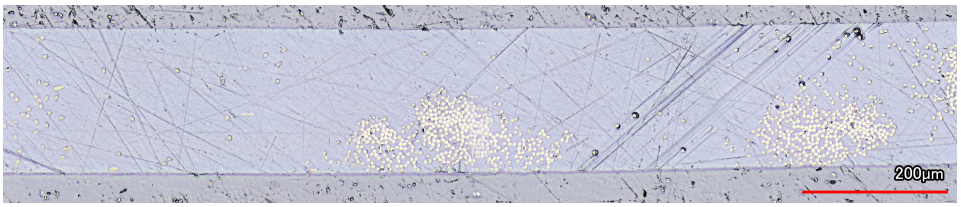

Figure D.22: Micrograph of Hybrid tape 2_1_2

Most conductive

Figure D.23 and Figure D.24 illustrate the cross sectional micrographs of the Hybrid tape sections of the most conductive 2_3 tape.

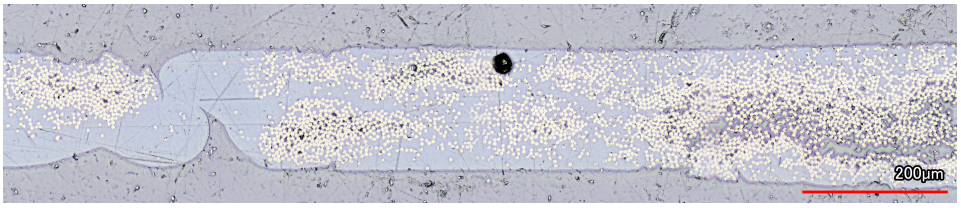

Figure D.23: Micrograph of Hybrid tape 2_3_1

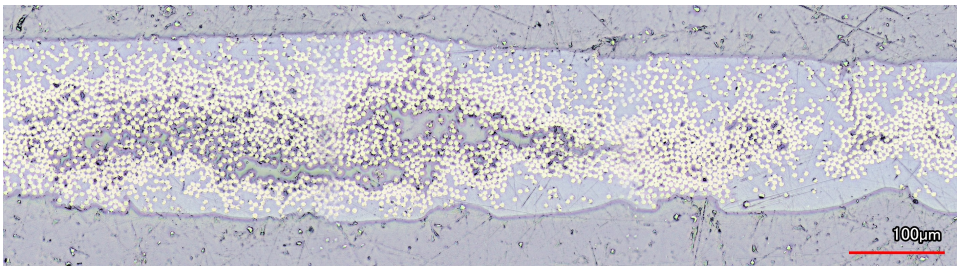

Figure D.24: Micrograph of Hybrid tape 2_3_2